Aus dem Institut für Zytobiologie
Geschäftsführender Direktor: Prof. Dr. Roland Lill

des Fachbereichs Medizin der Philipps-Universität Marburg

Investigation of the role of the mitochondrial ABC transporter ABCB7 in heme and iron-sulfur protein biosynthesis

Inaugural-Dissertation
zur Erlangung des Doktorgrades der gesamten Humanmedizin

dem Fachbereich Medizin der Philipps-Universität Marburg
vorgelegt von

Nadine Arlett Mathea aus Herdecke

Marburg, 2024

Angenommen vom Fachbereich Medizin
der Philipps-Universität Marburg am 27.05.2024

Gedruckt mit Genehmigung des Fachbereichs Medizin

Dekanin: Frau Prof. Dr. D. Hilfiker-Kleiner

Referent: Herr Prof. Dr. R. Lill

1. Koreferent: Herr Prof. Dr. A. Brehm

Table of contents

1. List of abbreviations

ABC	ATP-binding cassette
ABCB7	ATP-binding cassette subfamily B member 7
ABCB10	ATP-binding cassette subfamily B member 10
ACO	aconitase
ACP1	acyl-carrier protein 1
ADP	adenosine diphosphate
ALA	5-aminolevulinic acid
ALAS	5-aminolevulinic acid synthase
ALAD	5-aminolevulinic acid dehydratase
AMP-PNP	adenosine-5'-(β-γ-imido) triphosphate
approx.	approximate/approximately
APS	ammonium persulfate
ATP	adenosine triphosphate
ATPase	adenosine triphosphatase
BCA	bicinchoninic acid
BSA	bovine serum albumin
C	respiratory chain complex
cACO	cytosolic aconitase
CAT	catalase
cDNA	complementary desoxyribonucleic acid
cf.	confer
CIA	cytosolic iron-sulfur cluster assembly
cm^3	cubic centimeter
CoA	coenzyme A
Copro III	coproporphyrinogen III
COX	cytochrome *c* oxidase
CPO	coproporphyrinogen oxidase
CS	citrate synthase
Cryo-EM	cryo-electron microscopy
CTC	CIA targeting complex
C-terminal	carboxy-terminal
CYC1	cytochrome c_1
CYP	cytochrome
CYP450	cytochrome P450
ddH_2O	ultrapure H_2O

1. List of abbreviations

DDM	dodecylmaltoside
DGCR8	DiGeorge syndrome critical region gene 8 protein
DMEM	Dulbecco's modified Eagle's medium
DMSO	dimethylsulfoxid
DNA	desoxyribonucleic acid
DMT1	divalent metal-ion transporter 1
DTT	dithiothreitol
ECL	enhanced chemiluminescence
E. coli	Escherichia coli
EDTA	ethylenediaminetetraacetic acid
e.g.	exempli gratia
EGFP	enhanced green fluorescent protein
ER	endoplasmatic reticulum
F1 a/b	mitochondrial ATP-Synthase subunit alpha/beta
FAD	flavin adenine dinucleotide
FBXL5	F-box and leucine rich repeat protein 5
FCS	fetal calf serum
FDX2	ferredoxin 2
FDXR	ferredoxin-reductase
FECH	ferrochelatase
Fe/S	iron-sulfur
FLVCR1b	feline leukemia virus subgroup C receptor 1b
FOX	ferrous oxidation
FPN1	ferroportin 1
Ft	ferritin
Ft-H	heavy chain ferritin
Ft-L	light chain ferritin
FXN	frataxin
GAPDH	glycerinaldehyde-3-phosphate dehydrogenase
GLRX5	monothiol glutaredoxin
GRIM19	gene associated with retinoic and interferon-induced mortality 19 protein
GSH	glutathione
HA2X	histon A2
HCCS	holo cytochrome *c* synthase
HeLa cells	human cell line, derived from cervical cancer cells taken from Henrietta Lacks in 1951
HEPES	4-(2-hydroxyethyl)-1-piperazineethanesulfonic acid

1. List of abbreviations

HRP	horseradish peroxidase
HSC20	J-type co-chaperone protein homolog subfamily C member 20
HSPA9	heat shock protein 70 kDa protein 9 chaperone
IMM	inner mitochondrial membrane
IRE	iron-responsive element
IRP	iron-regulatory protein
ISC	iron-sulfur cluster
ISCU2	U-type scaffold protein 2
KH_2PO_4	monopotassium phosphate
kDa	Kilodalton
LB	lysogeny broth
LIAS	lipoyl synthase
LDH	lactate dehydrogenase
mACO	mitochondrial aconitase
MDV	mitochondria derived vesicles
MAM	mitochondria associated membrane
MES	2-(N-morpholino)ethanesulfonic acid
MFRN1	mitoferrin 1
MFRN2	mitoferrin 2
mRNA	messenger ribonucleic acid
miRNA	micro RNA
MoCo	molybdenum cofactor
Na_2HPO_4	disodium phosphate
NAD^+	oxidized nicotinamide adenine dinucleotide
NADH	reduced nicotinamide adenine dinucleotide
$NADP^+$	oxidized nicotinamide adenine dinucleotide phosphate
NADPH	reduced nicotinamide adenine dinucleotide phosphate
NDUF	NADH ubichinone oxidoreductase subunit
NoT	non-targeting control
N-terminal	amino-terminal
NTHL1	endonuclease III-like protein
OD	optical density
PAA	polyacrylamide
PAGE	polyacrylamide gel electrophoresis
PBGD	porphobilinogen deaminase
PBS	phosphate buffered saline
pH	potential of hydrogen (negative decimal logarithm of H^+ concentration)

1. List of abbreviations

PLP	pyridoxal phosphate
PMSF	phenylmethylsulfonylfluoride
PPGIX	protoporphyrinogen IX
PPIX	protoporphyrin IX
PPO	protoporphyrinogen oxidase
RNA	ribonucleic acid
RNAi	ribonucleic acid interference
rpm	revolutions per minute
SD	standard deviation
SDH	succinate dehydrogenase
SDS	sodiumdodecyl sulfate
siRNA	small interfering ribonucleic acid
sm	silent mutation/silently mutated
Steap3	six-transmembrane epithelial antigen of the prostate protein family member 3
TCA	tricarboxylic acid
TE	tris/EDTA
TEMED	tetramethylethylendiamine
TBS	tris buffered saline
TBST	tris buffered saline + Tween 20
Tf	transferrin
TfR	transferrin receptor
TMEM14C	transmembrane protein 14C
TOMM	translocase of the outer membrane
URO3S	uroporphyrinogen III synthase
UROD	uroporphyrinogen decarboxylase
UTR	untranslated region
VDAC1	voltage dependent anion channel 1
v-type	vacuolar-type
XLSA	X-linked sideroblastic anemia
XLSA/A	X-linked sideroblastic anemia and cerebellar ataxia

2. List of figures

3. List of tables

4. Introduction

4.1 Iron: overview and functions

Iron (Fe) is of major importance for biological systems (Sheftel & Lill, 2009). In proteins, iron-containing cofactors can be part of a catalytic center or be involved in redox reactions. On the other hand, iron can potentially be toxic as its ferrous (Fe^{2+}) form catalyzes the production of reactive hydroxyl radicals from hydrogen peroxide, a process known as Fenton reaction (Fenton, 1876; Sheftel & Lill, 2009). To prevent this toxic reaction and protect membranes, lipids, desoxyribonucleic acid (DNA) and proteins from damage, mammalian cells have developed dedicated mechanisms for the uptake, trafficking, storage and metabolism of Fe (Anderson & Frazer, 2017; Dutt et al., 2022).

Fe in the blood plasma is bound to transferrin (Tf) for transportation to target tissues (holo-Tf). At the cell surface, holo-Tf binds to transferrin receptor 1 (TfR1), is incorporated into the cell via clathrin-mediated endocytosis (Mayle et al., 2012; Muckenthaler et al., 2017; Richardson & Ponka, 1997) and subsequently delivered to the endosomal compartment. Upon acidification of endosomes by vacuolar-type (V-type) adenosine triphosphatases (ATPases) to less than pH 5.5, Fe is released from the Tf-TfR complex, reduced to Fe^{2+} by a specific ferrireductase (Steap3; Iwai, 2019; Knutson, 2007) and exported to the cytosol by the divalent metal transporter 1 (DMT1; Gunshin et al., 1997). Depending on the Fe requirement of the cell, the metal may afterwards either be trafficked to mitochondria for incorporation into heme or iron/sulfur (Fe/S) clusters or may be stored in the cytosolic compartment by loading into ferritin (Ft). Ft consists of varying proportions of heavy-chain (Ft-H) and light-chain (Ft-L) polypeptides, which are assembled as a rotund sphere with a large cavity in the center and can incorporate up to 4500 atoms of Fe (Harrison & Arosio, 1996; Munro & Linder, 1978; Zang et al., 2017).

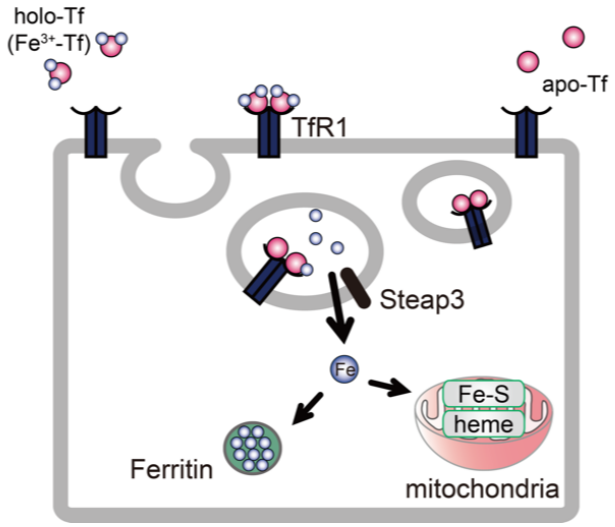

Figure 1: Fe binding and incorporation into the cell (adapted from Iwai, 2019).

The exact process of Fe delivery to mitochondria is still uncertain. While Fe^{2+} may pass freely through porins into the intermembrane space, the mitochondrial carrier family members mitoferrin 1 and 2 (MFRN1/2) appear to transport iron across the inner mitochondrial membrane (IMM; Mühlenhoff et al., 2015; Shaw, Cope, et al., 2006). Fe is subsequently utilized for the synthesis of heme and Fe/S cluster cofactors which are incorporated into mitochondrial proteins such as respiratory complexes and cytochromes. Heme and Fe/S cofactor maturation of extramitochondrial proteins including hemoglobin or catalase (CAT) is also dependent on mitochondria and requires further dedicated export and assembly systems.

4.1.1 Cellular iron regulation

In order to ensure cellular supply with appropriate amounts of Fe whilst protecting the cell against free radicals, sufficient regulation of cellular Fe levels is obligatory. Under Fe-replete conditions, the cellular Fe uptake mechanism is downregulated to prevent the cell from excessive and deleterious Fe uptake. Vice versa, when cellular Fe levels are low, Fe uptake needs to be increased. The major mechanism by which cellular Fe homeostasis is achieved in mammalian cells, is the posttranscriptional regulation via Fe-regulatory proteins (IRPs; Anderson & Frazer, 2017; Bjellqvist et al., 1993; Sanchez et al., 2011; Wilkinson & Pantopoulos, 2014).

Mammalian IRPs are present in two variants, IRP1 and IRP2. IRP1 possesses a double function. On the one hand, it acts as a cytosolic aconitase (cACO)

interconverting citrate and isocitrate when an Fe/S cluster is bound. On the other hand, when the Fe/S cluster cofactor is absent, IRP1 can bind to Fe-responsive elements (IREs) which are stem-loop structures in untranslated regions (UTRs) of messenger RNAs (mRNAs) of Fe-related proteins such as Ft or TfR (Martelli et al., 2015; Walden et al., 2006). When cellular Fe levels are low, IRP1 binds to the 5' IRE of Ft mRNA and blocks its translation, leading to a decrease in Ft protein levels and consequently to decreased cellular Fe storage capacities. Under these conditions, IRPs also bind to the 3' IREs of TfR mRNA, thereby stabilizing the messenger transcript, enhancing TfR1 production and concomitantly increasing Fe uptake. In contrast, IRE-binding of IRP2 is determined by the protein's steady-state levels which are regulated by Fe-dependent proteasomal degradation involving the ubiquitin-E3-ligase F-box and leucine rich repeat protein 5 (FBXL5) with an Fe-binding hemerythrin domain (Salahudeen & Bruick, 2009; Vashisht et al., 2009). Structural analyses have suggested that FBXL5 may also bind a [2Fe-2S] cluster to promote the interaction with IRP2 (Wang et al., 2020).

4.2 Heme

4.2.1 Heme: overview and functions

Hemes are tetrapyrrole-type protein cofactors and coordinate Fe as a central metal in their porphyrin ring. Sidechains of the ring can vary, resulting in different chemical properties and functions like for heme *a*, heme *b* and heme *c* (Figure 2). In humans, hemes are essential cofactors for electron transfer, catalysis of redox reactions, structural stability and oxygen transport (Ajioka et al., 2006; Balwani et al., 2020; Burden et al., 1999; Taketani et al., 2000).

The most prevalent and prototypical heme type in mammalian cells is heme *b*, which is present in several proteins including the erythrocytic oxygen transport protein hemoglobin (Gell, 2018; Yang et al., 2023), cytochrome P450 (CYP450) enzymes for example in liver (Correia et al., 2011), CAT in peroxisomes (Putnam et al., 2000), and respiratory chain complexes II and III.

The function of heme *b* in oxygen transport is well-known by hemoglobin. The protein is essential for oxygen binding and transport in erythrocytes and consists of four globin polypeptide chains each harboring a heme *b*. The heme *b* binds oxygen in respiratory capillaries of the lung and releases it in capillaries of peripheral tissues to be further processed for aerobic respiration (Ajioka et al., 2006; Caughey et al., 1975; Dlouhy & Outten, 2013; Hederstedt, 2012; Tsiftsoglou et al., 2006).

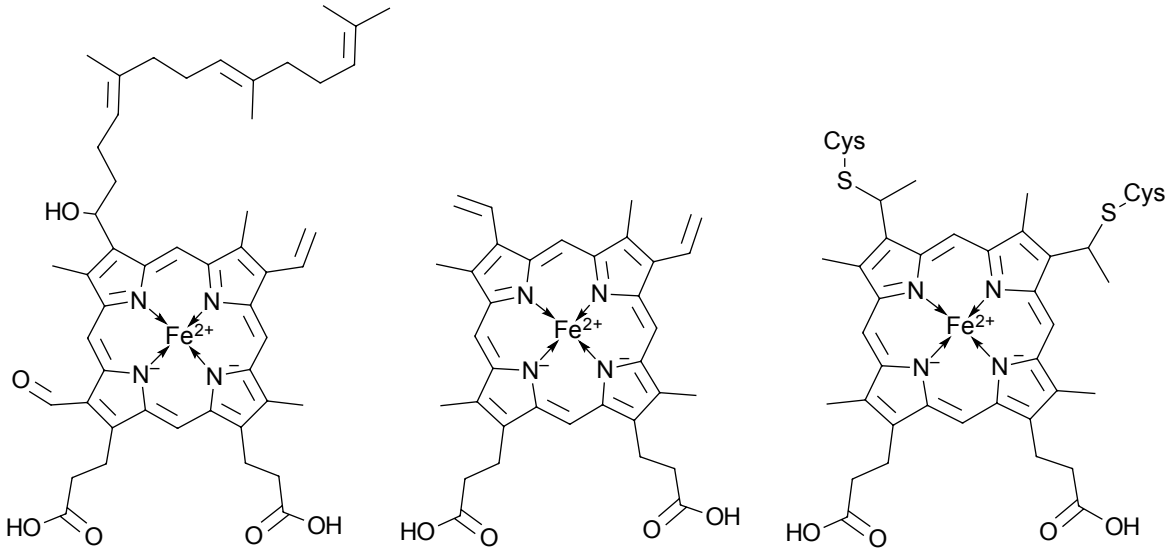

heme *a* heme *b* heme *c*

Figure 2: Hemes *a, b, c*; for details see text. Structures drawn up with ChemDoodle v11.0 by iChemLabs.

CYP450 proteins are oxygenases transferring electrons to oxygen or catalyzing the oxidation of organic compounds to protect the human cell against toxic agents (Manikandan & Nagini, 2018). CYP450s are essential for metabolism of bile acids, drugs, steroids and further chemicals (Guengerich et al., 2016).

CAT is a heme *b*-dependent homotetrameric peroxisomal enzyme harboring one heme cofactor per subunit. The enzyme catalyzes the conversion of two molecules of the highly reactive compound hydrogen peroxide to two molecules of water and one molecule of less reactive molecular oxygen ($2\ H_2O_2 \rightarrow O_2 + 2\ H_2O$), thus protecting the cellular constituents against oxidative damage (Goyal & Basak, 2010). Heme *b* directly participates in hydrogen peroxide turnover as its Fe^{3+} form becomes converted into a Fe^{4+}-containing porphyrin cation radical when the first hydrogen peroxide molecule is converted to water. In a second step, the porphyrin cation oxidizes a second hydrogen

peroxide and releases molecular oxygen and water (Putnam et al., 2000). Oxidative damage may become clinically relevant in patients with inherited Acatalasemia, who may suffer from methemoglobinemia or an early onset of diabetes mellitus due to CAT deficiency, leading to oxidative damage of the insulin-producing pancreatic beta-cells (Góth & Nagy, 2013).

Succinate coenzyme Q reductase or also referred to as succinate dehydrogenase (SDH) is a heterotetrameric enzyme at the IMM, operating at the interface between the respiratory chain (thus also designated as respiratory chain complex II) and the tricarboxylic acid (TCA) cycle (Van Vranken et al., 2015). SDH conveys a major reaction step of the TCA cycle, the oxidation of succinate to fumarate. Subunits A and B of SDH face towards the mitochondrial matrix where SDHA contains a covalently attached flavin adenine dinucleotide (FAD) moiety and converts the succinate substrate, and SDHB uses three Fe/S cofactors to transfer electrons to ubiquinone, a key component of the mitochondrial respiratory chain (Anderson et al., 2014). SDH subunits C and D are inserted into the IMM, with heme *b* bound at their interface. The functional significance of the heme *b* moiety is not clear, because its absence hardly interferes with SDH function (Rutter et al., 2010).

Heme types *a* and *c* are found in proteins of the respiratory chain where electrons are transferred to molecular oxygen to perform proton translocation across the IMM. This electron transfer is mainly enabled by heme-containing cytochromes which are subunits of the cytochrome *c* reductase complex (C III, containing heme *c*), the electron transfer factor cytochrome *c*, and cytochrome *c* oxidase complex (C IV or COX, harboring heme *a*).

C III is a multienzyme complex and harbors both heme *b* and heme *c* centers. The catalytic core of each C III monomer consists of cytochrome *b*, cytochrome c_1 and the Rieske Fe/S protein (Smith et al., 2012). Heme c_1 of cytochrome c_1 is involved in the transfer of two electrons from ubiquinol via the Rieske protein to cytochrome *c*. Cytochrome c_1 and the Rieske protein expose their prosthetic groups to the intermembrane space and are fixed in the IMM by their single transmembrane domains. In addition, C III contains hemes bL and bH which are involved in the Q cycle moving protons across the mitochondrial membrane and thereby contributing to the mitochondrial membrane potential. The eponymous cofactor of cytochrome *c* is heme *c* which in contrast to the other hemes is covalently bound to the protein via thioether bridges via catalysis by cytochrome c/c_1 heme lyases.

COX transfers electrons from reduced cytochrome *c* to dioxygen, resulting in the formation of water (Popović, 2013). To execute this reaction, COX contains four redox-active metal centers including a heme *a*, a copper center CuA and a binuclear complex consisting of heme a_3 and CuB as prosthetic groups. Reduced cytochrome *c* supplies CuA with electrons which are transferred to the active site via heme *a*. At the heme a_3/CuB active site, reduction of dioxygen takes place (Ferguson-Miller & Babcock, 1996; Kim & Hummer, 2012; Konstantinov et al., 1997; Ostermeier & Michel, 1997). During each reduction of dioxygen to water, eight protons are turned over, four by the formation of water, and four which are translocated across the IMM in an electron transfer-dependent fashion (Belevich et al., 2006).

4.2.2 Hemes are synthesized in a complex process

Heme synthesis in eukaryotes including human cells occurs through a highly conserved pathway and takes place in both the cytosolic and mitochondrial compartment (Ajioka et al., 2006; Dutt et al., 2022; Phillips, 2019; Stojanovski et al., 2019). The principal product is heme *b*, which is subsequently converted into other heme forms. The classical biosynthesis pathway of heme *b* (Figure 3) begins in mitochondria with the formation of 5-aminolevulinic acid (ALA) from glycine and succinyl-coenzyme A (succinyl-CoA; McKay et al., 1969). This condensation reaction is catalyzed by 5-aminolevulic acid synthase (ALAS) and is the rate-limiting reaction in the heme biosynthesis pathway. Two isoforms of ALAS occur in human tissue, the ubiquitously expressed ALAS1 and ALAS2, which is expressed specifically in erythroid cells (Peoc'h et al., 2019).

Subsequent to this initial step, ALA is exported from mitochondria into the cytosol where subsequent steps of heme synthesis take place. Little is known about how intermediates of the heme biosynthesis pathway are shuttled across the mitochondrial membranes, but it is suggested that adenosine triphosphate (ATP)-binding cassette (ABC) transporters may be involved (Martinez et al., 2020; Shirihai et al., 2000). In the cytosolic compartment, the enzyme ALA dehydratase (ALAD) catalyzes the second step of heme biosynthesis by converting ALA to porphobilinogen and water. Subsequently, porphobilinogen deaminase (PBGD) fuses four porphobilinogen molecules to the linear tetrapyrrole hydroxymethylbilane, which is then converted to ring-shaped Uroporphyrinogen III by Uroporphyrinogen III synthase (URO3S). In the last cytosolic step, acetate sidechains of the tetrapyrrole ring are converted to methyl

groups by decarboxylation, generating coproporphyrinogen III (Copro III). This Copro III is then reimported into mitochondria, possibly by assistance of a protein at the IMM known as transmembrane protein 14C (TMEM14C, Yien et al., 2014). Also at the IMM resides coproporphyrinogen oxidase (CPO) which oxidatively decarboxylates the propionate groups of Copro III to vinyl groups to form protoporphyrinogen IX (PPGIX; Rhee et al., 2013). PPGIX is subsequently oxidized to protoporphyrin IX (PPIX) by mitochondrial protoporphyrinogen oxidase (PPO; Donegan et al., 2019). In the final step of heme *b* biosynthesis, ferrochelatase (FECH) inserts Fe^{2+} into PPIX. FECH is a homodimeric protein at the inner surface of the IMM and with the active site facing the matrix. In many eukaryotes including humans each FECH protomer contains one [2Fe-2S] cluster as a cofactor (Dailey et al., 2000; Medlock et al., 2007; Taketani et al., 2000). FECH together with PPO, ATP-binding cassette subfamily B member 10 (ABCB10) and MFRN1 has been suggested to be part of a multienzyme complex which also requires TMEM14 for its function (Chen et al., 2010; Shaw, Cope, et al., 2006; Yien et al., 2014). Formation of such a complex is proposed to facilitate the coordinated import and turnover of PPIX and Fe in order to prevent the mitochondrial environment from potentially toxic effects of these substrate compounds.

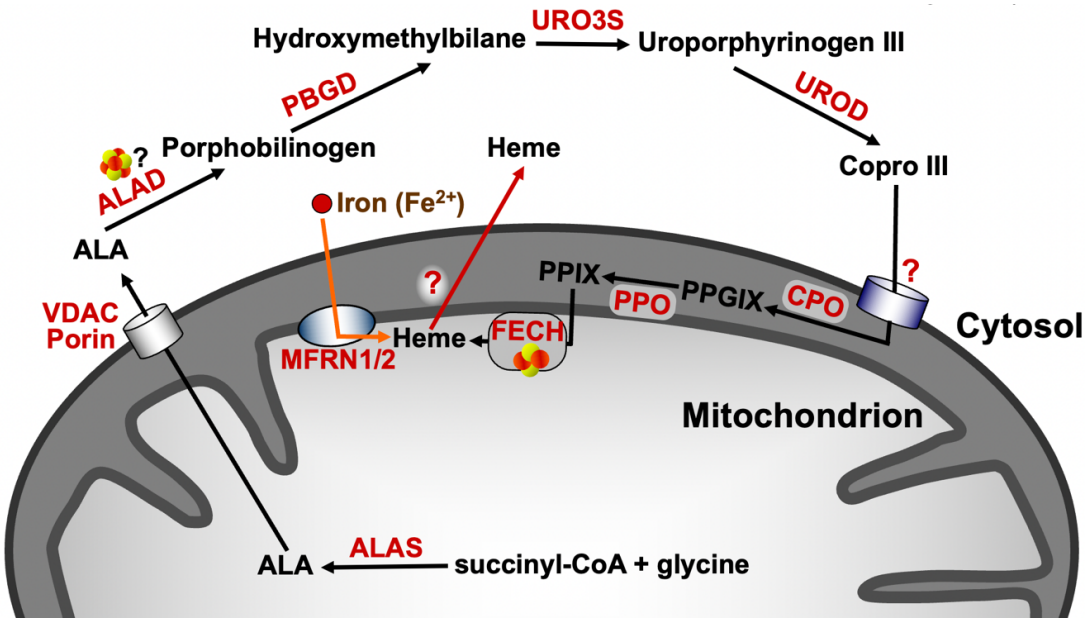

Figure 3: Overview of the heme biosynthesis and and its connection to Fe/S cluster metabolism. For details and abbreviations see text (adapted from an overview kindly provided by Roland Lill).

Formation of hemes *o*, *a*, and *c* occur from heme *b* (Swenson et al., 2020). The heme *a* biosynthetic pathway proceeds via heme *o* as an intermediate compound and involves two enzymes at the IMM, Heme *o* synthase (COX10) and Heme *a* synthase (COX15), respectively. In a first reaction step, COX10 catalyzes the modification of a

vinyl group of heme *b*. Subsequently, a methyl group is monooxygenated by COX15 to form heme *a* (Hederstedt, 2012). Heme *c* is formed by the covalent attachment of heme *b* to cytochrome *c* or c_1 via two cysteine residues of the apo-protein backbone. In mammals, both reactions are catalyzed by the same enzyme, holocytochrome *c* synthase (HCCS; Kranz et al., 2009; Moraes et al., 2004).

In each protein of the heme biosynthesis pathway, genetic dysfunctions may lead to a specific type of porphyric disorder in affected patients, e.g. X-linked erythropoietic protoporphyria (ALAS), ALA dehydratase deficiency porphyria (ALAD) or erythropoietic protoporphyria (FECH; Bissell et al., 2017; Kauppinen, 2005). The porphyric disorders are classified depending on the inheritance pattern and show erythroid, hepatic, or neurologic manifestations.

4.2.3 Mitochondrial heme *b* export

Subsequent to its biosynthesis, heme *b* can take different routes. Within mitochondria it may be modified to heme *a*, for use in C IV. It may also be trafficked to the intermembrane space where it is covalently attached to cytochrome *c* or c_1 by HCCS (cf. chapter 4.2.2). Heme *b* is also exported from mitochondria for insertion into extramitochondrial hemoproteins. The molecular mechanisms of heme trafficking and export from mitochondria are mostly unknown to date. A direct membrane-based delivery to the endoplasmic reticulum (ER) might be established via mitochondria-associated membranes (MAMs; Chambers et al., 2021; Vance, 2014). Mitochondria-derived vesicles (MDVs) have been suggested to transport molecules from mitochondria to peroxisomes and lysosomes (Neuspiel et al., 2008; Schumann & Subramani, 2008). The propionate side chains of heme *b* render the molecule hydrophobic, implying a requirement for an export system to allow transition through the two mitochondrial membranes. Yet, the protein Feline leukemia virus subgroup C receptor 1b (FLVCR1b) is suspected to export heme from mitochondria, as knockdown of FLVCR1b in human cervical cancer cells (HeLa cells) resulted in mitochondrial heme accumulation (Chiabrando et al., 2012). Vice versa, overexpression showed cytosolic heme accumulation. Consistently, knockdown of FLVCR1b in mice led to impaired erythroid differentiation due to heme accumulation in mitochondria (Chiabrando et al., 2012; Fleming & Hamza, 2012; Reddi & Hamza, 2016).

An alternative potential mitochondrial heme exporter complex consisting of FECH and the ABC proteins ABCB7 and ABCB10 has been proposed by a tissue culture model of

defective hemoglobinization in erythroid cells. In this model, the close spatial vicinity of the Fe importer MFRN1 and FECH to ABCB7 may support a potential heme export function of the ABC transporter (Maio et al., 2019).

4.3 Iron-sulfur clusters

4.3.1 Overview and structure

Fe/S clusters are essential inorganic cofactors present in all kingdoms of life (Lill & Freibert, 2020). In eukaryotes, Fe/S clusters are found in the cytosol, nucleus and mitochondria. The most common types are the rhombic [2Fe-2S] and the cubane [4Fe-4S] forms (Lill, 2020). In these structures, Fe and S atoms are alternatingly arranged to build the corners of the clusters, and each Fe atom is typically coordinated by one [4Fe-4S] or two [2Fe-2S] cysteine residues of the polypeptide backbone. Other ligands than cysteine are possible, for example in case of the so-called Rieske [2Fe-2S] cluster of respiratory chain C III in which one Fe atom is coordinated by two cysteine residues, and the other Fe by two histidine residues (Bak & Elliott, 2014).

4.3.2 Functions of Fe/S clusters

4.3.2.1 Fe/S proteins in the mitochondrion

Fe/S clusters in mitochondria participate in enzymatic catalysis reactions like in mitochondrial aconitase (mACO), or in electron transfer like in the respiratory chain complexes C I, C II and C III. The mACO catalyzes the second reaction of the TCA cycle by interconverting citrate to isocitrate via the intermediate aconitate. The [4Fe-4S] cluster is involved in the catalytic activity and coordinates hydroxyl groups of the reactants, thereby facilitating dehydration and aconitate formation. The TCA cycle reduces oxidized nicotinamide adenine dinucleotide (NAD^+) to reduced nicotinamide adenine dinucleotide (NADH)/H^+ which in turn feeds electrons into NADH dehydrogenase (C I) of the respiratory chain. C I adopts an “L-shaped” structure with a membrane-bound arm and an arm directing into the mitochondrial matrix and passes the NADH/H^+-derived electrons from the tip of its matrix arm through ubiquinone at the basis of this arm. A total of 8 [2Fe-2S] and [4Fe-4S] clusters are bound to C I subunits including NADH ubiquinone oxidoreductase subunit V2 (NDUFV2) and S8 (NDUFS8) and participate in the formation of the electron transfer conduit (Gnandt et al., 2016; Wu et al., 2016). Other subunits including NDUFB4 and gene associated with retinoic and interferon-induced mortality 19 protein (GRIM19, NDUFA13) of the membrane and the matrix arm, respectively, hold functions in the structural organization of C I.

As already pointed out above (cf. chapter 4.2.1) also respiratory chain C II (SDH) and C III transfer electrons in an Fe/S cluster-dependent fashion. SDH converts succinate to fumarate and reduces ubiquinone using a [2Fe-2S], a [3Fe-4S], and a [4Fe-4S] cluster each coordinated within subunit SDHB. In C III, electron transfer from ubiquinol to cytochrome *c* involves a Rieske-type [2Fe-2S] cluster. Electron transfer conducted by C I and C III supports the generation of a proton gradient across the IMM which is eventually used by the F_1F_o-ATP synthase complex to produce ATP.

Further Fe/S cluster proteins include lipoyl synthase (LIAS) which catalyzes the final step in the biosynthesis of the lipoyl cofactor (McCarthy & Booker, 2017) or ferredoxins which are essential for mitochondrial Fe/S protein maturation, heme and steroid hormone synthesis (Sheftel et al., 2010).

4.3.2.2 Extramitochondrial Fe/S clusters

Fe/S proteins are also present in the cytosolic and nuclear compartments where they hold essential regulatory and metabolic functions including DNA maintenance, nucleotide metabolism, and electron transfer (Lill & Freibert, 2020). A prominent example is IRP1 (c.f. 4.1.1) which is involved in cellular iron regulation by binding in its apoform to IREs of certain iron-trafficking-related proteins. With a bound [4Fe-4S] cluster it functions as a cytosolic aconitase (cACO; Walden et al., 2006). Another example for a nucleic acid-binding [4Fe-4S] protein is NTHL1, an endonuclease III-like enzyme. NTHL1 binds to DNA and supports the base excision repair of oxidatively damaged pyrimidines. The function of the cluster in this process is still ill-defined (Aspinwall et al., 1997), but is relevant for stabilizing NTHL1's interaction with DNA (Moe et al., 2022). Also, the metabolism of nucleotides, the building blocks of nucleic acids, is dependent on Fe/S proteins. *De novo* purine nucleotide biosynthesis is dependent on glutamine amidophosphoribosyltransferase (GPAT) which also depends on a [4Fe-4S] cluster (Iwahana et al., 1993). GPAT contains an N-terminal, 11 residues long propeptide which is autocatalytically cleaved upon the insertion of a [4Fe–4S] cluster to produce the mature and active enzyme (Brayton et al., 1994; Stehling et al., 2013). In the absence of the metallo-cofactor, propeptide processing is impaired, leading to GPAT destabilization and degradation (Martelli et al., 2007). Dihydropyrimidine dehydrogenase (DPYD) is the key enzyme for the modification of pyrimidine bases and their derivatives. The enzyme consists of two identical subunits, each containing four [4Fe-4S] clusters and two flavins to mediate electron transfer from

reduced nicotinamide adenine dinucleotide phosphate (NADPH) to pyrimidine (Porter & Spector, 1993; Schnackerz et al., 2004). DPYD is clinically significant for treatment of cancer patients with chemotherapeutics like the fluorouracil-derived therapeutic drug Capecitabine (Dean & Kane, 2012). Further extramitochondrial Fe/S proteins include ATP-binding cassette sub-family E member 1 (ABCE1), an essential factor of eukaryotic translation and ribosome biogenesis (Toompuu et al., 2016) and catalytic subunits of DNA polymerases like POLA1, POLD1 or POLE (Lill & Freibert, 2020; Paul & Lill, 2015). A full list of the human Fe/S proteome is found in Freibert and Lill 2020.

4.3.3 Biosynthesis of Fe/S clusters

In eukaryotes, complex and evolutionary conserved machineries mediate the assembly of Fe/S clusters and their subsequent insertion into apoproteins (Lill & Freibert, 2020; Stehling et al., 2014). Within mitochondria, the iron-sulfur cluster assembly (ISC) machinery conducts the *de novo* assembly of Fe/S clusters and the maturation of target proteins. The cytosolic iron-sulfur protein assembly (CIA) machinery is connected to the ISC system by a mitochondrial ISC export system (cf. chapter 4.3.3.2) and matures both cytosolic and nuclear Fe/S proteins. Due to the essential functions of cytosolic and nuclear Fe/S proteins (cf. chapter 4.3.2.2) also their biogenesis by the ISC and CIA systems is a vital process which includes three major assembly steps (Braymer et al., 2021; see also Figure 4):

1. *de novo* synthesis of an Fe/S cluster on scaffold proteins
2. Fe/S cluster trafficking via Fe/S cluster transfer proteins
3. insertion into apoproteins by targeting factors.

4.3.3.1 Mitochondrial Fe/S cluster assembly

The first assembly step is mediated by ISC factors that facilitate the *de novo* synthesis of a [2Fe-2S] cluster. The Fe required for Fe/S cluster assembly is imported into mitochondria by the mitochondrial carriers MFRN 1 and 2 and binds to U-type-scaffold protein 2 (ISCU2) via conserved active-site residues (Srour et al., 2022). A central component is the cysteine desulfurase complex NFS1-ISD11-ACP1 which converts cysteine to alanine in a pyridoxal phosphate (PLP)-dependent fashion and uses the abstracted sulfur for formation of a persulfide on the active cysteine residue of NFS1 (Zheng et al., 1994). Subsequently, the NFS1-linked persulfide sulfur is transferred to a cysteine residue of ISCU2, which serves as a scaffold for the assembly of a transiently

bound [2Fe-2S] cluster. The sulfur transfer reaction is stimulated by frataxin (FXN), a protein related to Friedreich's ataxia. In patients with Friedreich's ataxia, spinocerebellar and sensory atrophy lead to progressive ataxia with occasional blindness and deafness. Additionally, cardiological or metabolic symptoms can be found in affected patients (Gomes & Santos, 2013; Parkinson et al., 2013; Stehling et al., 2014). Defects in other ISC proteins may cause neurodegenerative, metabolic or hematological phenotypes and an overview is found in Stehling et al., 2014. In order to convert the persulfide sulfur to the sulfide S^{2-} present in the [2Fe-2S] cluster an electron supply by the NAD(P)H-ferredoxin reductase (FDXR)-ferredoxin (FDX2) redox chain is needed.

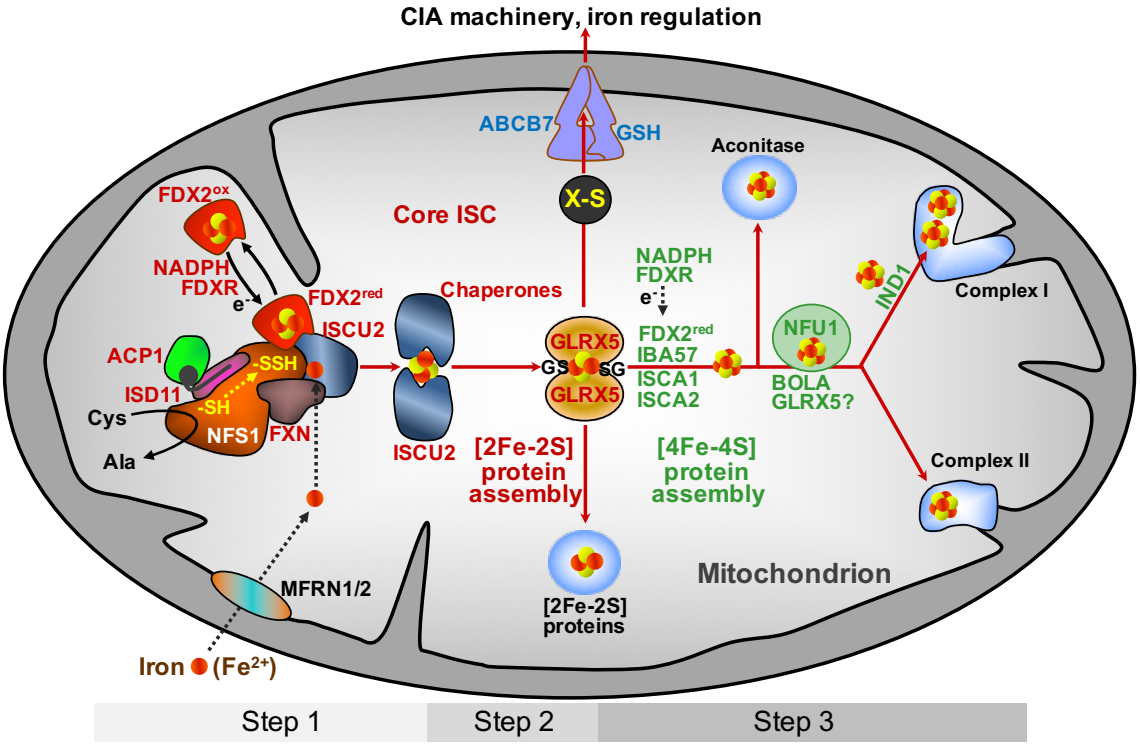

Figure 4: Model for the maturation of mitochondrial [2Fe-2S] and [4Fe-4S] proteins, adapted from Lill (2020).

In the second step, the assembled [2Fe-2S] cluster is released from ISCU2 by assistance of a dedicated chaperone system and transferred to the monothiol glutaredoxin 5 (GLRX5) which coordinates the cluster in a dimeric fashion in combination with two glutathione (GSH) peptides. GLRX5 holds a key position for the subsequent trafficking of the [2Fe-2S] cluster to different routes. The cluster is either directly inserted into [2Fe-2S] target proteins, converted into a [4Fe-4S] cluster, or is exported for use in the CIA system (cf. Figure 4). GLRX5 deficiency can lead to sideroblastic anemia 3 (Camaschella et al., 2007; Furuyama et al. 2013; Liu et al.

2016), which is characterized by anemia with iron overload and ring sideroblasts in affected patients.

In the third step of mitochondrial Fe/S protein assembly, [4Fe-4S] clusters are generated and inserted into apoproteins. In a so far ill-defined process, the ISC proteins ISCA1, ISCA2 and IBA57 are suspected to form a complex receiving [2Fe-2S] clusters from GLRX5 and fusing them to a [4Fe-4S] entity, again supported by electron delivery from NADPH to FDXR and FDX2 (Brancaccio et al., 2014; Sheftel et al., 2012; Weiler et al., 2020). Eventually, targeting proteins NFU1, IND1 or BOLA3 are assumed to be involved in the transfer of the assembled [4Fe-4S] cluster to target apoproteins (Lill & Freibert, 2020).

4.3.3.2 A role for ABCB7 in extramitochondrial Fe/S protein assembly

The assembly of cytosolic and nuclear Fe/S proteins is dependent on the mitochondrial core ISC system as well as on the ABC transporters of the IMM, Atm1 in yeast and ABCB7 in mammals (Kispal et al., 1999; Paul & Lill, 2015; Pondarre et al., 2006). The mitochondrial ISC system including the desulfurase NFS1 is proposed to synthesize a sulfur-containing compound called X-S of which the exact structure is not yet determined. X-S is assumed to be exported from mitochondria via ABCB7 in an energy-dependent fashion and to support cytosolic-nuclear Fe/S protein assembly (Li & Cowan, 2015; Pandey et al., 2018; Pandey et al., 2019).

ABCB7 and Atm1 are typical homodimeric ATP-binding cassette (ABC) transporters with their two nucleotide binding domains facing the mitochondrial matrix and their two transmembrane domains entangled with each other (Figure 5; Dawson & Locher, 2006; Ellinghaus et al., 2021; Srinivasan et al., 2014). The transmembrane domains form a substrate binding cavity at the level of the IMM-matrix interface for specific binding of X-S. ATP-binding and hydrolysis in the nucleotide binding domains powers the substrate transport towards the intermembrane space (Thomas & Tampé, 2020). Structural analyses have revealed three conformations of the ABCB7 homologs that characterize important aspects of the transport cycle of the protein. X-ray structures showed Atm1 in an inward open conformation with a large substrate binding cavity that is accessible from the matrix space (Srinivasan et al., 2014). The finding that some Atm1 crystals accommodated GSH in the substrate-binding cavity was in line with previous studies suggesting a requirement for GSH as well as mitochondrial iron for cytosolic iron-sulfur cluster assembly (Pandey et al., 2019; Sipos et al., 2002). This led

to the suggestion that X-S might be a glutathione coordinated Fe/S cluster (Pearson et al., 2020; Qi et al., 2014; Srinivasan et al., 2014). The closed conformation was observed in the adenosine-5'-(β-γ-imido) triphosphate (AMP-PNP)-bound cryo-electron microscopy (cryo-EM) structure of Atm1 (Ellinghaus et al., 2021). The two nucleotide binding domains are tightly bound thus forming a closed cavity between the

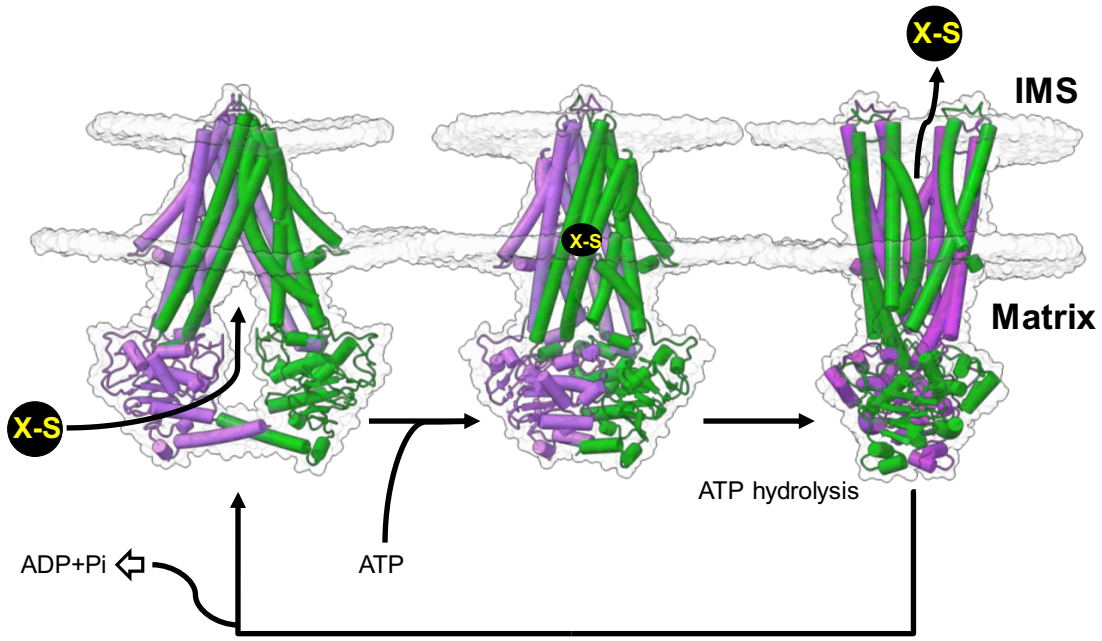

Figure 5: Three conformations of ABCB7, from left to right: the inward open, closed and outward open conformation (kindly provided by Roland Lill and Thomas Marcellino).

transmembrane segments for putative substrate binding. As observed for the plant homolog of Atm1, the outward open structure may release the trapped substrate by opening the transmembrane segments towards the intermembrane space (Fan & Rees, 2022). ATP hydrolysis, dissociation of adenosine diphosphate (ADP) and phosphate (P_i) and the subsequent re-opening of the nucleotide binding domains may eventually close the transport cycle.

ABCB7 appears to be particularly relevant for mitochondria-rich cells including hematopoietic tissue (Pondarre et al., 2007) or liver, the central organ for systemic iron homeostasis (Sikorska et al., 2016). Mutations in the ABCB7 gene are the cause for the rare disease X-linked sideroblastic anemia and cerebellar ataxia (XLSA/A; D'Hooghe et al., 2012; Maguire et al., 2001). Affected cells may contain iron-loaded mitochondria arranged in an arc-like shape around the nucleus and are thus called ring sideroblasts. XLSA/A was described in different families and is especially occurring in males as the gene of the exporter is located on the x-chromosome and is inherited recessively. The patients show varying neurological, mental as well as hematological

pathologic phenotypes like a severe form of spinocerebellar syndrome which is characterized by motor impairment and cerebellar atrophy. Additionally, they show a mild hypochromic, microcytic anemia.

4.3.3.3 Cytosolic and nuclear Fe/S cluster assembly

After transport of X-S to the cytosol, assembly of cytosolic and nuclear Fe/S proteins is mediated by a specific set of CIA factors. The process is dependent on mitochondria and like the ISC mechanism can be divided into three major steps (cf. Figure 6). First, a [4Fe-4S] cluster is synthesized *de novo* on a heterodimeric cytosolic scaffold complex consisting of CIA factors CFD1 and NBP35 (Netz et al., 2007; Stehling, Jeoung, et al., 2018; Stehling et al., 2008), a step dependent on an electron transfer

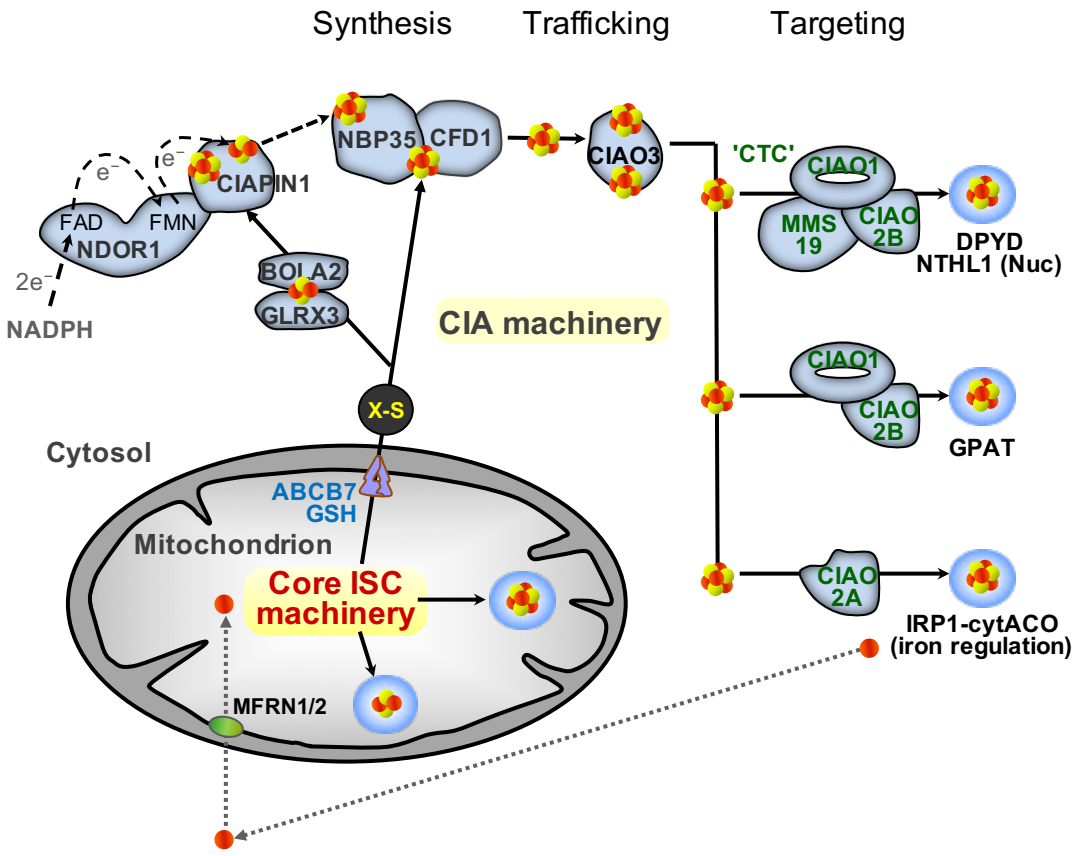

Figure 6: Model for the maturation of cytosolic and nuclear Fe/S proteins, adapted from Lill (2020).

chain involving NADPH, the flavin-dependent oxidoreductase NDOR1 and the Fe/S cluster protein CIAPIN1 (Netz et al., 2010; Zhang et al., 2008). Recent studies suggested that CIAPIN1 maturation may require [2Fe-2S] clusters provided by a

complex consisting of glutaredoxin 3 (GLRX3) and BOLA2 (Camponeschi et al., 2020; Frey et al., 2016; Patel et al., 2019).

In subsequent steps, the newly assembled [4Fe-4S] cluster is transferred to apoproteins with the help of CIAO3 and the three components of the CIA targeting complex (CTC), namely CIAO1, CIAO2B, and MMS19 (Gari et al., 2012; Srinivasan et al., 2007; Stehling et al., 2013; Stehling et al., 2012). These constituents are required for the maturation of almost all cytosolic-nuclear Fe/S proteins and have been suggested to act in different combinations. For example, maturation of GPAT is dependent on CIAO1 and CIAO2B but not on MMS19, whereas all CTC components are required for cluster insertion into DPYD or NTHL1 (Stehling et al., 2012). Fe/S cluster insertion into IRP1 requires the CIAO2B-related targeting factor CIAO2A, but none of the CTC components. This specificity points to a decoupling of common Fe-S protein assembly from IRP1-dependent cellular iron homeostasis (Stehling et al., 2013).

4.4 Rationale for the project

The aim of this study was to examine the role of human ABCB7 in both cytosolic Fe/S protein biogenesis and the maturation of (extramitochondrial) heme-containing proteins in more detail. The ABC transporter has been suggested to be involved in the export of the so far unknown sulfur-containing compound X-S serving as the substrate for eukaryotic cytosolic and nuclear Fe/S cluster assembly (cf. chapter 4.3.3.2). An additional role in heme export seems unlikely based on early studies in yeast showing a high enzyme activity of overexpressed CAT in cells lacking Atm1, the equivalent of human ABCB7. However, patients with XLSA/A show an anemia with protoporphyrin accumulation (Bekri et al., 2000). Moreover, a recent study found that heme biosynthesis is defective in ABCB7-depleted mammalian cells and suggested that heme could also be a potential ABCB7 substrate (Maio et al., 2019). An impact of cytosolic Fe/S cluster assembly on heme biosynthesis has been implicated by a study of Liu et al. (2020), suggesting that the second cytosolic step of heme biosynthesis by ALAD (cf. Figure 3) requires an Fe/S cluster, suggesting a potential role not only of the mitochondrial ISC (via the [2Fe-2S] protein ferrochelatase) but also of the ISC export and CIA systems in the activity of all cellular heme proteins. It remained unclear from all these studies in human cells, whether or not ABCB7 can transport heme towards the cytosol.

To address the relevance of ABCB7 for heme export and cytosolic Fe/S protein assembly, an ribonucleic acid interference (RNAi)-mediated ABCB7 knockdown was performed in HeLa cells, and mitochondrial and extramitochondrial heme- as well as Fe/S cluster-dependent marker proteins were analyzed. Besides the determination of Fe/S cofactor-dependent protein levels, assays also included the determination of enzyme activities, in particular of mitochondrial and cytosolic aconitase, SDH and COX. In order to assess the mitochondrial heme export, CAT was overexpressed in wild-type and ABCB7-depleted cells, similar to earlier studies in yeast (Kispal et al., 1997). Then, the heme maturation of CAT was analyzed by measuring its enzyme activity. The experimental setup, allowing the transient and rapid depletion of ABCB7 in human cell culture, should be suitable to clarify the primary function of ABCB7 in cytosolic-nuclear Fe/S protein biogenesis and/or heme export.

5. Material and Methods

5.1 Material

5.1.1 General Equipment

Table 1: General Equipment

Equipment Name	Source
12-channel pipettes 10, 200 µL	Brand (Wertheim, Germany)
5424 table centrifuge	Eppendorf (Hamburg, Germany)
5810R table centrifuge, refrigerated	Eppendorf (Hamburg, Germany)
Airflow control fume hood	Vinitex (Coswig, Germany)
Autoclave VX-150	Systec (Linden, Germany)
Automatic sarpette, pipette	Sarstedt (Nümbrecht, Germany)
Avanti J-20XP centrifuge, rotor JE-10	Beckman Coulter (USA)
Axiovert 100 microscope	Carl Zeiss (Oberkochen, Germany)
Biofuge primo centrifuge	Heraeus (Düsseldorf, Germany)
Biological safety cabinet BHA48	Faster S.r.l. (Cornaredo, Italy)
Cellometer Auto T4, cell counter	Nexcelom Biosciences (Lawrence, USA)
Chemostar imager	Intas science imaging (Göttingen, Germany)
Electrophoresis power supply EPS 301	GE Healthcare (Chicago, USA)
Function Line B6 heating oven	Heraeus (Hanau, Germany)
GenePulser Xcell electroporator	Bio-Rad (Hercules, USA)
Innova 4300 incubator shaker	New Brunswick Scientific (Enfield, USA)
Laboport pump	KNF (Trenton, USA)
M200 infinite plate reader	Tecan Group Ltd. (Crailsheim, Germany)
Mini-Protean tetra gel system	Bio-Rad (Hercules, USA)
MR Hei-Standard magnetic stirrer	Heidolph Instruments (Schwabach, Germany)
NanoDrop 2000c spectrophotometer	Thermo Scientific (Waltham, USA)
NuAire Autoflow IR direct heat CO_2 incubator	Integra (Fernwald, Germany)
NuAire Cellgard class II biological safety cabinet	Integra (Fernwald, Germany)
PerfectBlue semi-dry blotting chamber	Peqlab Biotechnology (Erlangen, Germany)
PerfectBlue vertical double gel system	Peqlab Biotechnology (Erlangen, Germany)
Pipetman pipettes 2, 10, 20, 100, 200, 1000 µL	Gilson (Middleton, USA)
Rocker-Shaker PMR-100	Grant-bio (Shepreth, UK)
Roto-Mini Plus rotator	Benchmark Scientific (Sayreville, USA)
Scale SBC 22	Scaltec (Dania, USA)
Scale SI-403	Denver Instrument (Arvada, USA)
SmartSpec Plus spectrophotometer	Bio-Rad (Hercules, USA)
Thermomixer comfort	Eppendorf (Hamburg, Germany)
Vortex Genius 2	Bender & Hobein AG (Ismaning, Germany)

5.1.2 General Consumables

Table 2: General Consumables

Consumable	Source
48-well cell culture plates	Greiner bio-one (Frickenhausen, Germany)
96-well cell culture plates	Greiner bio-one (Frickenhausen, Germany)
Blotting paper	Macherey-Nagel (Düren, Germany)
Bottle-top filters, 250 mL	Sarstedt (Nümbrecht, Germany)
Electroporation cuvettes, 4 mm gap	VWR (Darmstadt, Germany)
Filter tips: 20, 100, 1000 mL	Sarstedt (Nümbrecht, Germany)
Pasteur pipettes, different sizes	Carl Roth (Karlsruhe, Germany)
Petri dishes	Greiner bio-one (Frickenhausen, Germany)
Pipette tips, different sizes	Sarstedt (Nümbrecht, Germany)
Porablot nitrocellulose membrane	Macherey-Nagel (Düren, Germany)
Reaction cups 1.5 mL	Sarstedt (Nümbrecht, Germany)
Reaction cups 1.5 mL, SafeLock	eppendorf (Hamburg, Germany)
Reaction cups 2 mL	Sarstedt (Nümbrecht, Germany)
Reaction cups 2 mL, SafeLock	Eppendorf (Hamburg, Germany)
Reaction cups 5 mL	Sarstedt (Nümbrecht, Germany)
Reaction tubes 15, 50 mL	Sarstedt (Nümbrecht, Germany)
Serological pipettes: 5, 10, 25 mL	Sarstedt (Nümbrecht, Germany)
Sterican needle, different sizes	B. Braun (Melsungen, Germany)
Tissue culture flask for adherent cells, 75 cm^2, sterile	Sarstedt (Nümbrecht, Germany)
UV 96-well plates	Greiner bio-one (Frickenhausen, Germany)

5.2 Methods

5.2.1 Cell biological methods

5.2.1.1 Cell cultivation

Table 3: Cell culture reagents

Reagent	Source
Dulbecco's Modified Eagle Medium (DMEM)	Gibco, ThermoFisher (Waltham, USA)
Fetal bovine serum #FBS-11A	Capricorn Scientific (Ebsdorfergrund, Germany)
GlutaMAX, 100x	Gibco, ThermoFisher (Waltham, USA)
Nuclease-free water	Ambion, Applied Biosystems (Austin, USA)
On-Target plus control siRNA	Dharmacon (Lafayette, USA)
Penicillin/Streptomycin 10,000 U/mL	Gibco, ThermoFisher (Waltham, USA)
Trypsin/Ethylenediaminetetraacetic acid (EDTA)	Sigma Life Science (Darmstadt, Germany)

Table 4: Phosphate buffered saline (PBS) buffer, sterile-filtered

Sodium chloride (NaCl)	137 mM
Potassium chloride (KCl)	2.7 mM
Disodium phosphate (Na_2HPO_4)	7.3 mM
Monopotassium phosphate (KH_2PO_4)	1.5 mM

Cell culture handling was performed under a safety cabinet (Table 1) to maintain a protected environment; all buffers and materials used were sterile. Human epithelial cervix carcinoma (HeLa) cells were cultured in 75 cm^2 tissue culture flasks with filter cap (Table 2) in Dulbecco's Modified Eagle Medium (DMEM) with high glucose (25 mM), supplemented with 1 mM Glutamine, 1% Penicillin/Streptomycin and 7.5% fetal calf serum (FCS, Table 3) at 37°C and 5% CO_2 atmosphere. Usually, cells were maintained using a media volume of 20 mL.

Every three to five days, cell passaging was performed. After removing the cell culture medium, cells were incubated with 4 mL of Trypsin/Ethylenediamineteraacetic acid EDTA solution (Table 3) for 10-12 min at 37°C. By this treatment, extracellular adhesion proteins were cleaved by the protease trypsin. In addition, EDTA supported the detachment of the cells by chelating calcium ions (Ca^{2+}) which are required for cell adhesions. 8 mL of complete DMEM were added to stop the membrane protein degradation and to resuspend the cells. The cells were then subcultured in complete DMEM at a splitting ratio of 1:20 or 1:15. The medium of adherent cultures was changed the day before the harvest to minimize pH changes and to provide a constant nutrient supply. After harvest, the cell suspension was transferred into reaction tubes, centrifuged at 160 x g for 10 min, and the supernatant was discarded. The cell pellet was resuspended and washed in phosphate buffered saline (PBS) buffer (Table 4) to remove residual medium and trypsin/EDTA contaminations.

Cell numbers were quantified using the automatic cell counting device Cellometer Auto T4 (Table 1) according to the manufacturer's instructions. 21 µL of a cell suspension was added to a Neubauer-based cell counting chamber and cell number was determined. The cumulative cell number was determined by extrapolation of a given cell aliquot obtained from a total cell pool and expanded by repeated and quantitated subculturing cycles.

5.2.1.2 Cell transfection

Table 5: Small interfering ribonucleic acids (siRNAs)

siRNA	Origin
ABCB7 #2) SO-2834523G #2 CAACAGCAGUUCUGAUUGG #4) SO-2793724G #4 UAGACUCACUGCUGAAUUA	Dharmacon (Lafayette, USA)
FECH #1) s566 GCAUUUACCAGUGACCAUAtt #2) s567 CGAGUACUCUCAAGUUUUAtt #3) s568 GACACUUCCUAUUCAGAAUtt	Ambion, Applied Biosystems (Austin, USA)
On-Target plus control	Dharmacon (Lafayette, USA)

Table 6: Plasmids

Plasmid	Origin
pd2EYFP	Clontech, Saint-Germain-en-Laye, France
pMCS-ABCB7#sm2,4	Dr. O. Stehling, Marburg, Germany
pVA1	Group H.-P. Elsässer (Marburg, Germany), Biederbick et al., 1999
Sport6-CAT, Clone IRATp970B02136D	BioScience, Nottingham, United Kingdom

```
              541                                                    600
ABCB7(wt)       GCACCAAATACAGTTGCAACCATGGCAACAGCAGTTCTGATTGGCTATGGTGTATCAAGA
siRNA#2         -------------------------caacagcaguucugauugg----------------
ABCB7(sm)       GCACCAAATACAGTTGCAACCATGGCTACTGCTGTACTCATCGGCTATGGTGTATCAAGA

              961                                                   1020
ABCB7(wt)       GAAATGAACAAAGCAGATAATGATGCAGGTAATGCTGCTATAGACTCACTGCTGAATTAT
siRNA#4         ----------------------------------------uagacucacugcugaauua-
ABCB7(sm)       GAAATGAACAAAGCAGATAATGATGCAGGTAATGCTGCTATTGATAGTCTCTTAAACTAT
```

Figure 7: ABCB7 wildtype sequence nucleotides 541-600 and 961-1020 of the open reading frame, sequence of the ABCB7 siRNAs no. #2 and #4 (lowercase letters) and the sequence of the ABCB7 silent mutated plasmid (red: silent mutations).

Table 7: Electroporation buffer, sterile-filtered

HEPES	21 mM
NaCl	137 mM
KCl	5 mM
Na_2HPO_4	0.7 mM
D-Glucose	6 mM

Cell transfection describes the transfer of foreign DNA or RNA into a cell. Since HeLa cells are easy to handle and transfect (Stehling et al., 2009) they present a suitable model system for genetic manipulations followed by biochemical analyses. To introduce siRNA or DNA (Table 5, Table 6) molecules into HeLa cells, they were transfected by electroporation (Chu et al., 1987). For depletion of ABCB7, the cells were transfected with a pool of two different specific siRNAs (Table 5, Figure 7). Co-transfection of a pMCS-ABCB7#sm2,4 plasmid harboring two RNAi-resistant silent mutations (Figure 7) enabled complementation of the ABCB7 knockdown.

For electroporation, cells were harvested by trypsination, washed once with electroporation buffer (Table 7), counted, and suspended in electroporation buffer at a concentration of $6.5x10^6$-$8x10^6$ cells per 250 µL. This cell suspension was mixed with 3-6 µg of DNA plasmids, 3-6 µL of siRNA or a corresponding volume of nuclease-free water (serving as Mock control). After transfer to an electroporation cuvette (4 mm gap, Table 2), an electric pulse was applied using the Bio-Rad GenePulser Xcell device (capacity: 525 µF, voltage: 265 V; Table 1). The pulse time for optimal transfection efficacy and growth rate ranged from 26-28 ms and was frequently achieved by pre-adjusting the actual electroporation volume from around 250 µL. Subsequently, cells were transferred into a sterile 75 cm^2 flask and cultured in 20 mL medium consisting of 75% complete DMEM and 25% conditioned DMEM. Conditioned DMEM was freshly obtained from a confluent standard HeLa cell culture and had been found to support cell regeneration after electroporation (O. Stehling, personal communication). After three days of tissue culture, transfection was repeated to improve the efficiency of plasmid-based complementary DNA (cDNA) expression and/or RNAi-mediated gene silencing. After another three days of tissue culture, re-transfected cells were washed with PBS buffer (Table 4) and either immediately snap-frozen in liquid nitrogen as dry cell pellet or fractionated (see chapter 5.2.1.3) into crude cytosol and pellet fractions prior to quick-freezing. Frozen cell samples were stored at -80°C until use.

5.2.1.3 Cell fractionation

Table 8: DigiBuffer

Tris/HCl	25 mM, pH 7.4
Saccharose	250 mM
$MgCl_2$	1.5 mM
PMSF	1 mM
digitonin	0.008%

Table 9: MitoBuffer

Tris/HCl	25 mM, pH 7.4
Saccharose	250 mM
$MgCl_2$	1.5 mM

In order to analyze mitochondrial and extra-mitochondrial proteins separately, a crude digitonin-based cell fractionation into soluble cytosolic constituents and organelle-containing membrane fractions was performed (Drapier & Hibbs, 1996). In this preparation digitonin served as a chelator of cholesterol and subsequently impaired the barrier function of the plasma membrane which resulted its permeabilization. Organellar membranes such as the inner mitochondrial membrane remained intact due to their low content of cholesterol.

All fractionation steps were carried out on ice to maintain protein integrity. HeLa cells (cf. chapter 5.2.1.1) were resuspended in ice-cold DigiBuffer (Table 8) and incubated for 15 min. One third of the total lysate was removed as a reference sample. The remaining suspension was centrifuged at 13,000 revolutions per min (rpm) and 4°C for 10 min. The supernatant was removed and stored as cytosolic fraction. The membrane pellet was washed once in 1 mL MitoBuffer (Table 9) and subsequently resuspended in MitoBuffer at the same volume as the cytosolic fraction. Total lysate, cytosolic and pellet fractions were snap-frozen in liquid nitrogen and stored at -80°C until further use.

5.2.2 Molecular biology

Sequences and sources of siRNAs for the depletion of ABCB7 and FECH are given in Table 5 and Figure 7. Expression plasmids and their origins are listed in Table 6. In some experiments, ABCB7 deficiency mediated by combined transfection of two siRNAs (#2 and #4) was complemented by application of silently mutated, RNAi-resistant full-length human ABCB7 (pMCS-ABCB7#sm2,4; Table 6, Figure 7) which had been cloned into the backbone of an enhanced green fluorescent protein

(pEGFP)-derived plasmid (Clontech) by replacement of the EGFP sequence. Plasmids were expanded by standard molecular biology techniques as described below.

5.2.2.1 Transformation of competent bacteria

For plasmid propagation, *Escherichia coli (E. coli) DH5α cells* (Invitrogen) with the Genotype: *F Φ80dlacZ∆M15 ∆(lacZYA-argF)U169 recA1 endA1 hsdR17(r_k^- m_k^+) phoA supE44 thi-1 gyrA96 relA1 λ^-* were used.

Briefly, 10 µL of a highly diluted pMCS-ABCB7#sm2,4 plasmid (Table 6) were incubated with 200 µL of competent E. coli (OD_{600} about 7.5) for 30-45 min on ice. The bacterial suspension was shifted to 42°C for 60 sec under vigorous shaking and immediately cooled down for 2 min on ice. Then, 450 µL lysogeny broth (LB) Medium (1% tryptone, 0,5% yeast extract, 1% NaCl; Bertani, 1951) was added to each tube, and the sample was incubated at 37°C for 60 min. The suspension was centrifugated at 3000 x g for 5 min, 450 µL of the supernatant were removed, and the residual volume was used to resuspend the bacteria. The transformation sample was planted into LB culture plates (LB liquid medium, 2% agar agar) containing the antibiotic kanamycin (25 µg/mL kanamycin) and cultured at 37°C overnight. One bacterial colony was picked and expanded in 300 mL LB medium supplemented with 50 µg/mL kanamycin.

5.2.2.2 Plasmid DNA purification (Maxiprep)

An overnight LB liquid culture containing the transformed bacteria was centrifugated at 5000 rpm for 15 min. DNA plasmids were purified by the NucleoBond Xtra Maxi Kit (Macherey-Nagel) according to the manufacturer's instructions. Basically, the bacteria pellet was first resuspended in resuspension buffer. Subsequently, a sodiumdodecyl sulfate (SDS) / sodium hydroxide-containing lysis buffer was added to the suspension, and the mixture was incubated for 15 min at room temperature. The sample was neutralized by a potassium acetate buffer and carefully mixed by repeated inversions of the reaction tube. The lysate was then filtered through a pre-equilibrated ion-exchange column. After the column had been washed, plasmid DNA was eluted with 15 mL elution buffer and precipitated with 10.5 mL isopropanol. Following centrifugation at 15,000 x g for 30 min and 4°C, DNA pellets were washed with 70% ethanol, dried, and dissolved in 300 µL Tris/EDTA (TE) buffer (10 mM Tris/HCl, 1mM EDTA). Plasmid yield was determined using a NanoDrop spectrophotometer (Table 1).

5.2.3 Biochemical methods

5.2.3.1 Protein determination

Protein concentrations in cell suspensions and extracts were determined with the bicinchoninic acid (BCA) protein assay (BCA Assay Kit, Pierce, Waltham, USA), basically according to the manufacturer's instructions. The assay principle is based on the formation of an cupric ion (Cu^{2+}) complex and the subsequent reduction of Cu^{2+} to cuprous ion (Cu^{1+}) under alkaline conditions (cf. Scientific, 2020). The amino acids cysteine, tryptophan and tyrosine convey the reduction of Cu^{2+}. Then, reduced Cu^{1+} and BCA form a purple complex. The colorimetric change of the test solution is directly proportional to the protein level in the sample and was followed at 562 nanometer (nm). The comparison to a calibration curve with bovine serum albumin (BSA) allowed quantification of the protein content.

In order to determine the protein content of a given cell suspension, aliquots of up to 15 µL and BSA standard samples (1 to 30 µg) were applied to a flat-bottom 96-well plate and diluted with ultrapure H_2O (ddH_2O) to a total of 55 µL. After hypotonic cell lysis overnight at 4°C, 235 µL of a BCA working solution was added to each cell suspension or BSA sample. The absorption was repeatedly measured after 30, 60 and 90 min of incubation at 37°C using an M200 infinite plate reader (Table 1). Into each measurement blank samples were included, and corresponding blank values were subtracted from the OD of each sample at each time point. Protein concentrations of the cell samples were calculated from the colorimetric changes in the BSA standard samples.

5.2.3.2 Sodiumdodecylsulfate polyacrylamide gel electrophoresis (SDS-PAGE)

Table 10: Sample buffer

0.6 M Tris, pH 6.8	60 mM
Glycerol	10 %
SDS	2 %
Bromophenol blue	0.05 ‰
β-mercaptoethanol	5 %

Table 11: Gradient gel components

	Stacking gel	**Upper separating gel**	**Lower gel separating gel**	**Sealing gel**
Polyacrylamide*	4 %	6 or 10 %	14 or 20 %	15 %
Tris/HCl	84 mM, pH 6.8	372 mM, pH 8.8	372 mM, pH 8.8	558 mM, pH 8.8
SDS	0.1 %	0.1 %	0.1 %	-
Sucrose	-	-	392 mM	-
TEMED	0.1 %	0.05 %	0.05 %	0.4 %
APS	0.08 %	0.03 %	0.03 %	0.08 %
Bromophenol blue	for coloring	for coloring	for coloring	for coloring

*acrylamide : bisacrylamide 37.5:1

Table 12: SDS-PAGE running buffer

Tris	25 mM
SDS	0.1 %
Glycine	192 mM

Table 13: Tricine gel components

	Stacking gel	**Separating gel**
Polyacrylamide*	4 %	16 %
Glycerol	-	7.5 % (w/v)
3x gel buffer	6.7 %	8.3 %
TEMED	0.07 %	0.03 %
APS	0.04 %	0.03 %

* acrylamide : bisacrylamide 32:1

Separation of proteins according to their molecular weight was performed by sodiumdodecylsulfate polyacrylamide gel electrophoresis (SDS-PAGE) or tricine gel electrophoresis. Depending on the size of the proteins to be separated, different gels were chosen, or the acrylamide concentration was adjusted, with high-percentage or tricine gels better suited for separating small proteins and low-percentage gels suited for separating large proteins. For this study, the method according to Laemmli, 1970 was used and samples were prepared using the sample buffer provided in Table 10. Polymerization of the matrix was started by a decay of ammonium persulfate (APS) and the produced radical from this reaction reacted with tetramethylethylenediamine (TEMED) and initiated crosslinking.

Gradient gels (6-20% or 10-14% polyacrylamide) were casted in PerfectBlue dual gel systems (16 cm x 14 cm; Peqlab) according to Table 11. The composition of the

running buffer is provided in Table 12 (Stehling et al., 2018). Samples containing 20-40 µg protein as well as molecular weight markers (prestained protein ladder 11-170 kDa, low molecular weight ladder 6.5-97 kDa) were loaded per lane, and electrophoresis was performed at a maximum voltage of 240V and a constant current of 30 mA, which was increased to 50 mA after samples had entered the separating gel. Mini tricine gels were prepared using a Mini-Protean tetra gel system (6,8 cm x 8,6 cm; Bio-Rad) according to Table 13 (Schägger, 2006). Samples were prepared with tricine gel buffer (Tris/HCl 3 M, pH 8.45, SDS 0.3 %). 10-20 µg protein as well as molecular weight markers were loaded per lane, and electrophoresis was performed using cathode buffer (Tris 1M, Tricine 1M, SDS 1%) and anode buffer (Tris/HCl 1 M, pH 8.9) at a constant voltage of 60V which was increased to 100V after the samples had entered the separating gel.

5.2.3.3 Western blotting

Table 14: Transfer buffer

Tris	25 mM
Ethanol	20%
SDS	0.02%
Glycine	200 mM

Table 15: Membrane blocking buffer

Tris/HCl	50 mM, pH 7.5
NaCl	0.9%
Tween 20	0.1%
RotiBlock (Blocking reagent)	10%
Sodium azide	0.1%
Bovine serum albumin	1%

Proteins separated during SDS-PAGE were transferred from the polyacrylamide gel to a nitrocellulose membrane via semi-dry western blotting (Kyhse-Andersen, 1984). The composition of the transfer buffer used is provided in Table 14. After the transfer, the membrane was washed with H_2O and stained with a Ponceau staining solution (Ponceau S 0.2%, Trichloroacetic acid 0.3%) for 10 min. After washing with ddH_2O and TBST buffer (Tris/HCl 50 mM, pH 7.5, NaCl 0.9%, Tween 20 0.1%), the membrane was blocked 120 min to prevent non-specific antibody-binding during subsequent immunodetection. The composition of the blocking buffer is provided in Table 15.

5.2.3.4 Immunodetection of blotted antigens

Table 16: Primary antibodies

Antigen	Working dilution	Observed molecular weight (kDa)	Host	Source
ABCB7	2000	67	Rabbit	St. John's Laboratory (London, UK)
ACO2	2500	84	Rabbit	Invitrogen (Carlsbad, USA)
ACTB (β-Actin)	1000	44	Mouse	Santa Cruz Biotechnology (Santa Cruz, USA)
ATP5F1A/B (F1 a/b)	5000	50	Rabbit	Hermann Schägger (Frankfurt, Germany)
CAT	500	60	Mouse	Santa Cruz Biotechnology (Santa Cruz, USA)
COX6A/B	5000	10	Rabbit	Hermann Schägger, Frankfurt, Germany)
DPYD	175	111	Rabbit	Santa Cruz Biotechnology (Santa Cruz, USA)
FECH	1500	44	Rabbit	Harry Daily (Georgia, USA)
GAPDH	10000	36	Mouse	MerckMillipore
GPAT	5000	56	Rabbit	Helene Puccio (Illkirch, France)
HFT (Ferritin)	1000	22	Mouse	Santa Cruz Biotechnology (Santa Cruz, USA)
IRP1 (ACO1)	3000	98	Mouse	Richard Eisenstein (Wisconsin, USA)
IRP2	375 (ABC*)	105	Mouse	Santa Cruz Biotechnology (Santa Cruz, USA)
MT-CO2 (COX2)	2500	21	Rabbit	Hermann Schägger (Frankfurt, Germany)
NDUFA13 (Grim19)	2000	15	Mouse	Santa Cruz Biotechnology (Santa Cruz, USA)
NDUFB4	666 (ABC*)	14	Mouse	Abcam (Cambridge, UK)
NDUFS8	1000	23	Mouse	Santa Cruz Biotechnology (Santa Cruz, USA)
NDUFV2	1000	24	Mouse	Santa Cruz Biotechnology (Santa Cruz, USA)
Porin (VDAC1)	1500	34	Rabbit	Protein Tech Group
SDHB	1000	29	Mouse	Santa Cruz Biotechnology (Santa Cruz, USA)
TFR1	1000	90	Mouse	Invitrogen (Carlsbad, USA)
UQCRC2 (C III Core II)	5000	45	Rabbit	Hermann Schägger (Frankfurt, Germany)

UQCRFS1 (Rieske)	2500	23	Rabbit	Hermann Schägger (Frankfurt, Germany)

*Avidin-Biotin-Complex enhancement system

Table 17: Secondary antibodies

Antigen	**Working dilution**	**Host**	**Source**
α-mouse IgG HRP conjugate	2500	Goat	Bio-Rad (Feldkirchen, Germany)
α-rabbit IgG HRP conjugate	7500	Goat	Bio-Rad (Feldkirchen, Germany)
α-mouse biotinylated IgG conjugate	2500	Goat	Vectastain (Newark, USA)

* Horseradish peroxidase

Table 18: Enhanced chemiluminescence (ECL) solution 1

Tris/HCl	100 mM, pH 8.5
Luminol (from a DMSO stock)	2.5 mM in DMSO
p-coumaric acid (from a DMSO stock)	0.4 mM in DMSO

Table 19: Enhanced chemiluminescence (ECL) solution 2

Tris/HCl	100 mM, pH 8.5
H_2O_2	0.018% (v/v)

Table 20: TBST-based buffer for the dilution of primary antibodies

TBST buffer (Tris/HCl, NaCl, Tween 20)	Tris/HCl 50 mM, pH 7.5; NaCl 0.9%; Tween 20 0.1%
RotiBlock (Blocking reagent)	3%
Sodium azide*	0.1%
Bovine serum albumin	0.1%

*microbizide

Table 21: Buffer for the dilution of secondary antibodies

Tris/HCl	50 mM, pH 7.5
NaCl	0.9%
Tween 20	0.1%
Thiomersal*	0.02%
Bovine serum albumine	0.1%

*microbizide

Cellular proteins of interest blotted onto nitrocellulose membranes were detected by specific primary antibodies (Table 16) which were in turn labeled by a secondary

antibody conjugated to horseradish peroxidase (HRP, Table 17). Upon application of a 1:1 mixture of ECL solutions 1 and 2 (Table 18, Table 19) the HRP catalyzed the oxidation of luminol, and the light emitted by this reaction was detected by a digital camera.

In brief, dried nitrocellulose membranes were re-moistened by TBST buffer for several min and incubated in working solutions of primary antibodies (Table 20) for 90-120 min at room temperature in rotating hybridization tubes. Subsequent washing with TBST for three times removed residual traces of primary antibodies. Then, working solutions of the peroxidase-coupled secondary antibodies (Table 17, Table 21) were applied and membranes were incubated for 60 min at room temperature under moderate shaking. In cases of IRP2 and NDUFB4 the labeling was intensified by a biotin-based signal amplification approach (Vectastain Elite ABC-HRP Kit; Vector Laboratories, Newark, USA). Primary antibodies were bound by biotinylated secondary antibodies which in turn recruited multiple complexes consisting of avidin and biotinylated HRP. After each labeling step membranes were washed with TBST to remove secondary or tertiary reagents and were then subjected to chemiluminescence detection.

5.2.3.5 Enzyme activity analyses

Activities of enzymes in total cell lysates or crude fractions were measured spectrophotometrically in multi-well plates as triplicates at a temperature of 32.5° C, using a Tecan M200 infinite plate reader device (Table 1). Changes in the optical densities of reaction mixtures were in most cases recorded continuously, and linear regressions were calculated from the extinction values over time. Enzyme activities were calculated considering $E = \varepsilon * c * d$ (E - extinction, ε - molar extinction constant, c - solution concentration, d - length of sample; Mayerhöfer et al., 2020). The lightpath length was calculated from the total liquid volume applied to a particular well and its diameter. The specific activity of an enzyme present in a sample was determined from the protein amount applied to an individual well and the corresponding total activity measured. In order to prevent enzyme decay, samples and multi-well plates were kept on ice until addition of room-temperature reaction buffers.

5.2.3.5.1 Catalase (CAT) activity assay

Table 22: Ferrous oxidation (FOX) reagent

$(NH_4)_2Fe(SO_4)_2$	250 µM
Xylenol orange	100 µM
Sorbitol	0.1 M
H_2SO_4	25 mM

Catalase activity was determined according to Jiang et al., 1990 and Ou & Wolff, 1996. In this assay, ferrous ion (Fe^{2+}) is oxidized by hydrogen peroxide in dilute H_2SO_4, and ferric ions (Fe^{3+}) were detected upon complex formation with the dye xylenol orange at a wavelength of 585 nm.

In brief, cell lysates from digitonin-based cell fractionation were subjected to three freeze-thaw cycles to release catalase as efficient as possible and were further diluted with PBS buffer to a total volume of 200 µL. The diluted samples of 200 µL corresponding to 4-16 µg of total protein were loaded into wells of a 96-well-plate, and 20 µL of a 2.2 mM hydrogen peroxide stock was added to the 200 µL samples to start its CAT-mediated decay to H_2O and O_2. In 2-min intervals sample aliquots of 10 µL size were removed and mixed with 190 µL FOX reagent (Table 22) to stop the reaction and to assess the amount of residual H_2O_2 by the oxidation of Fe^{2+}. Formation of the colored Fe^{3+}-xylenol orange complex was allowed for 30 min at room temperature before the absorption was spectroscopically determined at 585 nm. To assess non-specific, CAT-independent formation of the Fe^{3+}-xylenol orange complex, CAT was inhibited in reference samples by addition of 3.3 mM hydroxylamine. For calculation of the CAT activities, the difference between total and nonspecific Fe^{3+}-xylenol orange complex formation was determined. The molar extinction coefficient for the Fe^{3+}-xylenol orange complex is ε_{585nm}= 2.35 x 10^5 M^{-1}* cm^{-1}.

5.2.3.5.2 Aconitase (ACO) activity assay

Table 23: ACO activity assay buffer

Triethanolamine	100 mM, pH 8.0
$MgCl_2$	1.5 mM
Triton X-100	0.1%

Table 24: ACO activity assay substrates

$NADP^+$	1.25 mM
Cis-aconitate	300 µM
Isocitrate dehydrogenase	40 mU/µL

The activities of cytosolic aconitase (cACO) and mitochondrial aconitase (mACO) were separately determined in the cytosolic and mitochondria-containing cell fractions, respectively, using a coupled aconitase-isocitrate-dehydrogenase assay (Drapier & Hibbs, 1996; Hausladen & Fridovich, 1996). This assay was based on the ACO-dependent production of isocitrate from cis-aconitate, the oxidative decarboxylation of isocitrate to α-ketoglutarate and the coupled reduction of oxidized nicotinamide adenine dinucleotide phosphate ($NADP^+$) to NADPH. The formation of NADPH was spectrophotometrically followed at its absorption maximum of 340 nm.

In brief, two identical cell samples were examined in parallel in a 96 well UV-plate, with protein amounts ranging from 3-20 µg. 250 µL ACO activity assay buffer (Table 23) was supplemented with respective substrates (Table 24) and added to one of the two cell samples. The second sample served as reference to determine the unspecific reduction of $NADP^+$, and the corresponding assay buffer was thus lacking both cis-aconitate and isocitrate dehydrogenase. After adding buffer and substrates, extinctions at 340 nm were measured every 20-30 sec for 60 min. The molar extinction coefficient of NADPH is ε_{340nm}= 6.22 mM^{-1}* cm^{-1}. For calculation of the actual ACO activities the difference between total and non-specific NADPH formation was determined.

5.2.3.5.3 Succinate dehydrogenase (SDH) activity assay

Table 25: SDH activity assay buffer

Tris/SO_4	50 mM, pH 7.4
EDTA	0.1 mM
Dichlorophenol-indophenol (DCPIP)	70 µM
Triton X-100	0.1%

Table 26: SDH activity assay substrates

Decylubiquinone	50 µM
Sodium succinate	0.2%
Sodium malonate	0.2%

SDH activity was determined in mitochondria-containing membrane fractions (cf. chapter 5.2.1.3), basically according to Hatefi & Stiggall, 1978; Robinson et al., 1991

with minor variations. During the oxidation of succinate to fumarate electrons were transferred to the blue reporter dye 2,6-dichloro-N-(4-hydroxyphenyl)-1,4-benzoquinoneiminedichlorophenol-indophenol (DCPIP) via decylubiquinone as an electron carrier. Reduction of DCPIP resulted in a color change from blue to pale and was followed spectrophotometrically at a wavelength of 600 nm.

For the activity measurements equal sample amounts corresponding to 4-10 µg protein were loaded into two wells of a 96-well-plate. 250 µL of SDH activity buffer (Table 25) was supplemented with the substrates (Table 26) and added to one of the two samples. The other sample served as reference to determine the non-specific reduction of DCPIP in the assay mixture. In this case the corresponding assay buffer was additionally supplemented with malonate, a specific inhibitor of SDH, and DCPIP reduction in this sample was entirely SDH-independent. After adding buffer and substrates, extinctions at 600 nm were measured every 15-20 sec for 30 min at 600 nm. The molar extinction coefficient for DCPIP is ε_{600nm}= 21 mM^{-1}* cm^{-1}. For determination of the specific SDH activities, the difference between total and nonspecific DCPIP bleaching was calculated.

5.2.3.5.4 Cytochrome *c* Oxidase (COX) activity assay

Table 27: COX activity assay buffer

2-(N-morpholino)ethanesulfonic acid (MES)	50 mM, pH 6.6
NaCl	50 mM
Bovine serum albumin	1%
Dodecylmaltoside (DDM)	0.5 mM (~ 0.025 %)
Cytochrome *c* (II)	100 µM

COX activity can be examined in mitochondria-containing membrane fractions via oxidation of cytochrome *c* (Birch-Machin & Turnbull, 2001; Trounce et al., 1996) which is associated by a color change from reddish to brownish and detectable at a wavelength of 550 nm.

Briefly, triplicate samples equivalent to less than 4 µg protein were applied to wells of a 96-well-plate. To start the reaction, 250 µL of COX activity assay buffer (Table 27) containing 100 µM cytochrome *c* (II) was added to each well. Three blank wells filled with COX activity assay buffer only served as reference to determine the COX-independent cytochrome *c* oxidation by ambient oxygen. Samples were measured every 10-15 sec for 20 min at 550 nm. The molar extinction coefficient for reduced

cytochrome *c* was ε_{550nm}= 19.1 mM^{-1}* cm^{-1}. The difference between total and nonspecific color change was calculated to determine the specific COX activity.

5.2.3.5.5 Citrate synthase (CS) activity assay

Table 28: CS activity assay buffer

Tris/HCl	50 mM, pH 8.0
NaCl	100 mM
5.5'-Dithio-bis-(2-nitrobenzoic acid) (DTNB, solved in DMSO)	0.5 mM
Triton X-100	0.1%

Table 29: CS activity assay substrates

Acetyl-CoA	125 µg/mL
Oxaloacetate	200 µg/mL

A mitochondrial matrix enzyme participating in the TCA cycle like ACO and SDH but not carrying any cofactor is citrate synthase (CS) which catalyzes the condensation of acetyl-coenzyme A (CoA) with oxaloacetate to form citrate. Since CS was not observed to react to changes in mitochondrial Fe/S cofactor synthesis it served as reporter for mitochondrial integrity (Stehling et al., 2009). The activity of CS was determined basically according to Srere, 1963. In this assay the condensation of acetyl-CoA with oxaloacetate into CoA and citrate results in the conversion of the almost colorless compound 5.5'-Dithio-bis-(2-nitrobenzoic acid) (DTNM) into the yellow dye 2-nitro-5-thiobenzoic acid (TNB) and the mixed thiol TNB-CoA. The activity of CS could thus be analyzed by the color change of the reaction mixture and was followed spectrophotometrically at the absorption maximum of TNB at 412 nm.

For the activity measurements equal amounts of HeLa cell fractions corresponding to 0.3-6 µg of total protein were loaded into two wells of 96-well-plates. 250 µL of CS activity buffer and substrates (Table 28, Table 29) were added to one of the two duplicates to determine total DTNB hydrolysis. The other sample served as reference to determine the non-specific, CS-independent cleavage of DTNB in the assay mixture and received a reaction buffer lacking the CS co-substrate oxaloacetate. Extinction of samples was measured every 20-30 sec for 30 min at 412 nm. The molar extinction coefficient for the DTNB hydrolysis product TNB is ε_{412nm}= 13.3 mM^{-1}* cm^{-1}. For calculation of the CS activities, the difference between total and nonspecific DTNB hydrolysis was determined.

5.2.3.5.6 Lactate Dehydrogenase (LDH) activity assay

Table 30: LDH activity assay buffer

Tris/HCl	50 mM, pH 7.4
EDTA	1 mM
Triton X-100	0.1%

Table 31: LDH activity assay substrates

Sodium pyruvate	750 µM
NADH	150 µg/mL

As a cytosolic reference enzyme lactate dehydrogenase (LDH) was used, which interconverts pyruvate and lactate with concomitant interconversion of NADH and NAD^+. LDH does not contain a cofactor and was not observed to react to changes in Fe/S and heme cofactor synthesis (Navarro-Sastre et al., 2011; Stehling et al., 2014). LDH enzymatic activity was measured in multi-well plates as published (Stehling et al., 2008).

Briefly, triplicate samples obtained from digitonin-based cell fractionation ranging from 0.25-7.5 µg of protein were transferred into 48-well-plates and supplemented with 750 µL of LDH activity assay buffer (Table 30) containing the LDH substrates (Table 31). To monitor non-specific LDH-independent oxidation of NADH, blank samples lacking cell material were also included. Samples was measured every 20-25 sec for 45 min at 340 nm. The extinction coefficient of NAD^+ is ε_{340nm}= 6.22 mM^{-1}* cm^{-1}. For determination of LDH activity, the difference between total and nonspecific NADH oxidation was calculated.

6. Results

6.1 Overexpression of catalase is a tool for the analysis of mitochondrial heme export in HeLa cells

The final step of heme biosynthesis is the insertion of Fe^{2+} into protoporphyrin IX, catalyzed by the IMM enzyme ferrochelatase (FECH) which is facing the mitochondrial matrix (Ajioka et al., 2006). FECH activity as well as heme export out of mitochondria are essential for the function of heme-dependent proteins including catalase (CAT), which binds heme in the cytosol and is then translocated to peroxisomes (Zeida et al., 2019). In these organelles, CAT is a key enzyme for the detoxification of hydrogen peroxide (H_2O_2) by catalyzing its conversion of H_2O_2 to water and oxygen (Walton et al., 2017).

Taking advantage of CAT's extramitochondrial localization, the enzyme was used as a reporter protein to analyze the involvement of ABCB7 in the mitochondrial export of heme to the cytosol. In an initial experiment to set up the assay, RNAi-mediated knockdown of FECH was performed in HeLa cells to assess the effects of a general heme deficiency on CAT maturation and activity. Different amounts of a FECH siRNA pool were transfected into HeLa cells by electroporation in order to determine the most efficient siRNA amount for FECH depletion without substantial loss of cell viability. Transfections were carried out twice at a three-day interval using either 0.84 µM, 1.32 µM or 1.8 µM FECH siRNA. For comparison, a control cell sample remained without siRNA (Mock). Because the endogenous activity of the heme enzyme CAT was low in HeLa cells, a CAT-encoding reporter plasmid was included during the second round of transfection in a second control cell sample (Mock/CAT). After a total of six days of FECH depletion, cells were harvested and processed for analyses by SDS-PAGE and immunoblotting (Figure 8a), or by CAT activity measurements (Figure 8b).

Immunoblotting revealed that FECH was efficiently depleted by RNAi, regardless of the transfected siRNA amount (Figure 8a, lanes 3-5). Endogenous CAT was hardly detectable in the Mock control sample (Figure 8a, lane 1), but plasmid-encoded CAT was well expressed (Figure 8a, lanes 2-5) and did not impair FECH immunoblotting signals (Figure 8a, lane 1, 2). Vice versa, transfection of FECH-directed siRNA did not impair steady-state levels of plasmid-expressed CAT (Figure 8a, lanes 3-5), an important prerequisite for the subsequent comparison of CAT activity in the various samples. CAT overproduction and FECH depletion provided the framework to establish an enzymatic assay for the determination of CAT activity, based on the determination

of H_2O_2 turnover (cf. chapter 5.2.3.5.1). In line with the immunoblot analyses, endogenous CAT activity was hardly detectable, but upon plasmid-based overexpression, H_2O_2-decomposing activity was well measurable (Figure 8b, column 2). Importantly, CAT activity severely decreased upon FECH depletion (Figure 8b, columns 3-5) to almost background levels of the CAT-lacking Mock sample (Figure 8b, column 1). In agreement with the immunoblot results above, each of the tested FECH siRNA concentrations was similarly effective in decreasing CAT activity, demonstrating that mitochondrial heme formation and export are essential for heme maturation of CAT.

In order to determine effects of FECH knockdown on hemoproteins other than CAT, maturation of respiratory chain complex III (C III) electron transfer protein cytochrome c_1 (CYC1) was assessed, since also CYC1 contains a heme cofactor. CYC1 is synthesized and processed in several steps (Steiner et al., 1995). Firstly, a precursor with a two-part signal sequence is synthesized. The precursor is then transferred to the matrix via the OMM and IMM. In the matrix, the first part of the signal sequence is removed. The remaining peptide is reexported into the intermembrane space where heme is attached. Then, the remaining presequence is removed. Being a subunit of the cytochrome bc_1 complex, CYC1 is essential for the electron transfer from the Rieske Fe/S protein to cytochrome *c* (Pérez-Mejías et al., 2020). CYC1's heme maturation is required for this function. Immunoblotting revealed that at high siRNA concentrations depletion of FECH was associated with decreased CYC1 levels, suggesting impaired CYC1 processing and stability due to disturbed heme formation (Figure 8a, lane 5 vs. lane 2). In contrast, lower FECH siRNA concentrations did not impair CYC1 immunoblot signals, indicating the requirement of profound FECH deficiency to elicit alterations in CYC1 steady-state protein levels (Figure 8a, lanes 2-4). Of note, the CYC1 immunoblotting signal slightly decreased upon overexpression of CAT (Figure 8a, lane 2 vs. lane 1) indicating a re-distribution of the available heme pool to respective target proteins.

Heme cofactors also contribute to electron transfer in cytochrome *c* oxidase (COX), the fourth complex (C IV) of the mitochondrial respiratory chain. Assembly of COX is critically reliant on the heme-dependent folding and stability of subunit COX1 (Kim et al., 2012), and COX integrity can be monitored by immunoblotting against the subunits COX2 and COX6A/B (Sheftel et al., 2012; Torraco et al., 2018). Steady-state levels of these two proteins were decreased when FECH was depleted by RNAi, indicating a destabilization of COX when heme formation is impaired (Figure 8a, lane 5).

Overproduction of CAT also affected COX2 levels, suggesting lowered availability of heme for COX maturation (Figure 8a, lane 1 and lanes 2-4).

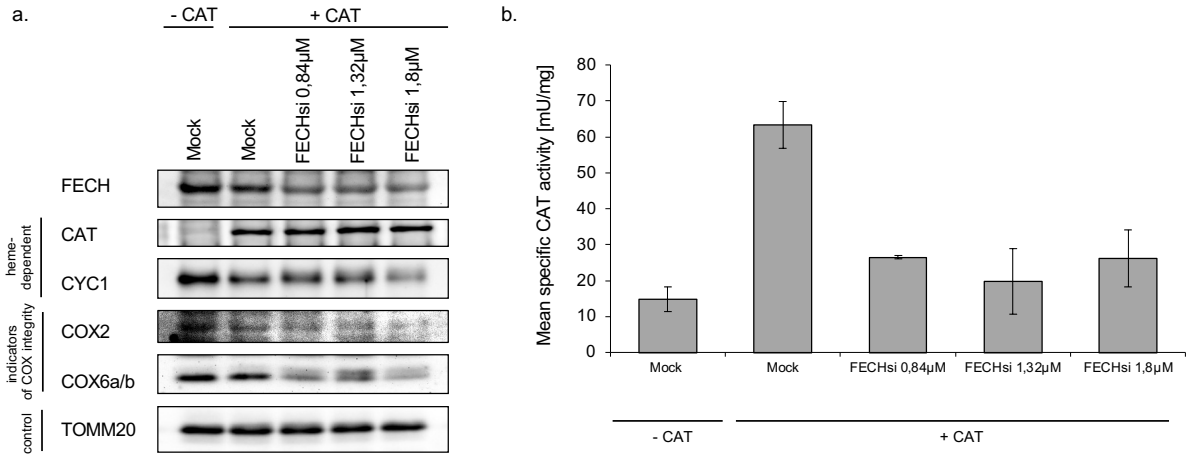

Figure 8: Steady-state protein levels and catalase activity upon depletion of FECH.

HeLa cells were transfected with three different amounts of FECH siRNA as shown or received no siRNA (Mock). Additionally, cells were transfected with a CAT-encoding plasmid or received no plasmid (-CAT/+CAT). After a total depletion time of 6 days cells were harvested and subjected to subsequent analyses. **a.** Cellular steady-state levels of indicated heme-dependent and reference proteins were determined by immunoblotting. Note that the highest FECH siRNA concentration impaired the levels of the heme-dependent mitochondrial proteins CYC1, which is part of complex III of the respiratory chain as well as COX2 and COX6A/B, which served as indicators for the structural integrity of the heme-containing respiratory chain complex IV (COX IV). TOMM20 served as a control. **b.** Specific CAT enzyme activity was determined in triplicates (Mean +/- SD). Catalase activity was substantially increased upon plasmid-based CAT overexpression, which was decreased again in the presence of FECH siRNA.

In contrast to the complex III and IV subunits above, the mitochondrial outer membrane protein TOMM20 did not exhibit changes in steady-state protein levels upon FECH siRNA application or CAT overproduction, indicating the absence of general mitochondrial effects upon siRNA or plasmid transfection. These results revealed TOMM20 as a suitable reference protein for immunoblotting.

Taken together, plasmid-based expression allowed effective and functional overproduction of CAT protein in HeLa cells. Concomitant knockdown of FECH impaired heme maturation not only of mitochondrial proteins but also of CAT, demonstrating that ectopic CAT expression is a suitable approach to study the mitochondrial export of heme via heme maturation of a cytosolic protein.

6.2 HeLa cells depleted for FECH or ABCB7 are growth-retarded

Though the final steps of heme synthesis within mitochondria are well characterized, the mechanistic link to the maturation of extramitochondrial heme proteins is still ill-defined because it is unclear how heme is transported to the cytosol. A potential mitochondrial heme exporter function has been proposed for ABCB7 (Maio et al., 2019), an ATP-binding cassette transporter at the IMM which is implicated in the mitochondrial export of an ill-defined substrate for the cytosolic iron-sulfur assembly (CIA) machinery to mature both cytosolic and nuclear Fe/S proteins (Lill & Freibert, 2020). To address the export function(s) of ABCB7 in the present study, an RNAi depletion system for ABCB7 was established, similar to the FECH knockdown set-up described above. The two depletion approaches were applied in combination with CAT overproduction and allowed the comparison of the requirement of ABCB7 and/or FECH for the maturation of mitochondrial and extramitochondrial heme proteins.

Alike in the initial FECH depletion approach above, HeLa cells were transfected twice at a three-day interval, this time with either no-targeting control siRNA (NoT) in order to monitor non-specific RNAi effects, with pools of ABCB7 or FECH siRNA, or without siRNA (Mock). Three days after the first transfection, cells additionally received the CAT-encoding plasmid (+CAT) except for an additional reference sample which received neither siRNA nor plasmid (Mock -CAT). After a total of six days of RNAi treatment, cells were harvested, counted, and processed for subsequent analyses. For CAT activity measurements cells were treated with digitonin to facilitate membrane permeabilization and enzyme accessibility (cf. chapter 5.2.1.3). Subsequently, permeabilized cells were subjected to a crude separation of soluble cytosolic constituents from insoluble organellar and membranous components by centrifugation (Drapier & Hibbs, 1996). The quality of this cell fractionation approach was assessed by the determination of specific activities of the cytosolic and mitochondrial marker enzymes lactate dehydrogenase (LDH) and citrate synthase (CS), respectively, in each cellular fraction (Figure 9) as described in chapter 5.2.3.5.

The specific LDH activities among the respective lysate, cytosolic and organellar fractions were comparable, indicating that neither CAT overexpression nor ABCB7 or FECH depletion affected the LDH marker enzyme (Figure 9a). The specific cytosolic LDH activity was approximately two-fold higher when compared to LDH of the total lysate since the protein concentration of the cytosolic fraction amounted to only about one half of the lysate concentration, yet the cytosol contained nearly the entire LDH

activity. The remaining LDH activity in the organellar fraction was approx. 10% at most when compared to the total lysate, corroborating LDH as a prototypical and reliable cytosolic marker enzyme. The low LDH activity in the organellar fraction also revealed an only minor contamination by cytosolic constituents.

CS activity was almost exclusively detectable in the organellar cell fractions. The residual CS activity in the cytosolic fraction amounted to approx. 1% of the respective activity in the total lysate (Figure 9b). This result assured that cytosolic enzyme activities could be measured without a major mitochondrial protein contamination. The CS activities in the Mock, Mock/CAT, NoT/CAT, and ABCB7-depleted samples were comparable, indicating that neither CAT overproduction nor ABCB7 knockdown exerted effects on CS. In contrast, CS activity was slightly decreased in FECH-deficient HeLa cells (Figure 9b, column 5), suggesting the occurrence of a general mitochondrial defect as an indirect consequence of impaired heme formation.

Taken together, digitonin-based cell fractionation allowed an efficient separation of mitochondrial and cytosolic constituents for subsequent enzymatic analyses. Measurement of marker enzymes indicated that LDH activity was mainly detectable in the cytosolic fraction whereas CS activity was almost exclusively present in the mitochondria-containing organellar fraction.

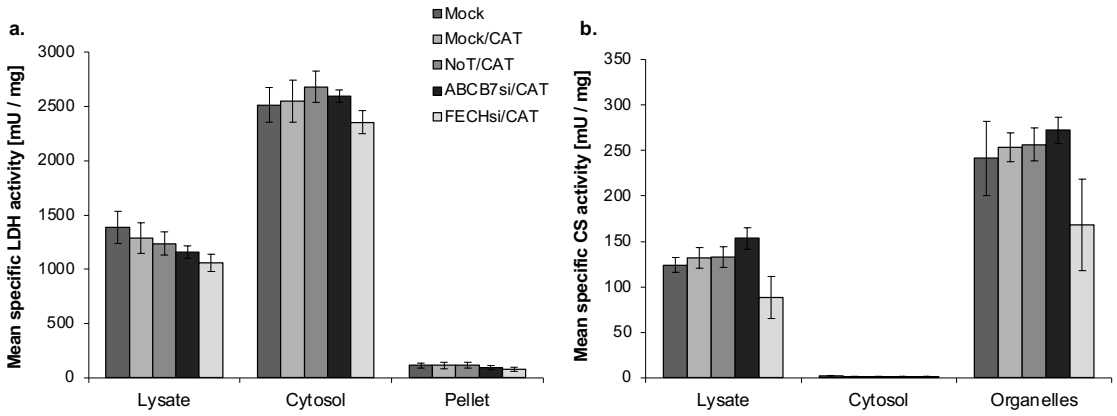

Figure 9: Fractionation efficacy upon depletion of ABCB7 or FECH in CAT-overexpressing cells.

HeLa cells were transfected and processed as described in the text. Cytosolic and organellar fractions were subjected to enzymatic activity assays. Efficient digitonin-based cell fractionation was confirmed by enzymatic activity analyses of LDH (a) and CS (b) as reference enzymes for the cytosolic and organellar fraction, respectively (Mean +/- SD). Note that CS activity was mildly impaired upon FECH depletion.

Immunoblotting of cytosolic and organellar fractions revealed that ABCB7 and FECH protein levels were substantially diminished upon siRNA treatment (Figure 10a, lanes 4, 5), and were not altered upon transfection of the CAT plasmid (Figure 10a, lane 2). Vice versa, immunoblot signals of plasmid-expressed CAT were uniform, indicating that neither ABCB7 nor FECH deficiency affected CAT overproduction (Figure 10a, lanes 2-5). As shown above, immunoblot signals for endogenous CAT were not detectable (Mock -CAT) (Figure 10a, lane 1). Endogenous levels of VDAC1, a protein of the mitochondrial outer membrane, and of cytosolic actin were neither altered upon ABCB7 or FECH knockdown nor responding to the transfection of the CAT plasmid.

In order to assess in how far ectopic CAT expression might cause general adverse effects, cell growth was evaluated. Within the six days of tissue culture, growth analyses of the reference samples Mock (-CAT), Mock/CAT and NoT/CAT showed typical and comparable proliferation patterns which were independent of CAT plasmid transfection, suggesting that CAT protein overproduction did not exert detrimental effects on cell viability as measured by cell number (Figure 10b). In contrast, depletion of ABCB7 or FECH led to a decrease of cell growth by approx. 50% compared to control samples (Mock, Mock/CAT, NoT/CAT), indicative of an essential requirement of both ABCB7 and FECH for cell proliferation.

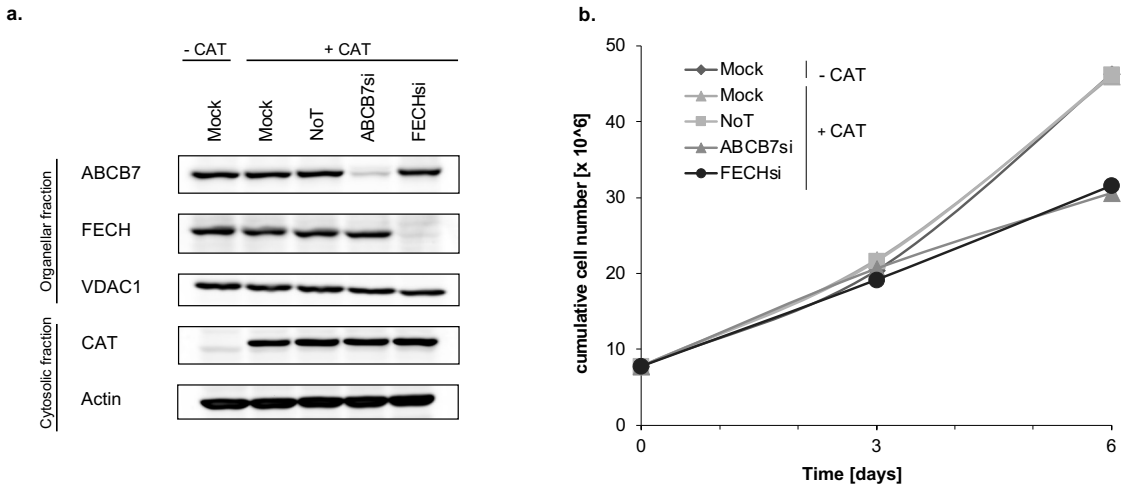

Figure 10: Steady-state protein levels and cell growth of HeLa cells upon depletion of ABCB7, FECH and overexpression of CAT.

HeLa cells were transfected twice at a three-day interval with control siRNA (NoT), ABCB7 siRNA, FECH siRNA or received no siRNA (Mock). After depletion for 3 days, cells were additionally transfected with or without a catalase-encoding plasmid (-CAT/+CAT). After a total of 6 days of growth, cells were harvested, lysed by digitonin, and total lysate, cytosolic and organellar fractions were collected. Cytosolic and organellar fractions were subjected to SDS-PAGE and immunoblotting. **a**. Mitochondrial and cytosolic proteins were immunostained in the respective cellular fractions as shown. VDAC1 and actin served as mitochondrial and cytosolic controls, respectively. Representative blots are shown. **b**. Cell growth was measured by cell counting and is displayed in a cumulative mode (n=4). Growth was impaired upon ABCB7 and FECH depletion in the second growth period.

Taken together, CAT plasmid transfection into HeLa cells did not exert severe detrimental effects as indicated by normal cell proliferation. In contrast, loss of both ABCB7 or FECH decreased cell growth substantially, in line with their critical function in the synthesis of essential iron-containing cofactors.

6.3 Catalase activity is not dependent on ABCB7

In order to test how far the growth phenotype of ABCB7-depleted cells (chapter 6.2) correlated with a potential extramitochondrial heme maturation defect, the specific activity of plasmid-expressed CAT was determined in digitonin-permeabilized total lysates derived from four independent experimental ABCB7-knockdown series (Figure 11a, b). Variations among the individual sample preparations were taken into account by relating specific CAT activities to the corresponding activities of LDH (Figure 11c). LDH served as an independent cytosolic reference enzyme since its activity is not dependent on heme or Fe/S cluster formation.

Despite the rather uniform plasmid-based CAT overproduction, the specific enzyme activities varied profoundly among the four sample series (Figure 11a). Nevertheless, ectopic CAT expression resulted in a substantial increase in specific CAT activity, except in samples depleted for FECH by RNAi. This observation was further substantiated after elimination of the inter-assay variability by normalization of the specific CAT activities to that of Mock/CAT samples (Figure 11b), and further after relation to LDH (Figure 11c). Consistent with the initial FECH knockdown experiments above (cf. chapter 6.1) this analysis underscores that FECH is essential for CAT activity and emphasizes the critical role of FECH for extramitochondrial heme maturation.

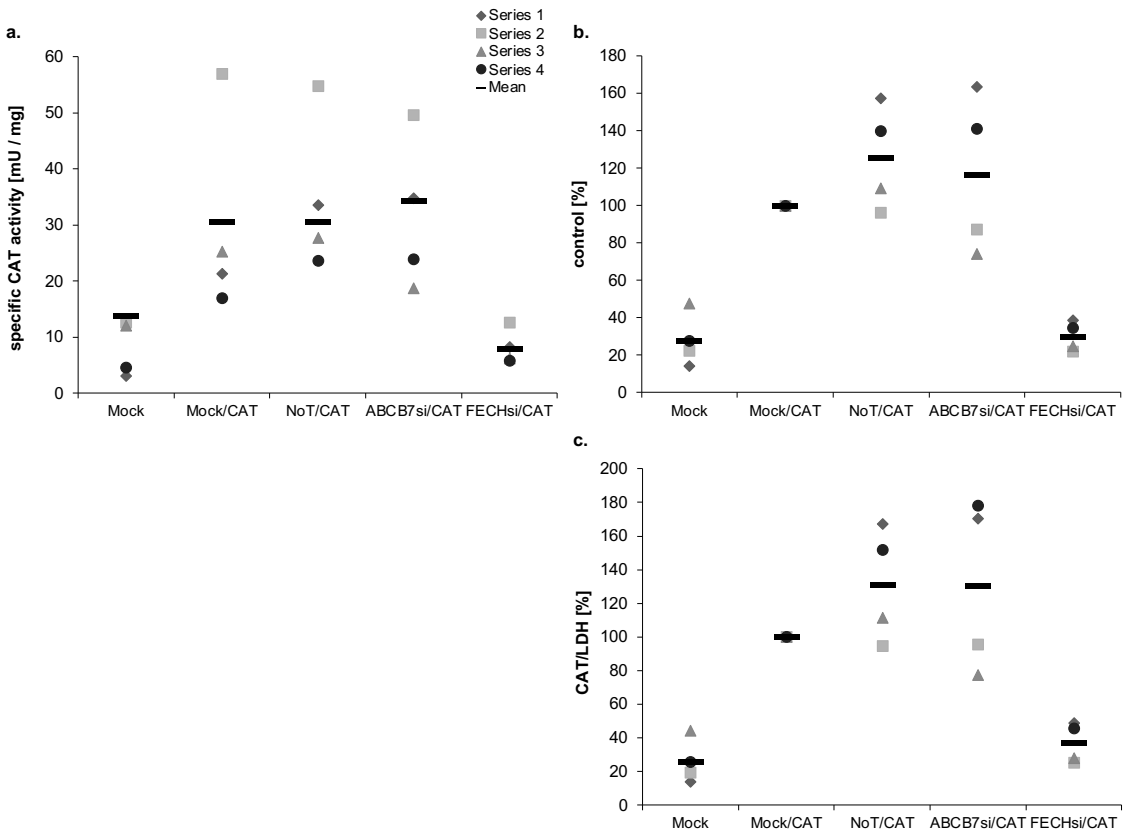

Figure 11: Catalase activities in HeLa cells are not decreased upon depletion of ABCB7.

Lysates from Fig. 9 were subjected to enzymatic activity assays. a. Specific enzyme activity [mU/mg protein] of heme-dependent catalase was determined in the lysate of 4 experiments. b. Specific catalase activity in relation to control (Sample 2: Mock/CAT) is shown for 4 experimental series. c. Catalase activity is depicted in relation to LDH as cytosolic reference enzyme for 4 experimental series (n=4).

Importantly, CAT activity in ABCB7-deficient cells was still comparable to the Mock/CAT and NoT/CAT reference samples which were overproducing CAT but were not depleted for ABCB7 or FECH (Figure 11a-c, ABCB7si/CAT). This result unequivocally demonstrated that ABCB7 is not required for heme maturation of CAT, despite CAT overexpression requiring higher heme amounts. This result implicates that ABCB7 is not involved in the export of heme out of mitochondria. Consequently, the growth retardation observed in cells lacking the ABCB7 exporter (cf. chapter 6.2) was not caused by extramitochondrial heme deficiency.

Taken together, these results underline the importance of FECH for the maturation of all cellular heme proteins but do not support the hypothesis that ABCB7 executes a significant function in mitochondrial heme export.

6.4 ABCB7 but not FECH deficiency impairs maturation of cytosolic and nuclear Fe/S proteins

Since the CAT activity measurements (cf. chapter 6.3) did not detect alterations in extramitochondrial heme availability upon ABCB7 deficiency, the observed growth retardation (cf. Figure 10b) was likely to be caused by the disruption of other vital processes. A critical function has been ascribed to ABCB7 in the maturation of extramitochondrial Fe/S proteins including IRP1 (cf. chapter 4.1.1 and 4.3.2.2). IRP1 is a bifunctional protein that in its apo-form can bind to certain mRNA stem-loop structures to regulate cellular iron metabolism. In its Fe/S cluster containing holo-form, IRP1 acts as a cytosolic aconitase (cACO), catalyzing the conversion of citrate to isocitrate (cf. chapter 4.1.1; Stehling et al., 2008). The enzymatic activity of cACO was thus assessed as a marker for cytosolic Fe/S cluster maturation to determine its dependency on ABCB7.

Analyses were performed in samples of the same cells used for CAT activity measurements (cf. chapter 6.3). Cytosolic fractions of digitonin-permeabilized, CAT overproducing, and ABCB7 or FECH deficient HeLa cells served to determine IRP1's cACO activity independent of mACO, which had been separated into organellar fractions by centrifugation (c.f. chapter 6.2, Figure 9). The successful separation of cytosolic and organellar constituents allowed the selective determination of IRP1's cACO activity in the cytosolic fractions of RNAi-treated and control cells (Figure 12) without substantial contamination by mACO. Among the four independent sample series already used for CAT activity measurements (cf. chapter 6.3), only slight variations of specific cACO activity were determined, ranging from 8 to 12 mU per mg protein in Mock (-CAT) control cells (Figure 12a). Normalization of the specific cACO activities to Mock/CAT samples (Figure 12b) and in relation to LDH (Figure 12c) revealed comparable cACO activities in all samples with maximum deviations of 10%, except for samples depleted for ABCB7. Neither CAT overproduction (Figure 12, +CAT) nor FECH knockdown (Figure 12, sample 5) affected the activity of cACO. In contrast, RNAi-mediated ABCB7 knockdown (Figure 12, sample 4) decreased cACO activity to approx. only 20% of control levels, indicating a requirement of ABCB7 in cytosolic Fe/S cluster assembly.

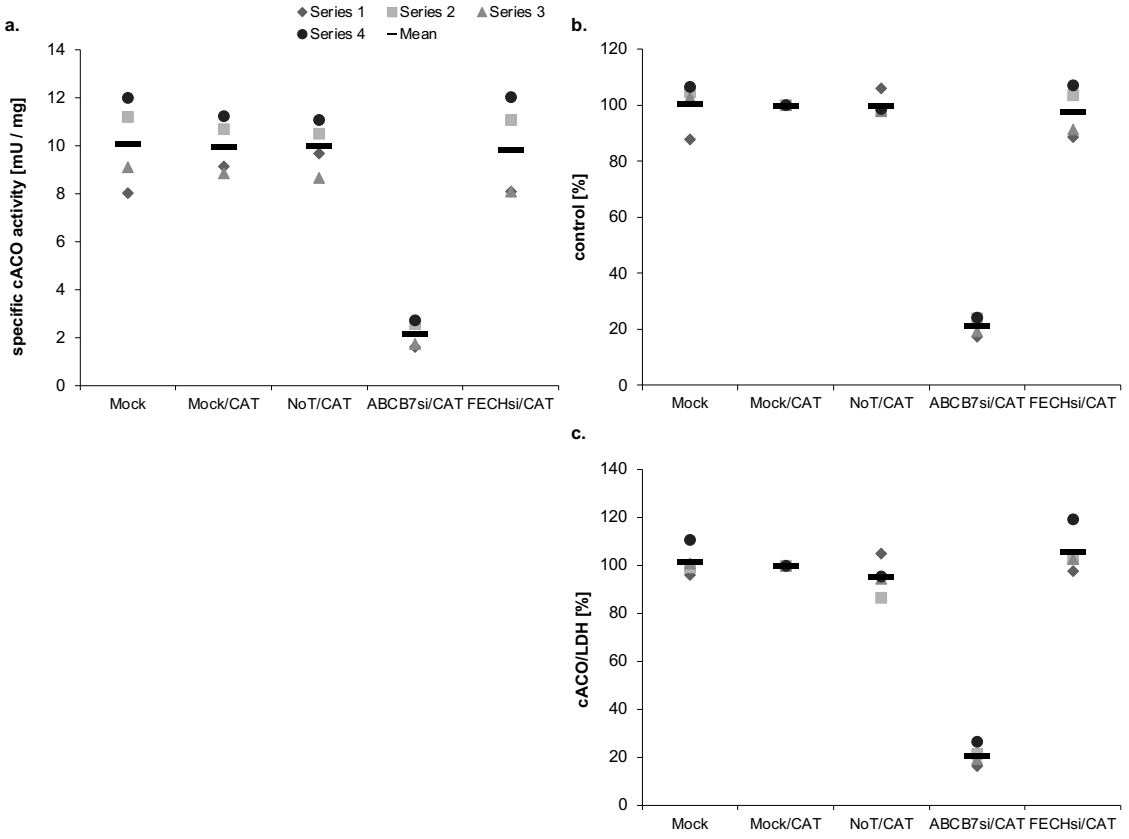

Figure 12: Cytosolic aconitase activity upon depletion of ABCB7 or FECH in CAT-overexpressing cells.

HeLa cells were transfected and processed as described in Fig. 2. Cytosolic and organellar fractions were subjected to enzymatic activity assays. **a.** Specific activity [mU/mg protein] of cytosolic aconitase (cACO) was determined in the cytosolic fraction. **b.** cACO activity in relation to the Mock/CAT control (sample 2). **c**. cACO activity is depicted in relation to LDH as cytosolic reference enzyme for 4 experimental series (n=4).

Since hampered Fe/S cofactor insertion is frequently associated with protein destabilization (cf. chapter 4.3.2.2), steady-state protein levels of IRP1 were determined (Figure 13a). Immunoblotting revealed a profound decline in IRP1 levels in ABCB7-deficient cells in comparison to control cells, whereas levels of actin and VDAC1 were not affected (Figure 13a, lane 4), in line with a severe maturation defect of IRP1 (cf. Biederbick et al., 2006). In contrast, CAT overproduction (Figure 13a, lane 2) or FECH knockdown (Figure 13a, lane 5) did not result in any alterations in steady-state levels of IRP1 or of the marker proteins actin or VDAC1.

Taken together, enzyme activity assays and immunoblotting demonstrated that cytosolic ACO activity and stability of IRP1 are unaffected by impaired mitochondrial heme formation but are strictly dependent on ABCB7. These results reinforce the well-known observation that mitochondria export a compound essentially required for cytosolic Fe/S cluster assembly including cofactor maturation of IRP1, but do not support a function of ABCB7 in mitochondrial heme export.

At the cell physiological level, maturation of IRP1 is a critical determinant of cellular iron homeostasis in mammalian cells and is known to affect both ferritin-mediated iron storage and transferrin receptor (TfR1)-mediated iron uptake. A second layer of iron regulation is mediated by IRP2, an IRP1 homologue whose cellular abundance is governed by the E3 ubiquitin ligase F-box/leucine rich repeat protein 5 (FBXL5; cf. chapter 4.1.1). FBXL5's cellular levels are dependent on Fe-dependent stabilization of its N-terminal hemerythin domain (Salahudeen & Bruick, 2009; Vashisht et al., 2009). The interaction of FBXL5 with IRP2 may be favored by a C-terminal [2Fe-2S] cluster (Wang et al., 2020). In line with previous observations (Cavadini et al., 2007; Pondarre et al., 2006) IRP2 and TFR1 levels were substantially increased in ABCB7 knockdown cell samples whereas the amount of ferritin was decreased (Figure 13a, lane 4). These changes are consistent with compromised Fe/S cluster biosynthesis pathways eliciting an iron starvation phenotype despite presence of sufficient iron supply and support the finding that ABCB7 is connected to cytosolic-nuclear Fe/S protein maturation.

In contrast, FECH deficiency did not exert detectable effects on iron-regulatory proteins (IRPs), ferritin, and TFR1, indicating that heme formation does not play a decisive role in cellular iron regulation in the HeLa cell model (Figure 13a, lane 5). Notably, according to Mock- and NoT-transfected cells, CAT overproduction did not alter steady-state protein levels of the tested iron homeostasis-regulating factors, suggesting that the surplus amount of CAT protein did not produce an appreciable iron sink which might have led to relevant changes in intracellular iron handling.

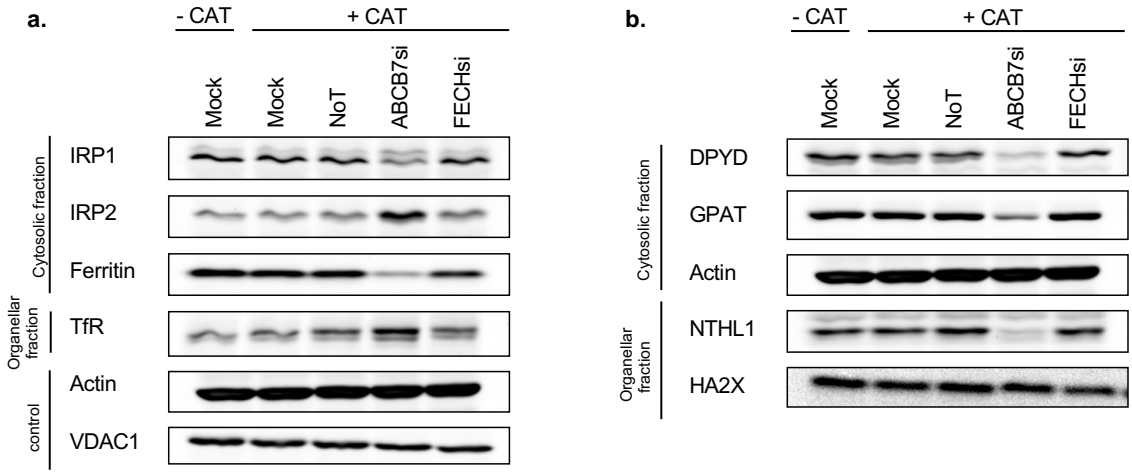

Figure 13: Steady-state protein levels of HeLa cells upon depletion of ABCB7, FECH and overexpression of CAT.

HeLa cells were transfected and processed as described in chapter 6.2. Cytosolic and organellar fractions were subjected to SDS-PAGE and immunoblotting. **a**. Proteins involved in iron homeostasis were assessed as displayed. ABCB7 deficient cells impair levels of IRP, Ferritin and Transferrin receptor. VDAC1 and actin served as mitochondrial and cytosolic controls, respectively. Representative blots are shown. **b**. Mitochondrial, nuclear and cytosolic proteins were immunostained in the respective cellular fractions as shown. Fe/S dependent proteins IRP1, NTHL1, DPYD and GPAT show a decrease in expression upon ABCB7 depletion.

The decrease in IRP1's steady-state protein level accompanying the loss of the protein's ACO activity upon ABCB7 deficiency is paradigmatic for the destabilization of many Fe/S proteins in the absence of their metallo-cofactor, i.e. in their apoform. Accordingly, immunoblotting is a useful and easy approach to assess the efficiency of cytosolic-nuclear Fe-S protein assembly (Stehling, Paul, et al., 2018). For example, previous studies have revealed that, similar to IRP1, also the steady-state levels of the non-mitochondrial Fe/S proteins dihydropyrimidine dehydrogenase (DPYD), glutamine amidophosphoribosyltransferase (GPAT), and Nth-like DNA Glycosylase 1 (NTHL1) were affected by loss of the Fe/S cofactor (Paul & Lill, 2015; Stehling et al., 2013). Hence, immunoblotting was employed to analyze the abundance of the three proteins in the same samples of ABCB7- and FECH-deficient HeLa cells like IRP1 (Figure 13b) using actin and Histon A2X (HA2X) as a control.

DPYD is a homodimeric cytosolic enzyme which is involved in the modification and degradation of pyrimidines and pyrimidine derivatives and which carries a total of eight [4Fe-4S] clusters (Porter & Spector, 1993). Immunoblotting revealed decreased DPYD levels upon ABCB7 knockdown (Figure 13b, lane 4), indicating defective maturation of the enzyme. In contrast, HeLa cells with overproduced CAT (Figure 13b, lane 2) or FECH knockdown (Figure 13b, lane 5) did not show any deficiencies in DPYD steady-

state levels compared to control samples. Thus, the immunoblotting analyses demonstrated that stability of DPYD is dependent on ABCB7, but was unaffected by impaired mitochondrial heme formation, supporting the view that ABCB7 is essential for cytosolic Fe/S protein assembly including maturation of DPYD.

GPAT is a cytosolic enzyme of the *de novo* purine nucleotide biosynthesis and requires incorporation of a [4Fe-4S] cluster to mature to an active enzyme (Iwahana et al., 1993). Similar to IRP1 and DPYD, knockdown of ABCB7 diminished GPAT's steady state levels, indicating impaired cluster assembly on the protein (Figure 13b, lane 4). In contrast, protein levels of GPAT were apparently not affected by CAT overproduction (Figure 13b, lane 2) or RNAi-mediated FECH depletion (Figure 13b, lane 5), demonstrating that GPAT maturation and stability are independent of mitochondrial heme formation.

NTHL1 is a [4Fe-4S] DNA glycosylase enzyme involved in the repair of oxidatively damaged pyrimidines in nuclear DNA (cf. chapter 4.3.2.2). Accordingly, the protein was preferentially localized in the nuclei-containing organellar fraction of digitonin-permeabilized HeLa cells and staining for the histone marker H2AX served as nuclear control (Figure 13b). Steady-state levels of NTHL1 were substantially decreased in samples depleted for ABCB7 (Figure 13b, lane 4), indicating that ABCB7 is required for stability of this DNA glycosylase. At the same time, neither FECH siRNA treatment (Figure 13b, lane 5) nor CAT plasmid transfection (Figure 13b, lane 2) affected the NTHL1 signal.

Taken together, immunostaining detected decreased steady-state levels of the three well-established non-mitochondrial Fe/S marker proteins DPYD, GPAT and NTHL1 (Paul & Lill, 2015; Stehling et al., 2013) upon ABCB7 depletion, in line with a requirement of this mitochondrial exporter for cytosolic-nuclear Fe/S protein assembly. On the other hand, loss of FECH and consequently of heme did not affect the three extramitochondrial Fe/S marker proteins.

6.5 RNAi-mediated depletion of FECH and ABCB7 elicits mitochondrial defects

The enzymatic activity and immunoblotting analyses in this study have confirmed a critical function of mitochondria in cofactor maturation of extramitochondrial heme and Fe/S proteins. In order to compare these cytosolic-nuclear maturation defects with consequences of FECH and ABCB7 depletion on mitochondria, steady-state levels and functions of mitochondrial proteins were examined in the organellar fractions of the same CAT-overproducing, digitonin-permeabilized cells that have been described above (cf. chapter 6.3 and 6.4). Immunoblotting indicated that the F1 a/b subunits of mitochondrial ATP synthase (Complex V) neither were altered upon ABCB7 or FECH knockdown nor were responding to transfection of the CAT plasmid (Figure 14a). Together with the fact that complex V does not contain any cofactor the unchanged steady-state levels render F1 a/b subunits as suitable reference antigens in subsequent mitochondrial analyses.

In line with the initial results in chapter 6.1, specific COX activity as well as steady-state levels of COX2 and COX6A/B were decreased in FECH-depleted, CAT-overproducing cells (Figure 14a, lane 5; Figure 14h-j), confirming impaired COX assembly upon heme deficiency. However, the low COX activity (Figure 14h) did not become evident in relation to CS activity due to generally lowered CS activity in FECH-deficient cells (Figure 14j; cf. Figure 9b). Knockdown of FECH also revealed the dependency of respiratory chain complex III integrity on heme availability. Not only the heme-containing subunit CYC1 but also the core 2 and the Fe/S Rieske proteins were diminished (Figure 14a, lane 5), suggesting a destabilization of the three subunits due to improper cofactor maturation and subsequent hampered complex formation (Allen, 2011; San Francisco et al., 2013).

Respiratory chain complex II (SDH) contains a heme cofactor in its membrane domain, suspected to play a role in electron transfer to ubiquinone. Consistently, ubiquinone-dependent specific SDH activity was severely decreased upon FECH depletion (Figure 14e,f, sample 5), even in relation to CS (Figure 14g, sample 5), thereby underlining the requirement of heme for proper SDH function. At the same time, immunoblotting demonstrated that SDH's Fe/S cluster-binding subunit SDHB was not affected by FECH knockdown (Figure 14a, lane 5). Since SDHB is sensitive to the lack of its cofactors, impaired Fe/S maturation was an unlikely cause for SDH inactivation. Similar to SDH, immunoblotting for the [2Fe-2S] and [4Fe-4S] cluster subunits NDUFV2 and

NDUFS8 of C I, did not reveal FECH-dependent changes in their integrity (Figure 14a, lane 5), supporting the observation that mitochondrial Fe/S protein assembly is not influenced by heme availability. Also other markers of C I stability including the membrane and matrix arm subunits NDUFB4 and GRIM19, respectively (Gnandt et al., 2016; Wu et al., 2016), did not respond to FECH deficiency, in line with the fact that none of the C I subunits contains heme.

Alike the Fe/S subunits of the respiratory chain also the mitochondrial Fe/S enzyme ACO (mACO) did not reveal changes in its steady-state protein level in samples of FECH siRNA-treated cells (Figure 14a, lane 5). However, the specific mACO activity decreased by 50% in FECH-depleted cells (Figure 14b, sample 5), an effect that was almost abolished by relation to the also diminished CS activity (Figure 14d, sample 5) and was thus likely not attributable to impaired Fe/S cluster assembly but rather to a heme-dependent pleiotropic mitochondrial defect.

Taken together, enzyme activity assays and immunoblotting showed that FECH depletion substantially affected activity and stability of mitochondrial hemoproteins, indicating an efficient abrogation of mitochondrial heme formation as a sound basis for extramitochondrial heme deficiency including impaired CAT activity (cf. Figure 8). Insufficient heme supply had significant consequences for mitochondrial function in general (cf. Kim et al., 2012; Smith et al., 2012), as indicated by impaired activities of for example citrate synthase (cf. Figure 9) and mACO, but the defect was not severe enough to compromise steady-state protein levels of mitochondrial Fe/S proteins.

Next, the effects of ABCB7 depletion on mitochondrial enzymes were analyzed. Enzyme activity analyses of the mitochondria-containing organellar fraction derived from digitonin-permeabilized cells revealed that mACO activity was impaired by 50% upon ABCB7 knockdown when compared to the Mock- or NoT-transfected samples (Figure 14b-d, sample 4). However, mACO immunoblot analysis showed no difference in the signal intensity to controls (Figure 14a, lane 4), indicating a rather moderate mACO enzyme defect without detectable protein destabilization. Moreover, compared to the fivefold decrease in cACO activity (cf. Figure 12, sample 4), the twofold diminution for mACO appeared to be rather mild.

In order to assess the integrity of additional mitochondrial Fe/S cluster-containing proteins in ABCB7-depleted cells, steady-state levels of selected C I subunits were assessed by immunoblotting, including NDUFV2, NDUFS8, NDUFB4, and GRIM19.

Similar to mACO, a destabilization of neither subunit was detectable, suggesting that at least the assembly of C I was not affected by ABCB7 loss. In contrast, SDH was substantially affected in ABCB7-depleted cells. Besides its activity (Figure 14e-g, sample 4) also the steady-state protein level of the Fe/S subunit SDHB was strongly diminished (Figure 14a, lane 4). Overall, the effect on SDH activity during ABCB7 depletion was similar to the depletion of FECH.

Due to the severe SDH defect, an enzyme dependent on two different types of Fe-dependent cofactors (Fe/S cluster and heme *b)*, the analyses were extended to the integrity and function of mitochondrial heme-containing complexes. Immunoblotting for CYC1, Core II or Rieske proteins did not reveal profound C III defects and thus did not allow any conclusions about the efficiency of heme formation in ABCB7-depleted mitochondria (Figure 14a, lane 4). However, steady-state COX2 level as well as activity of the heme-dependent enzyme COX were lower in ABCB7-deficient than in Mock- and NoT-transfected control samples (Figure 14a, h-j, sample 4). Other mitochondrial enzymes that lack a cofactor including CS (cf. chapter 6.2) were apparently not affected by ABCB7 depletion suggesting an iron-dependent cause of these defects.

Taken together, the analyses of mitochondrial proteins demonstrated an impact of RNAi-mediated ABCB7 depletion on the iron-dependent enzymes mACO, SDH and COX. Since ABCB7 is considered to act as an exporter, this effect was surprising. The effect may be indirect and similar to the situation of Atm1-deficient yeast mitochondria which accumulate iron as a result of deregulated iron homeostasis (Kispal et al., 1997; Kispal et al., 1999). This eventually caused oxidative stress conditions with a severe impact on several mitochondrial enzymes such as c-type cytochromes whose heme cofactor was absent. Since the RNAi-mediated ABCB7 knockdown also affected cytosolic regulators and components of cellular iron homeostasis, a similar effect as in yeast seemed possible, suggesting that the observed decreases in mitochondrial iron-dependent proteins were indirectly caused by a potential feedback from the disturbed cellular iron metabolism. This interpretation would explain why SDH, an enzyme dependent on both Fe/S clusters and heme, might be particularly sensitive. Moreover, the much weaker effect on mACO activity compared to cACO also suggested that the defects on individual mitochondrial Fe/S or heme proteins were an indirect consequence of the alterations in mitochondrial iron metabolism caused by disturbances upon ABCB7 depletion.

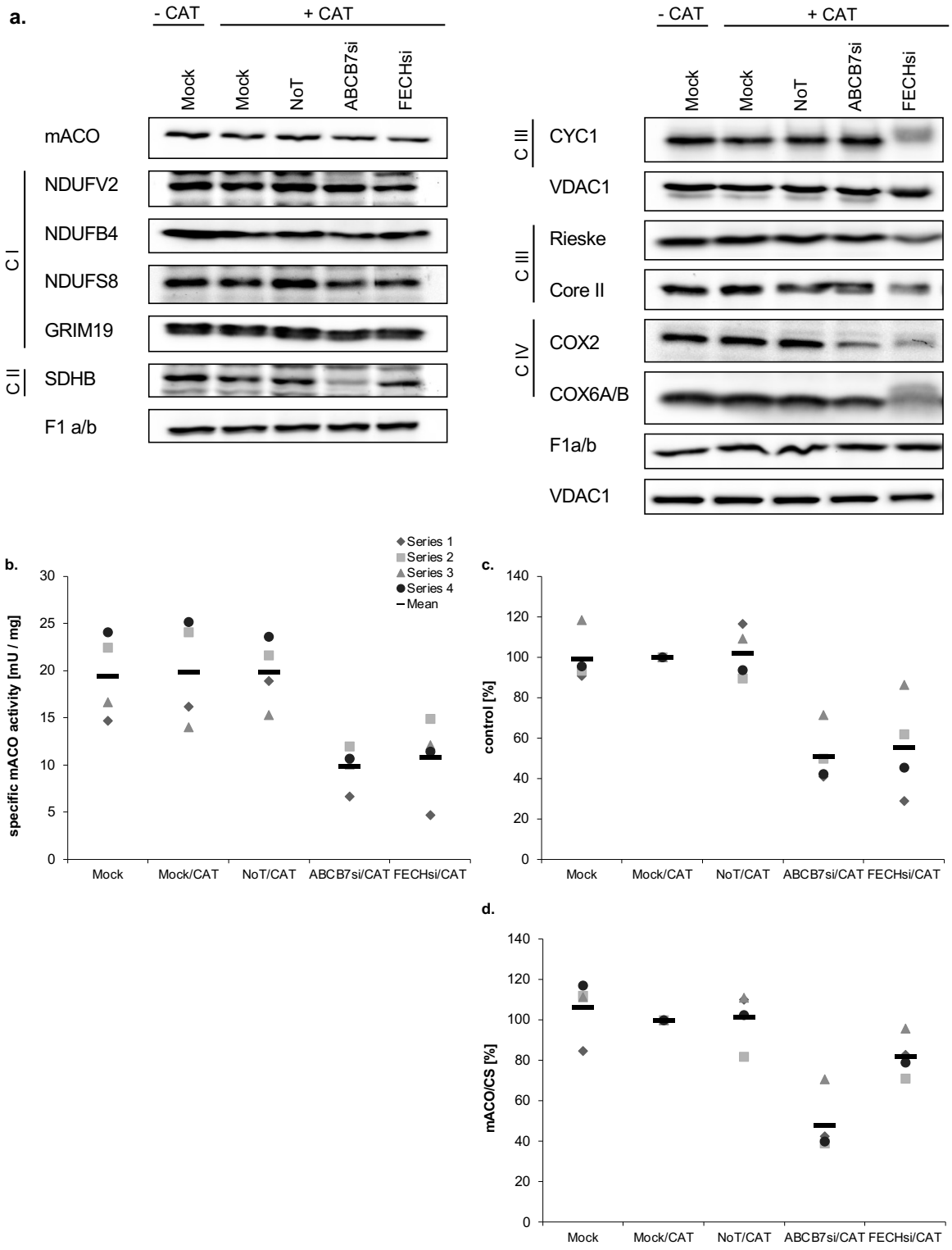

Figure 14a-d: Steady-state protein levels and enzymatic activities of mitochondrial proteins upon depletion of ABCB7, FECH and overexpression of CAT.

HeLa cells were transfected and processed as described in chapter 6.2. Cytosolic and organellar fractions were subjected to SDS-PAGE, immunoblotting and enzymatic activity assays. **a.** Steady-state levels of mitochondrial proteins such as marker proteins for respiratory chain complexes I, II, III, IV and V were analyzed as indicated. VDAC1 was stained as a mitochondrial control. Representative blots are shown. **b.** Specific activity [mU/mg protein] of mitochondrial aconitase (mACO) was determined in the organellar fraction. **c.** mACO activity in relation to control (Sample 2: Mock/CAT). **d.** Mean mACO activity is depicted in relation to CS as mitochondrial reference enzyme (+/- SD, n=4).

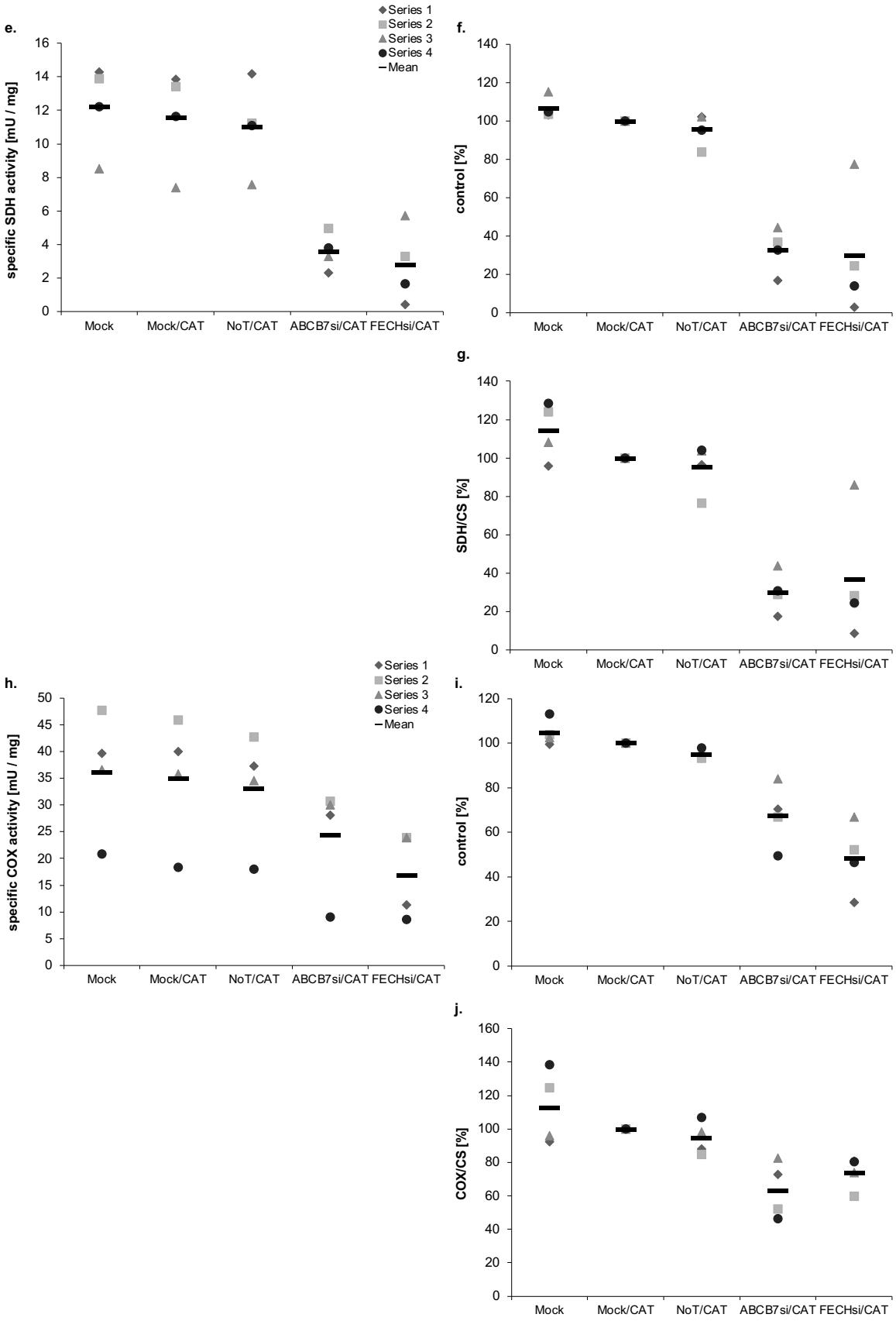

Figure 14e-j: Enzymatic activities of mitochondrial proteins upon depletion of ABCB7, FECH and overexpression of CAT.

e. Specific activity [mU/mg protein] of mitochondrial SDH was determined in the organellar fraction. **f.** SDH activity in relation to control (Sample 2: Mock/CAT). **g.** Mean SDH activity is depicted in relation to CS as mitochondrial reference enzyme (+/- SD, n=4). **h.** Specific activity [mU/mg protein] of mitochondrial COX was determined in the organellar fraction. **i.** COX activity in relation to control (Sample 2: Mock/CAT). **j**. Mean COX activity is depicted in relation to CS as mitochondrial reference enzyme (+/- SD, n=4).

6.6 The mitochondrial defects associated with ABCB7 deficiency are specific consequences of the transporter knockdown

In order to verify that the observed consequences of RNAi-mediated ABCB7 depletion were indeed caused by loss of the transporter protein and not by non-specific siRNA (off-target) effects particularly on mitochondria (cf. chapter 6.5), the specificity of the transporter knockdown was assessed by a complementation approach. In this approach, plasmid-based expression of an RNAi-resistant, silently mutated ABCB7 version (ABCB7sm) was performed concurrently to the transfection of ABCB7-directed siRNAs. If the ABCB7 depletion phenotype could be reverted by ABCB7sm overexpression, the observed consequences of the transporter knockdown would be specific. If complementation of the ABCB7 RNAi phenotype would not be successful, the used siRNAs would have exerted off-target effects which were not related to the loss of the ABCB7 protein but may have impacted particularly on mitochondrial physiology.

In the complementation experiments, HeLa cells were transfected twice at a three-day interval with either ABCB7 or control NoT siRNA or were Mock-transfected as before. A fourth sample was treated not only with ABCB7 siRNA, but additionally received a plasmid encoding the silently mutated, RNAi-resistant version of ABCB7 (ABCB7sm). Six days after the first transfection cells were harvested and fractionated using the digitonin-permeabilization approach described above (chapter 6.2). In line with the results in chapter 6.2, application of ABCB7-directed siRNA caused a substantial decrease in ABCB7 steady-state protein level in comparison to Mock- and NoT-transfected control cells (Figure 15a, lane 3). Co-transfection of the ABCB7sm-encoding plasmid in addition to ABCB7-directed siRNAs restored the ABCB7 protein to almost control levels (Figure 15a, lane 4), demonstrating a successful complementation of ABCB7 expression.

The plasmid-based recovery of ABCB7 was now used to re-confirm the requirement of the transporter for cytosolic-nuclear Fe/S protein assembly. First, maturation of IRP1 to cACO was assessed. As before, ABCB7 siRNAs led to a decrease in the cACO activity compared to Mock- or NoT-transfected cells (Figure 15b-d, sample 3). Concomitant expression of plasmid-encoded ABCB7sm substantially recovered cACO activity (Figure 15b-d, sample 4), indicating an indispensable role of ABCB7 for Fe/S cofactor maturation on IRP1, and at the same time ruling out an siRNA off-target effect on IRP1 maturation. In line with the activity assays, immunoblotting of samples from ABCB7-

depleted cells revealed an improvement of the IRP1 signal upon complementation with plasmid-encoded ABCB7 (Figure 15a, lane 4), suggesting a cluster-dependent stabilization of the IRP1 holo-enzyme. Similar effects were observed for the extramitochondrial Fe/S proteins NTHL1, DPYD and GPAT. Consistent with results above (cf. chapter 6.4) immunoblotting detected a destabilization of the three proteins in ABCB7-deficient HeLa cells (Figure 15a, lane 3), whereas ABCB7 complementation efficiently recovered their steady-state protein levels to almost wild-type amounts, suggesting restoration of cytosolic-nuclear Fe/S cofactor maturation.

Taken together, complementation of siRNA-mediated ABCB7 depletion by ectopic expression of a silently mutated, RNAi-resistant version of ABCB7 unequivocally showed both the essential function of the ABC transporter for cytosolic-nuclear Fe/S protein assembly and the specificity of the experimental RNAi approach.

In order to examine whether also the mitochondrial ABCB7 knockdown phenotype could be reversed by complementation, enzyme and immunoblotting analyses were extended to the organellar fraction of digitonin-permeabilized cells. Determination of mACO activity in ABCB7-knockdown cells confirmed the previous observation of an approx. 50% decrease in comparison to reference samples (Figure 15e-g, sample 3). Co-transfection of the RNAi-resistant ABCB7sm version recovered mACO activity to roughly 80% of control levels, but higher individual values were also possible (Figure 15f, sample 4), suggesting a distinct effect of ABCB7 deficiency on mACO function rather than a non-specific siRNA off-target effect on mitochondria. Neither loss of ABCB7 nor complementation by ABCB7sm altered the mACO steady-state protein level, in line with a rather moderate mACO cofactor defect already observed above (Figure 15a; cf. chapter 6.5).

A more severe ABCB7 knockdown phenotype was confirmed for SDH (Figure 15a, h-j; c.f. chapter 6.5), but even this strong SDH effect was complementable by ABCB7sm expression, restoring not only SDH activity (Figure 15h-j, sample 4), but also recovering SDHB protein level (Figure 15a, lane 4). In line with the mACO analyses these results revealed a direct dependency of SDH function and integrity on the presence of ABCB7 and rendered the existence of off-target-related artefacts unlikely.

Similar to observations above, siRNA-mediated depletion of ABCB7 exerted only minor effects on COX (Figure 15a, k-m; c.f. chapter 6.5). The enzyme activity decreased by 30% at most (Figure 15k-m, sample 3) with COX2 steady state levels being affected,

whereas the amount of COX6A/B remained even more or less constant (Figure 15a, lane 3). In this mild phenotypic background, the overproduction of ABCB7sm did not lead to detectable complementation and this could thus not help to interpret the ABCB7 deficiency phenotype.

Taken together, complementation of siRNA-mediated ABCB7 depletion by an RNAi-resistant ABCB7sm plasmid version suggested that the mitochondrial ABCB7 knockdown phenotype was a specific consequence of ABCB7 deficiency and not caused by siRNA off-target effects. The fact that particularly Fe-dependent mitochondrial enzymes were affected in the absence of ABCB7 might implicate disturbances of mitochondrial iron handling as one cause of impaired mACO and SDH activity.

In summary, the present study has established a plasmid-based reporter assay for the analysis of extramitochondrial heme protein maturation in HeLa cells where endogenous CAT levels are low. In order to assess the function of ABCB7 for the maturation of hemoproteins, we depleted the CAT-overproduction cells for ABCB7 and used FECH depletion as a reference knockdown approach. Both ABCB7 and FECH loss led to decreased cell growth of the respective CAT overexpressed cell samples, suggesting their essential function for cell viability. FECH was essentially important for the maturation of heme proteins like CAT, but importantly the ABCB7 knockdown approach and subsequent CAT activity analysis did not support the view that ABCB7 holds a significant function in mitochondrial heme export as suggested (Maio et al., 2019). At the same time, analyses of ABCB7-knockdown cells detected decreased steady-state levels of cytosolic Fe/S marker proteins. In contrast, loss of FECH and consequently of heme did not impair cellular steady-state levels of Fe/S proteins, demonstrating a heme-independent involvement of ABCB7 in the Fe/S cluster maturation of cytosolic apoproteins. Mitochondrial analyses revealed that ABCB7 loss affected stability and function of mitochondrial proteins, especially the Fe/S cluster dependent proteins. In order to assess the specificity of this transporter knockdown approach, complementation of ABCB7 was established via plasmid-based expression of an RNAi-resistant ABCB7 version concurrent to ABCB7 RNAi treatment. Subsequent analyses indicated that cytosolic and mitochondrial defects upon ABCB7 knockdown were specific effects of the transporter knockdown. Loss of ABCB7 led to potential indirect mechanisms in mitochondria which require further discussion.

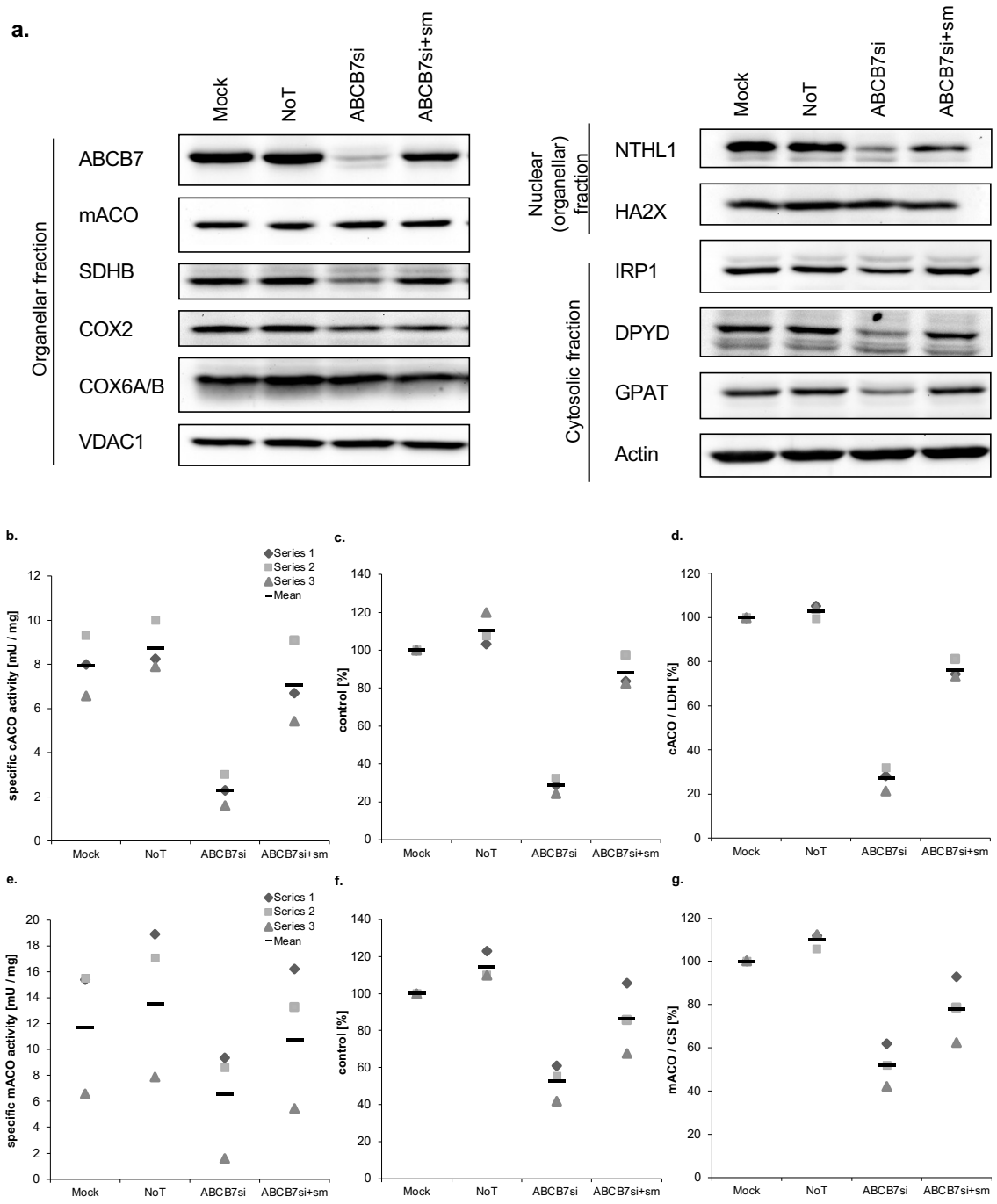

Figure 15a-g: Steady-state protein levels and enzymatic activities in HeLa cells upon complementation of ABCB7.

HeLa cells were transfected twice at a three-day interval with either control siRNA (NoT), ABCB7 siRNA, or obtained no siRNA (Mock). One sample treated with ABCB7 siRNA additionally received an ABCB7 silent mutation-encoding plasmid. Only one sample remained without siRNA. Samples were processed as described in the text. Experiments were performed in triplicates. **a**. Steady-state levels of mitochondrial, nuclear and cytosolic proteins such as marker proteins for respiratory chain complex I, II, III, IV and V were analyzed as indicated. ABCB7, SDHB, NTHL1, IRP1, DPYD and GPAT show a recovery upon complementation of ABCB7 NTHL1: n=1). VDAC1, Histon A2X and Actin served as mitochondrial, nuclear and cytosolic controls, respectively. Representative Blots are shown. **b**. Specific activity [mU/mg protein] of cytosolic ACO (cACO) was determined in the cytosolic fraction of 3 experimental series. **c.** cACO activity in relation to control (Sample 1: Mock) is shown for 3 experimental series. **d**. Mean cACO activity is depicted in relation to LDH as cytosolic reference enzyme (+/- SD, n=3). **e.** Specific activity [mU/mg protein] of mitochondrial ACO (mACO) was determined in the organellar fraction of 3 experimental series. **f**. mACO activity in relation to control (Sample 1: Mock) is shown for 3 experimental series. **g**. Mean mACO activity is depicted in relation to CS as mitochondrial reference enzyme (n=3).

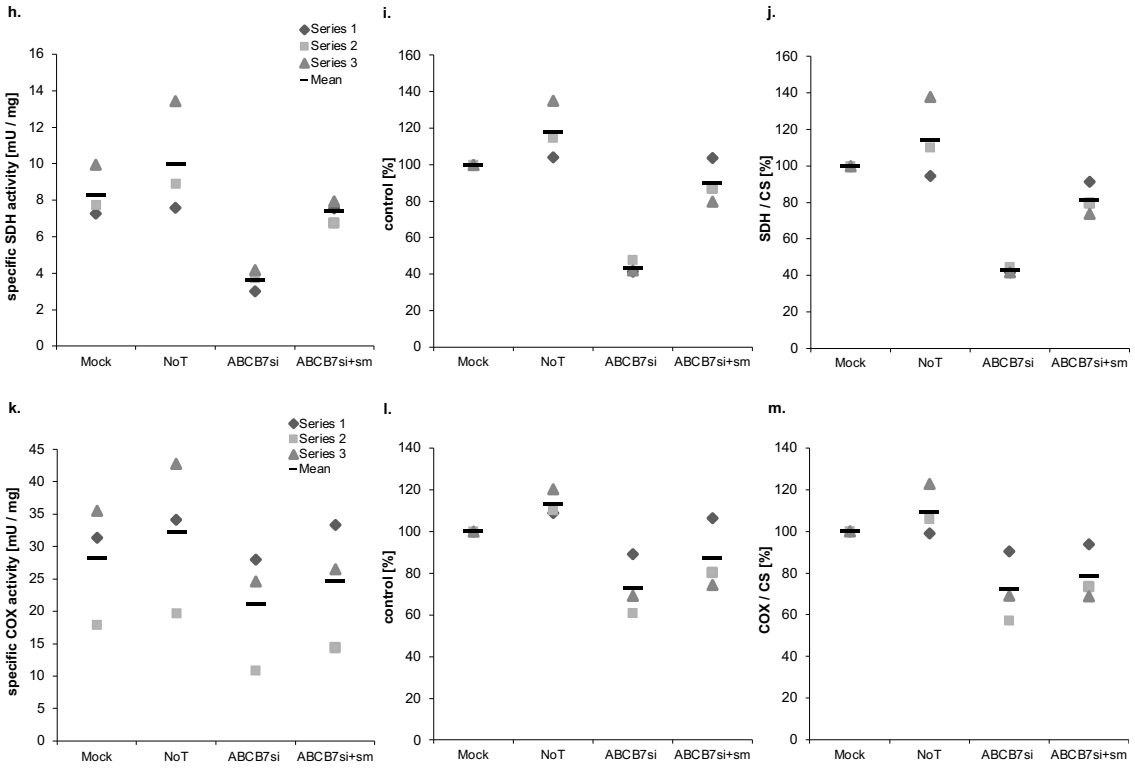

Figure 15h-m: Enzymatic activities in HeLa cells upon complementation of ABCB7.

h. Specific activity [mU/mg protein] of mitochondrial SDH was measured in the organellar fraction of 3 experimental series. **i**. SDH activity in relation to control (Sample 1: Mock) is shown for 3 experimental series. **j**. Mean SDH activity is depicted in relation to CS as mitochondrial reference enzyme (n=3). **k**. Specific activity [mU/mg protein] of mitochondrial COX was determined in the organellar fraction of 3 experimental series. **l**. COX activity in relation to control (Sample 1: Mock) is shown for 3 experimental series. **m**. Mean COX activity is depicted in relation to CS as mitochondrial reference enzyme (n=3).

7. Discussion

7.1 The effects of ABCB7 depletion in human cells

The ABC transport protein ABCB7 exports an unknown sulfur-containing compound from mitochondria for cytosolic Fe/S cluster biosynthesis and, in a defective state, is associated with a disease condition called XLSA/A (Allikmets et al., 1999; Bekri et al., 2000; Boultwood et al., 2008; Maguire et al., 2001; Sheftel et al., 2009; Xiong et al., 2021). This disease is characterized, inter alia, by sideroblastic anemia and is accompanied by cerebellar symptomatology called ataxia (Allikmets et al., 1999; Bekri et al., 2000; Pagon et al., 1985; Shimada et al., 1998). The ataxia demonstrates the relevance of ABCB7 to neural tissue function (Chiabrando et al., 2020), as previously observed in Friedreich's ataxia in the case of frataxin deficiency (Parkinson et al., 2013). The cause of the rare condition of XLSA/A is attributable to several mutations in the gene of the ABCB7 transporter and may have effects on heme synthesis (Boultwood et al., 2008; Maguire et al., 2001; Pondarre et al., 2007; Xiong et al., 2021). At the cellular level, mitochondrial Fe accumulation is a typical feature of XLSA/A. This Fe accumulation is, for example in cells of the hematopoietic tissue, regularly found as an accumulation of Fe-loaded mitochondria around the cell nucleus, the so-called ring sideroblasts (Cazzola & Invernizzi, 2011). Fe accumulation in the form of ring sideroblasts in ABCB7 deficiency may not only occur systemically as in XLSA/A but may also be observed in the hematopoietic system as is the case in the pathogenesis of refractory anemia with ring sideroblasts (RARS; Boultwood et al., 2008; Nikpour et al., 2013; Stehling et al., 2014; Visconte et al., 2012).

Mitochondrial Fe accumulation in cells with cytosolic Fe/S assembly defects has already been studied in numerous cell culture models using depletion of ABCB7 or its orthologs from other species (Cavadini et al., 2007; Csere et al., 1998; Kispal et al., 1997). In yeast, it was shown that Atm1 function is linked to the export of a sulfur- and possibly iron-containing species termed X-S (Kispal et al., 1999; Pandey et al., 2019). Cavadini et al. (2007) summarized from their analyses that Fe accumulates in ABCB7-deficient cells and is therefore not available for heme synthesis. In contrast, Maio et al. (2019) speculated that loss of ABCB7 function primarily leads to mitochondrial defects, the cause of which, along the lines of Taketani et al. (2003), is a physical interaction of ABCB7 and the FECH. In ABCB7 defects in XLSA/A, this interaction could lead to decreased mitochondrial heme synthesis and in turn impaired mitochondrial heme export. Since functional connections between heme synthesis and mitoferrins, the mitochondrial Fe import proteins, have been described (Chen et al., 2010; Martelli et

al., 2015; Shaw, Cope, et al., 2006; Shaw, Langer, et al., 2006), indirect effects of functional ABCB7 deficiency on mitochondrial Fe homeostasis, including Fe accumulation, seem possible (Maio et al., 2019). In yeast cells depleted of Atm1 there is also a profound heme defect (Kispal et al., 1999). However, this was shown to be a secondary effect due to heme degradation, because these cells could support the assembly of the heme-containing cytosolic enzyme CAT.

To better understand the cellular function of human ABCB7, a HeLa cell culture model was developed in the present work in which the ABCB7 transport protein was depleted, and cofactor maturation of selected heme and Fe/S cluster proteins was examined. The analyses showed that ABCB7 loss affected the stability and function of Fe-dependent proteins in both the cytosol and mitochondria. The Fe/S maturation of cytosolic aconitase (cACO), whose apo-form IRP1 plays an important role in cellular Fe regulation (cf. chapter 4.1.1) was impaired by ABCB7 deficiency (cf. chapter 6.4). ABCB7-depleted cells developed phenotypic signs of Fe deficiency involving activation of cellular Fe uptake components and a diminution in Fe storage capacity. Similar phenotypes were also observed in mitochondrial Fe accumulation in XLSA/A. In contrast, upon depletion of FECH, both cytosolic-nuclear Fe/S protein maturation and components of cellular Fe homeostasis were not affected. In addition, there were no signs of Fe deficiency as observed for ABCB7-depleted cells detectable. Moreover, studies of mitochondrial Fe/S enzymes mACO and SDH in ABCB7-depleted cells also revealed decreased activities and stabilities (cf. chapter 6.5). Complementation of ABCB7 deficiency by plasmid-based expression of an RNAi-resistant ABCB7 version reversed the dysfunction of both cytosolic and mitochondrial Fe/S enzymes (cf. chapter 6.6), verifying the specificity of the siRNA approach also with respect to the ABCB7-dependent mitochondrial phenotype.

Extramitochondrial heme protein maturation was analyzed by the prominent heme marker protein CAT in the present analyses (Putnam et al., 2000). For this purpose, a plasmid-based CAT reporter assay was established in the previously introduced HeLa cell model with ABCB7 depletion (cf. chapter 6.2). The effect of ABCB7 deficiency was compared with the consequences resulting from RNAi-mediated FECH depletion. Knockdown of both ABCB7 and FECH resulted in decreased cell yield in each case, indicating an essential function for cell growth of these two enzymes (cf. chapter 6.2). FECH knockdown, as a model for defective heme synthesis, led to expected mitochondrial defects, particularly in the heme-dependent respiratory chain complexes (cf. chapter 6.1; Kim et al., 2012; Smith et al., 2012). FECH depletion further impaired

the maturation of the extramitochondrial heme enzyme CAT, thereby confirming the general dependence of extramitochondrial heme proteins on mitochondrial heme synthesis (Hamza & Dailey, 2012; Sinclair & Hamza, 2015). In contrast, knockdown of ABCB7 did not affect CAT activity, ruling out a relevant function of the transporter in both mitochondrial heme synthesis and export (cf. chapter 6.3). Rather, since the maturation of cytosolic nuclear Fe/S proteins was impaired, these findings confirmed the function of ABCB7 as an essential link between mitochondria and extramitochondrial Fe/S protein assembly as expected from yeast studies (Lill et al., 2014). Therefore, the present study rendered a role for ABCB7 in cellular heme metabolism as a central cause of XLSA/A and associated mitochondrial Fe accumulation unlikely. Rather, it supported the concept of impaired maturation of cytosolic nuclear Fe/S proteins with downstream disruption of cellular Fe homeostasis as the etiology of XLSA/A.

7.2 Maturation of extramitochondrial hemoproteins occurs independently of ABCB7

The disease XLSA/A is caused by mutations of the ABCB7 gene and the associated loss of function of the mitochondrial transporter ABCB7. One of the most prominent features of this disease is the anemic phenotype which may result from impaired maturation of hemoproteins. Taketani et al. (2003) and Maio et al. (2019) thus investigated the functional link between ABCB7 and the synthesis of heme. Both studies identified a physical interaction of ABCB7 with the enzyme FECH and used this to develop the hypothesis that ABCB7 affects heme synthesis through specific binding to FECH. Maio et al. (2019) further suggested that ABCB7 in complex with FECH and the protein ABCB10 may have additional responsibility for the export of heme out of the mitochondrion. However, this idea competed with numerous indications that the substrate of ABCB7 is a sulfur-containing compound synthesized depending on the mitochondrial ISC machinery, which is exported from mitochondria to the cytosol where it is required for cytosolic-nuclear Fe/S cofactor synthesis (Biederbick et al., 2006; Kispal et al., 1999; Stehling & Lill, 2013). To contribute to the biochemical characterization of ABCB7 function and thus the pathogenesis of XLSA/A, the present work systematically examined features related to the maturation of both mitochondrial heme proteins and the extramitochondrial heme enzyme CAT in human ABCB7-deficient cells and compared these effects with the consequences of FECH loss. Since a possible involvement of ABCB7 in mitochondrial heme export was a central question of the present work, for the analyses presented here an existing reporter assay was

further modified for the specific inhibitor-based detection of CAT activity. In contrast, Maio et al. (2019) used a simple commercial CAT assay based on the reactive fluorescent dye Amplex-Red (Miwa et al., 2016; Zhou et al., 1997; Zhou et al., 2003) without further verification of substrate specificity. Compared to the HeLa analyses of Maio et al., 2019, the assay used in this work revealed only low specific activity of endogenous CAT, which was, however, consistent with the barely detectable CAT protein levels in HeLa total cell lysates (cf. chapter 6.1). In the present study and similar to work performed in yeast (Kispal et al., 1997), human CAT was further transiently overproduced from an ectopic CAT plasmid to avoid possible experimentally influenced fluctuations in endogenous CAT levels. Additionally, the preparation of peroxisomes was bypassed by the transient overproduction. The overproduction of CAT was found to be robust, increased the detectable enzyme activity several-fold and was not affected by further cell manipulation. Thus, this CAT overproduction system offered the possibility to additionally deplete ABCB7 or FECH by RNAi, and to analyze the CAT activities in the various cells.

Loss of FECH affected the integrity and activity of cellular heme proteins, both inside and outside of mitochondria, as shown for example by CAT analysis (cf. chapter 6.1). The experimental approach of FECH depletion thus underscored the importance of mitochondria for cofactor maturation of all cellular heme proteins and provided a suitable model for the characterization of general heme deficiency. In contrast, depletion of ABCB7 in a cell culture model for the diseases XLSA/A and RARS revealed no signs of a CAT defect (cf. chapter 6.3). This result on the one hand excluded an insufficient mitochondrial heme export in the cells, and on the other hand also refuted a role of ABCB7 in mitochondrial heme synthesis. While some effects of ABCB7 loss on heme-containing enzymes like COX were observed at the mitochondrial level, the stability of heme-related mitochondrial proteins was less affected than in the case of FECH deficiency. This was especially the case for the heme subunit CYC1 of respiratory chain complex III, but also for the COX2 and COX6A/B subunits of COX. Conversely, the non-heme protein ACO was also affected by ABCB7 deficiency, indicating a general rather than a heme-specific mitochondrial defect (cf. chapter 6.5). In conclusion, the lack of an extramitochondrial heme defect and the moderate, rather pleiotropic mitochondrial heme phenotype suggested that ABCB7 does neither have a central function in the regulation of FECH activity nor in mitochondrial heme export.

Previous studies of experimental ABCB7 deficiency in both the HeLa cell culture model (Cavadini et al., 2007) and an XLSA/A mouse model (Pondarre et al., 2006) also considered a direct involvement of ABCB7 in heme synthesis unlikely. Similar conclusions were obtained from studies on the function of ABCB7 orthologs in other model organisms. Bernard et al. (2009) depleted the mitochondrial exporter Atm3 in plants and, consistent with the present work, found no loss of function of endogenous CAT, nor any significant impairment of mitochondrial heme synthesis. In yeast, Kispal et al. (1997), however, found impaired maturation of both mitochondrial and extramitochondrial heme proteins upon characterization of Atm1-deficient cells, but the synthesis of heme was not substantially impaired, similar to the ABCB7-depleted cells in the present study. Rather, heme was degraded in these cells by an unknown mechanism. Thus, in synopsis of the analyses from previous work and the findings from this study, it is unlikely that the pathobiochemical basis for XLSA/A and RARS is related to a direct involvement of ABCB7 in mitochondrial heme synthesis or ABCB7-mediated mitochondrial heme export.

7.3 The importance of ABCB7 for the maturation of extramitochondrial Fe/S proteins

Although a function of ABCB7 in the maturation of extramitochondrial hemoproteins could be excluded by the present results, ABCB7-depleted cells showed significant deficiencies in the stability and function of extramitochondrial Fe/S proteins (cf. chapter 6.4). Previous functional analyses of ABCB7 and its orthologs from various species such as plants (Bernard et al., 2009; Kushnir et al., 2001), trypanosomes (Horáková et al., 2015), yeast (Kispal et al., 1999), and mammals (Cavadini et al., 2007; Pondarre et al., 2006) already revealed the importance of mitochondrial exporters for cytosolic Fe/S cluster biogenesis and maturation of cytosolic-nuclear proteins. In all of these studies, loss of the corresponding transporters mainly resulted in impaired function of extramitochondrial Fe/S proteins, and thus suggested a role in their maturation. In addition, structural and functional studies of recombinant Atm1 found indications of a possible substrate consistent with the export of a glutathione-coordinated [2Fe-2S]-cluster as a precursor for cytosolic-nuclear Fe/S protein biosynthesis (Li et al., 2022; Pearson et al., 2020; Srinivasan et al., 2014). Hence, the analyses of the HeLa cell model developed in the present work supported the results of these articles and substantiated the central role of ABCB7 in the maturation of cytosolic-nuclear proteins. Here, inactivation of the mitochondrial ABCB7 transporter affected Fe/S proteins of nucleotide metabolism (DPYD, GPAT) as well as DNA repair (NTHL1) and

underscored the importance of *de novo* Fe/S-cluster synthesis in mitochondria (Lill & Freibert, 2020; Lill et al., 2014) and for genome stability in the nucleus (Paul & Lill, 2015; Stehling et al., 2012).

An additional direct link between Fe/S protein maturation and, in turn, heme synthesis was suggested by Liu et al., 2020 with ALAD. ALAD catalyzes the second step in heme synthesis by converting 5-aminolevulinates to porphobilinogen and water (cf. chapter 4.2.2). Additional to potential cysteine ligands, the authors identified an alanine-phenylalanine-arginine (AFR) motif in the ALAD amino acid sequence, which mediates the interaction with maturation factors of Fe/S cluster synthesis according to Maio et al., 2014. Indeed, analyses of recombinant mammalian cell-derived ALAD revealed indications for the presence of a corresponding cofactor. Especially, ALAD catalytic activity decreased when the AFR motif was modified. However, the interaction of cytosolically localized ALAD with the mitochondrial co-chaperone HSC20 was described as a basis for cofactor maturation by Liu et al., 2020. Moreover, the influence of ALAD on heme synthesis was only incompletely investigated by the authors using the two extramitochondrial hemoproteins CAT and CYP1A2. They omitted to investigate effects on critical mitochondrial hemoproteins, whose maturation is much more directly dependent on ALAD (cf. chapter 4.2.1). With the analyses performed in this work, it was possible to directly compare the importance of ABCB7 for cytosolic Fe/S protein maturation with the relevance of FECH for heme synthesis. Although ALAD and FECH are equally indispensable for heme synthesis, ABCB7 depletion did not show effects on heme maturation of extramitochondrially localized CAT, nor of the mitochondrial heme enzyme CYC1 (cf. chapter 6.3, 6.5). In contrast, FECH loss led to inactivation or destabilization of both proteins. Fe/S cofactor maturation of ALAD was therefore not necessary for the *in vivo* function of the enzyme (Maio et al., 2014). Accordingly, the moderate defects in COX caused by depletion of ABCB7 are unlikely to be directly attributable to impaired heme synthesis, in contrast to the severe phenotype of FECH knockdown on COX (cf. chapter 6.5). Taken together, the hypothesis of Liu et al. (2020) suggesting that the function of ALAD in the heme synthesis pathway relies on its Fe/S cluster maturation cannot be supported with the results of the present work.

7.4 ABCB7 affects cellular iron regulation

Analyses of the cells studied in this work ruled out a central role of ABCB7 in the maturation of hemoproteins but supported the participation of the mitochondrial

exporter in the maturation of cytosolic nuclear Fe/S proteins (cf. chapter 6.3). Depletion of ABCB7 led to impaired maturation of cACO and consequently, the apo-form IRP1 induced alterations in two components of cellular Fe homeostasis, TfR1 and ferritin (cf. chapter 4.1). ABCB7 depletion was also accompanied by markedly elevated levels of IRP2, a homolog of IRP1, which itself does not carry an Fe/S cofactor. Instead, IRP2 is regulated by the E3 ubiquitin ligase F-box/leucine-rich repeat protein 5 (FBXL5), whose cellular levels are in turn dependent on Fe-dependent stabilization of its N-terminal hemerythrin domain (Salahudeen & Bruick, 2009; Vashisht et al., 2009). Further, the interaction of FBXL5 with IRP2 may be favored by a [2Fe-2S] cluster bound to the C terminus of FBXL5 (Wang et al., 2020). Thus, a functional loss of ABCB7 would affect Fe/S cluster-dependent FBXL5-mediated degradation of IRP2, which is consistent with the findings presented in this study. Further, a decreased Fe availability in the cytosol also leads to the increase in cellular IRP2 levels via proteasomal degradation of FBXL5 mediated by the E3 ligase HERC2 (Moroishi et al., 2014). Accordingly, the high IRP2 levels of the ABCB7-deficient cells examined in this work were consistent with both decreased cytosolic [2Fe-2S] cluster and Fe availability (cf. chapter 6.5). As a consequence of the decreased cofactor maturation of IRP1 and increased IRP2 levels, there was more efficient binding of both proteins to mRNA-IREs. This binding lead to an impairment of ferritin translation and an increased expression of TfR1 (Anderson & Frazer, 2017) as observed in the present cell culture model (cf. chapter 6.4). ABCB7-dependent dysfunctions of cellular Fe homeostasis have been previously studied in cell culture models by Cavadini et al. (2007) and Maio et al. (2019) as well as in mouse models by Pondarre et al. (2006) and resulted in comparable phenotypic changes.

Combined with the findings of the present work that ABCB7 has no direct function for cofactor maturation of extramitochondrial hemoproteins, the analyses of iron-regulatory proteins provide a possible causal chain for the (long-term) heme deficiency not only in XLSA/A but also in RARS. In both diseases, ABCB7 deficiency is found in hematopoietic cells, leading to increasing IRE binding activity of both IRPs (Maio et al., 2019). In hematopoietic tissues, these two proteins participate in heme synthesis by regulating the enzyme ALAS2, an isoform of the ubiquitous ALAS1 (Peoc'h et al., 2019; Taylor & Brown, 2022). ALAS2 also catalyzes the first step of heme biosynthesis, the formation of 5-aminolevulinate, but unlike ALAS1, translation of the enzyme is controlled by an IRE in the 5'-UTR region. Thus, ALAS2 represents an important regulatory interface between the Fe/S and heme biosynthesis pathways in hematopoietic cells. ABCB7 deficiency in hematopoietic cells leads to increased occupancy of the IRE of ALAS2 mRNA, downregulation of the ALAS2 enzyme (Maio et

al., 2019; Nikpour et al., 2013) and consequently impaired heme synthesis (Cavadini et al., 2007; Sheftel et al., 2009; Stehling et al., 2014). The similarity of the hematologic phenotypes of patients with ALAS2 and ABCB7 mutations (Stehling et al., 2014) is consistent with these considerations. The similarity of the phenotypes suggests that the reason for the hematopoietic defect in patients with XLSA/A is found in the Fe/S cluster-dependent regulation of the heme synthesis enzyme ALAS2 (cf. Ye et al., 2010).

The significance of the IRP system in hematopoiesis is also corroborated by further studies on the maturation and function of extramitochondrial Fe/S proteins. For example, Haunhorst et al. (2013) showed that in HeLa cells, deficiency of GLRX5 impaired the maturation of cytosolic Fe/S proteins. In particular, Fe/S cofactor insertion into IRP1 was impaired, which increased its IRE binding activity. Accordingly, ferritin levels were decreased and TfR levels were increased. Consistent with this, downregulation of GLRX3 in a zebrafish model led to a substantial decline in ALAS2 and consequently to impaired heme synthesis (Haunhorst et al., 2013). Similarly, Wang et al. (2022) found indications that extensive oxidative stress resulting from impaired mitochondrial respiratory chain activity may affect Fe regulation and heme formation in human erythroleukemia cells. They examined K562 cells and described that conversion of cACO from the aconitase form to the IRP1 form not only altered cellular Fe regulation but also led to inhibition of ALAS2 production and heme synthesis. The results of Haunhorst et al., 2013 and Wang et al., 2022, in combination with the present findings, support the hypothesis that defects in IRE/IRP1-dependent Fe regulation cause a heme phenotype in patients with ABCB7 deficiency via interference with ALAS2.

7.5 The effects of ABCB7 loss in mitochondria

A characteristic feature of XLSA/A and RARS diseases caused by loss of ABCB7 function is mitochondrial Fe accumulation in the form of ring sideroblasts (Boultwood et al., 2008; Cavadini et al., 2007; Malcovati et al., 2009). This Fe accumulation is accompanied by the disruption of cellular Fe homeostasis (cf. chapter 7.4), which is possibly also related to the mitochondrial phenotype observed in the present work upon experimental ABCB7 depletion (cf. chapter 6.5). Precipitation of Fe in mitochondria has been consistently detected in various cross-species models of ABCB7 deficiency, including human cell culture (Cavadini et al., 2007; Csere et al., 1998), medakefish (Miyake et al., 2008), nematodes (González-Cabo et al., 2011), and

yeast (Kispal et al., 1997). Biophysical studies on yeast Atm1-depleted mitochondria revealed that the Fe precipitates are composed of nanoparticles of Fe^{3+} phosphate (Miao et al., 2009), which is not bioavailable in this insoluble form (Cavadini et al., 2007; Sheftel & Lill, 2009). Indeed, increased Fe uptake into mitochondria not only occurs upon functional ABCB7 deficiency but was also regularly observed during impaired mitochondrial *de novo* synthesis and transfer of [2Fe-2S] clusters, including ISCU2, FXN, or GLRX5 deficiencies in humans (Camaschella et al., 2007; Crooks et al., 2012; Huang et al., 2009; Sanaker et al., 2010), or ferredoxin (Yah1) and frataxin (Yfh1) deficiencies in yeast (Miao et al., 2009). In case of human GLRX5 deficiency, which is the cause for the sideroblastic anemia 3, even the formation of ring sideroblasts occurred (Camaschella et al., 2007, Furuyama et al., 2018), indicating a common cytopathological basis for mitochondrial Fe accumulation in core ISC and ABCB7 defects. In contrast, the role of ABCB7 in heme synthesis, postulated by Maio et al. (2019), cannot be directly linked to mitochondrial Fe accumulation. Individuals with FECH defects may suffer from impaired heme formation but not mitochondrial Fe accumulation (Ward & Cloonan, 2019). Consistent with this, in the present work, experimental FECH depletion did not result in detectable changes in cellular Fe regulation. Thus, the phenotype of mitochondrial Fe accumulation in XLSA/A and RARS cannot be explained by FECH and subsequent heme deficiency and is not consistent with the suggestion by Maio et al. (2019) that ABCB7 contributes significantly to maturation of heme proteins. Merely ALAS2 defects lead to the formation of ring sideroblasts in the context of XLSA/A, but this involves relative mitochondrial Fe accumulation exclusively in hematopoietic tissues as a result of lack of Fe incorporation into protoporphyrin IX (Ward & Cloonan, 2019).

Indications for a mechanism possibly leading to mitochondrial Fe accumulation in the presence of deficient mitochondrial Fe/S cluster synthesis were found by Huang et al. (2009). They investigated this process in more detail in Friedreich’s ataxia, an Fe/S disease caused by FXN deficiency (cf. chapter 4.3.3.1). Huang et al. (2009) observed in FXN knockout mice, besides general changes in Fe metabolism, an upregulation of the mitochondrial Fe importer MFRN2, with the potential consequence of increased mitochondrial Fe uptake. Moreover, cellular IRP2 levels were elevated in Friedreich's ataxia patients, as shown by studies in lymphocytes (Li et al., 2008). Thus, one can assume that mitochondrial Fe accumulation occurs at the expense of cytosolic Fe, and this cytosolic Fe depletion is consequently indicated by high IRP2 levels (c.f. chapter 7.4). Comparable changes in mitoferrins or IRP2 were also found in ABCB7 deficiency by Maio et al. (2019), by Pondarre et al. (2006), and in the present work, suggesting a

similar mechanism of mitochondrial Fe accumulation as in FXN deficiency. Indeed, Maio et al. (2019) demonstrated that the increased IRP2 level following ABCB7 depletion in turn increased cellular Fe uptake, thereby driving mitochondrial Fe accumulation.

Cytopathological accumulation of Fe in mitochondria is regularly associated with the development of oxidative stress (Crooks et al., 2012; Miao et al., 2009), which can negatively affect oxidation-sensitive structures including Fe/S clusters in these organelles. Early on, Kispal et al. (1997) therefore suggested that it is the oxidative stress observed in various organisms (González-Cabo et al., 2011; Miao et al., 2009) that causes impairments in mitochondrial Fe/S and heme proteins when ABCB7 orthologs are deficient. Maio et al. (2019) also detected oxidative stress in their cell culture models of ABCB7 deficiency, including increased ROS levels and a markedly elevated protein level of manganese superoxide dismutase 2 (SOD2), the mitochondrially localized SOD. At the same time, consistent with oxidative damage to Fe/S clusters, the authors demonstrated destabilization of the respiratory chain subunits NDUFS1, NDUFS8, SDHB, the mACO, the FECH, and the mitochondrial Fe/S cluster biogenesis factor GLRX5. On the one hand, the GLRX5 deficiency suggests a vicious circle of mitochondrial Fe accumulation and oxidative stress (c.f. above). On the other hand, it suggests further consequences for cellular Fe/S protein maturation that, in addition to FECH deficiency, may also affect heme biosynthesis, including the decreased CYC1 and CYT heme cofactor maturation observed by the authors. Taken together, the experimental depletion of ABCB7 performed by Maio et al. (2019) thus resulted in a severe pleiotropic mitochondrial phenotype that was associated with Fe accumulation, and not only affected heme but also Fe/S proteins. This phenotype is therefore only partially suitable for assessing the authors' initially mentioned postulate that ABCB7 is directly involved in mitochondrial heme synthesis and/or mitochondrial heme export.

In other models of ABCB7 deficiency, however, only weak or no mitochondrial changes were found (Bernard et al., 2009; Cavadini et al., 2007; Pondarre et al., 2006). Also in the cells studied in this work, only minor effects of ABCB7 deficiency on mitochondrial Fe-dependent proteins were detected (cf. chapter 6.5). The RNAi-induced weak mitochondrial phenotype could be reversed by plasmid-based complementation and was therefore not an off-target artifact of the RNAi treatment, but a specific consequence of ABCB7 depletion (cf. chapter 6.6). A comparison of ACO enzyme activities as well as stability of Fe/S proteins from the present work showed that the

effects on mitochondria were much weaker than on the cytosolic-nuclear compartment (cf. chapter 6.4), suggesting a more indirect character of mitochondrial impairment upon ABCB7 depletion. Cavadini et al. (2007) had already demonstrated that ABCB7 deficiency also leads to mitochondrial Fe accumulation in HeLa cells. Thus, oxidative damage, especially to mitochondrial Fe/S proteins, was also likely to be responsible for the disruption of cellular Fe regulation (cf. chapter 7.4) observed in the present work.

In contrast to mitochondrial Fe/S proteins, mitochondrial heme synthesis and trafficking was basically unaffected (cf. chapter 7.3). In a likely indirect manner, COX activity under ABCB7 depletion conditions dropped to about 70% of control. Unlike in the case of COX destabilization due to FECH deficiency and the resulting heme *a/a*$_3$ deficiency, the protein level of the mitochondrially encoded COX2 subunit was reduced, but not the protein level of the nuclear encoded COX6A/B subunits. Recent results may provide an explanation for the COX2 deficiency. COX2 is dependent on mitochondrial protein biosynthesis, which in turn requires the mitochondrial Fe/S protein METTL17 (Zhong et al., 2023). METTL17 promotes mitochondrial translation in a [4Fe-4S]-cluster-dependent manner, and its activity may be impaired due to diminished ISC activity as a result of the Fe accumulation and deficiency of bioavailable Fe upon ABCB7 loss. Hence, COX may respond more sensitive to damage of mitochondrial Fe/S cofactor synthesis than other heme proteins that were not affected by ABCB7 deficiency, such as mitochondrial CYC1 and peroxisomal CAT. Based on the results of the present work, together with studies on other species (including Cavadini et al., 2007; Kispal et al., 1997; Pondarre et al., 2006), the common conclusion is that the mitochondrial phenotype of ABCB7-deficient organisms may be an indirect consequence of the loss of its transport function.

7.6 Conclusion and Outlook

In conclusion, the present study could exclude a direct role of the mitochondrial exporter ABCB7 in FECH function or mitochondrial heme export. Rather, the findings support a crucial role for ABCB7 in the context of cytosolic-nuclear Fe/S cluster biogenesis and the associated regulation of cellular Fe homeostasis. The mitochondrial and erythropoietic defects observed in patients with XLSA/A and RARS as a result of ABCB7 deficiency are most likely indirect consequences of an altered Fe metabolism with mitochondrial Fe accumulation and consequent oxidative stress, in combination with anemia due to misregulation of ALAS2 and impairment of the Fe/S enzyme FECH.

Although the present work was able to exclude heme as a transport substrate of the ABCB7 transporter, the identity of its actual substrate remains unresolved. It is likely that it is a precursor for extramitochondrial Fe/S cluster synthesis, but other substrates are not completely ruled out. This includes cyclic pyranopterin monophosphate (cPMP), which is synthesized in mitochondria to later serve as a substrate for the synthesis of molybdenum cofactors (MoCo) in the cytosol (Kruse et al., 2018; Mendel, 2013). Analyses in plants have suggested that cPMP may be transported from mitochondria to the cytosol by the plant ortholog of ABCB7, Atm3 (Teschner et al., 2010). Characterization of the cargo molecules transported by ABCB7 will help to further elucidate the role of the transporter in cellular processes such as Fe/S cluster biosynthesis and MoCo biosynthesis. ABCB7 thus remains an exciting subject of future cell biologic research.

8. Summary

Mutations in the gene encoding the human mitochondrial transporter ABCB7 have been associated with X-linked sideroblastic anemia and cerebellar ataxia and refractory anemia with ring sideroblasts. ABCB7 is located in the mitochondrial inner membrane and considered to serve as an exporter of sulfur-containing compounds crucial for cytosolic and nuclear iron-sulfur protein biogenesis. While a few previous studies have also demonstrated a deficiency in heme-containing proteins in ABCB7-depleted cells, the precise molecular mechanisms behind these observations remain ill-defined. Various cytosolic-nuclear iron-sulfur proteins play pivotal roles in cellular iron and heme metabolism, and consequently could explain the X-linked sideroblastic anemia and cerebellar ataxia or refractory anemia with ring sideroblasts-related patient phenotypes. Other studies have suggested physical as well as functional interactions between ABCB7 and ferrochelatase, an enzyme associated with the matrix side of the mitochondrial inner membrane and mediating the final step in heme biosynthesis by inserting iron into protoporphyrin IX. These observations raised the question of a direct involvement of ABCB7 in both heme synthesis and mitochondrial heme export with possible consequences for erythropoiesis. This study aimed to assess the role of ABCB7 in hemoprotein maturation in human cells. To examine a potential mitochondrial heme export function of ABCB7, a HeLa tissue culture system overexpressing the peroxisomal heme-containing enzyme catalase was established. Using this system, RNA interference was applied to deplete ABCB7, and the consequences for both heme formation and mitochondrial export were compared to those of a ferrochelatase deficiency by using a combination of cell fractionation, enzymatic activity and immunoblotting assays. In addition, the maturation of selected mitochondrial and cytosolic-nuclear iron-sulfur proteins were assessed to study the requirement of ABCB7 in iron-sulfur protein biosynthesis. Upon depletion of either ABCB7 or ferrochelatase, the HeLa cell yield declined markedly, highlighting the indispensable nature of both ABCB7 and ferrochelatase for cell viability. Knockdown of ferrochelatase specifically affected the stability and function of hemoproteins both within and outside mitochondria, including respiratory chain complex II, cytochrome c_1 of respiratory chain complex III, respiratory chain complex IV and catalase. In contrast, deficiency of ABCB7 did not significantly impair catalase activity, clearly indicating that ABCB7 does not play a role in heme export from mitochondria and the subsequent maturation of extramitochondrial hemoproteins. Moreover, the present study did not identify a general requirement of ABCB7 for mitochondrial heme proteins, arguing against a functional influence of the transporter on heme formation by ferrochelatase.

Rather, loss of ABCB7 led to a compromised maturation of cytosolic and nuclear Fe/S proteins including GPAT, DPYD and NTHL1, three enzymes involved in nucleotide metabolism and DNA repair, and iron-regulatory protein 1. Plasmid-based expression of RNA interference-resistant ABCB7 reverted these effects. Together, the results corroborated earlier findings which had indicated the requirement of ABCB7 for cytosolic and nuclear iron-sulfur cluster biosynthesis. In agreement with an ABCB7 function in maturation of iron-regulatory protein 1, ABCB7 deficiency also influenced the levels of two iron regulatory protein-regulated key proteins of cellular Fe homeostasis, the iron storage protein ferritin and the iron uptake component transferrin receptor, resulting in a cellular iron deficiency phenotype. Consistently, ABCB7 deficiency triggered an increase in iron-regulatory protein 2 levels, an effect indicating decreased iron levels in the cytosolic compartment. Moreover, RNA interference-mediated depletion of ABCB7 elicited defects in mitochondrial iron-sulfur proteins, likely caused by the altered iron metabolism. Taken together, the current investigation clearly refutes critical roles of human ABCB7 in both mitochondrial heme synthesis and heme export to the cytosol and thus contradicts a direct involvement of ABCB7 in erythropoiesis. In accordance with previous studies on ABCB7 orthologs from multiple model organisms, this transporter was found to be required for the biogenesis of cytosolic-nuclear iron-sulfur proteins. The exact substrate of the transporter remains unclear and thus will be an exciting subject of future cell biological research. The concomitant, yet weaker effects on mitochondrial iron-sulfur proteins were likely caused by the oxidative stress resulting from the iron accumulation observed in ABCB7-deficient cells. The results of the present study may explain the mitochondrial phenotypes of X-linked sideroblastic anemia and cerebellar ataxia and refractory anemia with ring sideroblasts. Similar pathological mechanisms may be effective in other iron-overload diseases such as Friedreich's ataxia (caused by frataxin deficiency) and sideroblastic anemia 3 (caused by GLRX5 deficiency). Other cellular processes involving cytosolic-nuclear iron-sulfur proteins, such as iron metabolism, genome integrity and protein biosynthesis, are also affected in the case of ABCB7 deficiency, and contribute to the complex phenotype of patients who suffer from X-linked sideroblastic anemia and cerebellar ataxia or refractory anemia with ring sideroblasts.

9. Zusammenfassung

Mutationen im Gen, das für den menschlichen mitochondrialen Transporter ABCB7 kodiert, stehen in Zusammenhang mit den Krankheiten X-chromosomale sideroblastische Anämie mit zerebellärer Ataxie sowie refraktäre Anämie mit Ringsideroblasten. ABCB7 ist in der inneren Mitochondrienmembran lokalisiert und gilt als Exporteur von schwefelhaltigen Verbindungen, die für die zytosolische und nukleäre Eisen-Schwefel-Proteinbiogenese entscheidend sind. Ebenfalls haben einige frühere Studien in ABCB7-depletierten Zellen auch einen Mangel an hämhaltigen Proteinen nachgewiesen. Die genauen molekularen Mechanismen, die dieser Beobachtung zugrunde liegen, sind nach wie vor unklar. Diese Beobachtungen warfen die Frage nach einer direkten Beteiligung von ABCB7 sowohl an der Hämbiosynthese als auch am mitochondrialen Hämexport auf, mit möglichen Konsequenzen für die Erythropoese. Zusätzlich dazu könnten verschiedene zytosolisch-nukleäre Eisen-Schwefel-Proteine, die eine zentrale Rolle im zellulären Eisen- und Hämstoffwechsel spielen, die assoziierten Phänotypen der Patienten erklären. Andere Studien deuten auf physikalische und funktionelle Wechselwirkungen zwischen ABCB7 und der Ferrochelatase hin, einem Enzym, das mit der Matrixseite der inneren Mitochondrienmembran assoziiert ist und den letzten Schritt der Hämbiosynthese vermittelt. Ziel der vorliegenden Studie war es, die Rolle von ABCB7 bei der Reifung von Hämoproteinen in menschlichen Zellen zu charakterisieren. Um eine mögliche mitochondriale Hämexportfunktion von ABCB7 zu untersuchen, wurde ein HeLa-Zellkultursystem etabliert, in dem das peroxisomale, hämhaltige Enzym Katalase überexprimiert wurde. In diesem System wurde ABCB7 mittels RNA-Interferenz depletiert. Über die Messung von Enzymaktivitäten und Immunoblotting an mitochondrialen und zytosolischen Zellfraktionen wurden Effekte auf die Bildung und den mitochondrialen Export von Häm ermittelt. Diese wurden mit einem analogen Zellsystem verglichen, in dem die für die Hämbiosynthese essenzielle Ferrochelatase mittels RNA-Interferenz depletiert wurde. Darüber hinaus wurde die Synthese ausgewählter mitochondrialer sowie zytosolischer und nukleärer Eisen-Schwefel-Proteine untersucht, um die Rolle von ABCB7 in der Eisen-Schwefel-Proteinbiosynthese zu ermitteln. Nach Depletion von ABCB7 oder Ferrochelatase ging die erreichte Zellzahl deutlich zurück, was die Bedeutung sowohl von ABCB7 als auch der Ferrochelatase für Wachstum und Zellteilung zeigte. Die Depletion der Ferrochelatase wirkte sich speziell auf die Stabilität und Funktion von Hämoproteinen innerhalb und außerhalb der Mitochondrien aus, darunter der Atmungskettenkomplex II, das Cytochrom c_1 des Atmungskettenkomplexes III, der Atmungskettenkomplex IV

und Katalase. Im Gegensatz dazu beeinträchtigte ein Mangel an ABCB7 die Stabilität und Funktion von Hämoproteinen wie die Katalase-Aktivität nicht signifikant, was eindeutig darauf hindeutete, dass ABCB7 keine Rolle beim Hämexport aus den Mitochondrien und der anschließenden Reifung von extramitochondrialen Hämoproteinen spielt. Darüber hinaus konnte in der vorliegenden Studie keine Rolle von ABCB7 für mitochondriale Hämproteine identifiziert werden, was gegen einen funktionellen Einfluss des Transporters auf die Hämbildung durch Ferrochelatase spricht. Vielmehr führte der Verlust von ABCB7 zu einer beeinträchtigten Reifung von zytosolischen und nukleären Eisen-Schwefel-Proteinen, darunter GPAT, DPYD und NTHL1, drei Enzyme, die am Nukleotidstoffwechsel und an der DNA-Reparatur beteiligt sind, sowie des iron-regulatory proteins 1. Insgesamt bestätigten die Ergebnisse frühere Befunde, die auf die Notwendigkeit von ABCB7 für die zytosolische und nukleäre Eisen-Schwefel-Clusterbiosynthese hingewiesen hatten. Der ABCB7-Mangel beeinflusste auch die Spiegel zweier Proteine der zellulären Eisen-Homöostase, des Eisenspeicherproteins Ferritin und des Transferrinrezeptors, was zum Phänotyp eines zellulären Eisenmangels führte. Der ABCB7-Mangel führte zusätzlich zu einem Anstieg eines Markers für eine erhöhte mitochondriale Eisenaufnahme auf Kosten des zytosolischen Kompartiments. Darüber hinaus führte die RNA-Interferenz-vermittelte Depletion von ABCB7 zu Defekten bei mitochondrialen Eisen-Schwefel-Proteinen, die mutmaßlich durch den veränderten Eisenstoffwechsel verursacht wurden. Insgesamt widerlegte die aktuelle Untersuchung eindeutig eine Rolle des humanen ABCB7 sowohl bei der mitochondrialen Hämsynthese als auch beim Hämexport in das Zytosol. Die direkte Beteiligung von ABCB7 an der Erythropoese scheint somit fragwürdig. In Übereinstimmung mit früheren Studien über ABCB7-Orthologa aus mehreren Modellorganismen wurde festgestellt, dass ABCB7 für die Biogenese von zytosolisch-nukleären Eisen-Schwefel-Proteinen unabdingbar ist. Zelluläre Prozesse, an denen diese Eisen-Schwefel-Proteine beteiligt sind, wie der Eisenstoffwechsel, die Genomintegrität und die Proteinbiosynthese, sind bei ABCB7-Mangel ebenfalls betroffen. Sie tragen zum komplexen Phänotyp von Patienten mit X-chromosomaler sideroblastischer Anämie mit zerebellärer Ataxie sowie refraktärer Anämie mit Ringsideroblasten bei. Die gleichzeitigen, jedoch schwächer ausgeprägten Auswirkungen eines ABCB7-Mangels auf mitochondriale Eisen-Schwefel-Proteine wurden möglicherweise durch oxidativen Stress verursacht, der aus einer in ABCB7-defizienten Zellen beobachteten Eisenakkumulation resultierte. Ähnliche pathologische Mechanismen könnten auch bei anderen Krankheiten mit Eisenüberladung wie der Friedreich-Ataxie (verursacht durch Frataxin-Mangel) und der sideroblastischen Anämie 3 (verursacht durch GLRX5-Mangel) wirksam sein.

10. Bibliography

Ajioka, R. S., Phillips, J. D., & Kushner, J. P. (2006). Biosynthesis of heme in mammals. *Biochim Biophys Acta*, *1763*(7), 723-736.

Allen, J. W. (2011). Cytochrome c biogenesis in mitochondria--Systems III and V. *Febs j*, *278*(22), 4198-4216.

Allikmets, R., Raskind, W. H., Hutchinson, A., Schueck, N. D., Dean, M., & Koeller, D. M. (1999). Mutation of a putative mitochondrial iron transporter gene (ABC7) in X-linked sideroblastic anemia and ataxia (XLSA/A). *Hum. Mol. Gen.*, *8*, 743-749.

Anderson, G. J., & Frazer, D. M. (2017). Current understanding of iron homeostasis. *Am J Clin Nutr*, *106*(Suppl 6), 1559s-1566s.

Anderson, R. F., Shinde, S. S., Hille, R., Rothery, R. A., Weiner, J. H., Rajagukguk, S., . . . Cecchini, G. (2014). Electron-transfer pathways in the heme and quinone-binding domain of complex II (succinate dehydrogenase). *Biochemistry*, *53*(10), 1637-1646.

Aspinwall, R., Rothwell, D. G., Roldan-Arjona, T., Anselmino, C., Ward, C. J., Cheadle, J. P., . . . Hickson, I. D. (1997). Cloning and characterization of a functional human homolog of Escherichia coli endonuclease III. *Proc Natl Acad Sci U S A*, *94*(1), 109-114.

Bak, D. W., & Elliott, S. J. (2014). Alternative FeS cluster ligands: tuning redox potentials and chemistry. *Curr Opin Chem Biol*, *19*, 50-58.

Balwani, M., Sardh, E., Ventura, P., Peiró, P. A., Rees, D. C., Stölzel, U., . . . Gouya, L. (2020). Phase 3 Trial of RNAi Therapeutic Givosiran for Acute Intermittent Porphyria. *N Engl J Med*, *382*(24), 2289-2301.

Bekri, S., Kispal, G., Lange, H., Fitzsimons, E., Tolmie, J., Lill, R., & Bishop, D. F. (2000). Human ABC7 transporter: Gene structure and mutation causing X-linked sideroblastic anemia with ataxia (XLSA/A) with disruption of cytosolic iron-sulfur protein maturation. *Blood*, *96*, 3256-3264.

Belevich, I., Verkhovsky, M. I., & Wikström, M. (2006). Proton-coupled electron transfer drives the proton pump of cytochrome c oxidase. *Nature*, *440*(7085), 829-832.

Bernard, D. G., Cheng, Y., Zhao, Y., & Balk, J. (2009). An allelic mutant series of ATM3 reveals its key role in the biogenesis of cytosolic iron-sulfur proteins in Arabidopsis. *Plant Physiol*, *151*(2), 590-602.

Bertani, G. (1951). Studies on lysogenesis. I. The mode of phage liberation by lysogenic Escherichia coli. *J Bacteriol*, *62*(3), 293-300.

Biederbick, A., Rose, S., & Elsässer, H. P. (1999). A human intracellular apyrase-like protein, LALP70, localizes to lysosomal/autophagic vacuoles. *J Cell Sci*, *112 (Pt 15)*, 2473-2484.

Biederbick, A., Stehling, O., Rösser, R., Niggemeyer, B., Nakai, Y., Elsässer, H. P., & Lill, R. (2006). Role of human mitochondrial Nfs1 in cytosolic iron-sulfur protein biogenesis and iron regulation. *Mol. Cell. Biol.*, *26*, 5675-5687.

Birch-Machin, M. A., & Turnbull, D. M. (2001). Assaying mitochondrial respiratory complex activity in mitochondria isolated from human cells and tissues. *Methods Cell Biol*, *65*, 97-117.

Bissell, D. M., Anderson, K. E., & Bonkovsky, H. L. (2017). Porphyria. *N Engl J Med*, *377*(9), 862-872.

Bjellqvist, B., Sanchez, J. C., Pasquali, C., Ravier, F., Paquet, N., Frutiger, S., . . . Hochstrasser, D. (1993). Micropreparative two-dimensional electrophoresis allowing the separation of samples containing milligram amounts of proteins. *Electrophoresis*, *14*, 1375-1378.

Boultwood, J., Pellagatti, A., Nikpour, M., Pushkaran, B., Fidler, C., Cattan, H., . . . Wainscoat, J. S. (2008). The role of the iron transporter ABCB7 in refractory anemia with ring sideroblasts [Research Support, Non-U.S. Gov't]. *PloS one*, *3*(4), e1970.

Brancaccio, D., Gallo, A., Mikolajczyk, M., Zovo, K., Palumaa, P., Novellino, E., . . . Banci, L. (2014). Formation of [4Fe-4S] clusters in the mitochondrial iron-sulfur cluster assembly machinery [Research Support, Non-U.S. Gov't]. *Journal of the American Chemical Society*, *136*(46), 16240-16250.

Braymer, J. J., Freibert, S. A., Rakwalska-Bange, M., & Lill, R. (2021). Mechanistic concepts of iron-sulfur protein biogenesis in Biology. *Biochim Biophys Acta Mol Cell Res*, *1868*(1), 118863.

Brayton, K. A., Chen, Z., Zhou, G., Nagy, P. L., Gavalas, A., Trent, J. M., . . . Zalkin, H. (1994). Two genes for de novo purine nucleotide synthesis on human chromosome 4 are closely linked and divergently transcribed. *J Biol Chem*, *269*(7), 5313-5321.

Burden, A. E., Wu, C., Dailey, T. A., Busch, J. L., Dhawan, I. K., Rose, J. P., . . . Dailey, H. A. (1999). Human ferrochelatase: crystallization, characterization of the [2Fe-2S] cluster and determination that the enzyme is a homodimer. *Biochim Biophys Acta*, *1435*(1-2), 191-197.

Camaschella, C., Campanella, A., De Falco, L., Boschetto, L., Merlini, R., Silvestri, L., . . . Iolascon, A. (2007). The human counterpart of zebrafish shiraz shows

sideroblastic-like microcytic anemia and iron overload. *Blood*, *110*(4), 1353-1358.

Camponeschi, F., Prusty, N. R., Heider, S. A. E., Ciofi-Baffoni, S., & Banci, L. (2020). GLRX3 Acts as a [2Fe-2S] Cluster Chaperone in the Cytosolic Iron-Sulfur Assembly Machinery Transferring [2Fe-2S] Clusters to NUBP1. *J Am Chem Soc*, *142*(24), 10794-10805.

Caughey, W. S., Smythe, G. A., O'Keeffe, D. H., Maskasky, J. E., & Smith, M. I. (1975). Heme A of cytochrome c oxicase. Structure and properties: comparisons with hemes B, C, and S and derivatives. *J Biol Chem*, *250*(19), 7602-7622.

Cavadini, P., Biasiotto, G., Poli, M., Levi, S., Verardi, R., Zanella, I., . . . Arosio, P. (2007). RNA silencing of the mitochondrial ABCB7 transporter in HeLa cells causes an iron-deficient phenotype with mitochondrial iron overload. *Blood*, *109*(8), 3552-3559.

Cazzola, M., & Invernizzi, R. (2011). Ring sideroblasts and sideroblastic anemias [Comment Editorial Research Support, Non-U.S. Gov't]. *Haematologica*, *96*(6), 789-792.

Chambers, I. G., Willoughby, M. M., Hamza, I., & Reddi, A. R. (2021). One ring to bring them all and in the darkness bind them: The trafficking of heme without deliverers. *Biochim Biophys Acta Mol Cell Res*, *1868*(1), 118881.

Chen, W., Dailey, H. A., & Paw, B. H. (2010). Ferrochelatase forms an oligomeric complex with mitoferrin-1 and Abcb10 for erythroid heme biosynthesis. *Blood*, *116*(4), 628-630.

Chiabrando, D., Bertino, F., & Tolosano, E. (2020). Hereditary Ataxia: A Focus on Heme Metabolism and Fe-S Cluster Biogenesis. *Int J Mol Sci*, *21*(11).

Chiabrando, D., Marro, S., Mercurio, S., Giorgi, C., Petrillo, S., Vinchi, F., . . . Tolosano, E. (2012). The mitochondrial heme exporter FLVCR1b mediates erythroid differentiation. *J Clin Invest*, *122*(12), 4569-4579.

Chu, G., Hayakawa, H., & Berg, P. (1987). Electroporation for the efficient transfection of mammalian cells with DNA. *Nucleic Acids Res*, *15*(3), 1311-1326.

Correia, M. A., Sinclair, P. R., & De Matteis, F. (2011). Cytochrome P450 regulation: the interplay between its heme and apoprotein moieties in synthesis, assembly, repair, and disposal. *Drug Metab Rev*, *43*(1), 1-26.

Crooks, D. R., Jeong, S. Y., Tong, W. H., Ghosh, M. C., Olivierre, H., Haller, R. G., & Rouault, T. A. (2012). Tissue specificity of a human mitochondrial disease: differentiation-enhanced mis-splicing of the Fe-S scaffold gene ISCU renders patient cells more sensitive to oxidative stress in ISCU myopathy [Research Support, N.I.H., Extramural Research Support, N.I.H., Intramural Research

Support, U.S. Gov't, Non-P.H.S.]. *The Journal of biological chemistry*, *287*(48), 40119-40130.

Csere, P., Lill, R., & Kispal, G. (1998). Identification of a human mitochondrial ABC transporter, the functional orthologue of yeast Atm1p. *FEBS Lett.*, *441*, 266-270.

D'Hooghe, M., Selleslag, D., Mortier, G., Van Coster, R., Vermeersch, P., Billiet, J., & Bekri, S. (2012). X-linked sideroblastic anemia and ataxia: a new family with identification of a fourth ABCB7 gene mutation [Case Reports]. *European journal of paediatric neurology : EJPN : official journal of the European Paediatric Neurology Society*, *16*(6), 730-735.

Dailey, H. A., Dailey, T. A., Wu, C. K., Medlock, A. E., Wang, K. F., Rose, J. P., & Wang, B. C. (2000). Ferrochelatase at the millennium: structures, mechanisms and [2Fe-2S] clusters. *Cell Mol Life Sci*, *57*(13-14), 1909-1926.

Dawson, R. J., & Locher, K. P. (2006). Structure of a bacterial multidrug ABC transporter [Research Support, Non-U.S. Gov't]. *Nature*, *443*(7108), 180-185.

Dean, L., & Kane, M. (2012). Capecitabine Therapy and DPYD Genotype. In V. M. Pratt, S. A. Scott, M. Pirmohamed, B. Esquivel, M. S. Kane, B. L. Kattman, & A. J. Malheiro (Eds.), *Medical Genetics Summaries*. National Center for Biotechnology Information (US).

Dlouhy, A. C., & Outten, C. E. (2013). The iron metallome in eukaryotic organisms. *Met Ions Life Sci*, *12*, 241-278.

Donegan, R. K., Moore, C. M., Hanna, D. A., & Reddi, A. R. (2019). Handling heme: The mechanisms underlying the movement of heme within and between cells. *Free Radic Biol Med*, *133*, 88-100.

Drapier, J. C., & Hibbs, J. B., Jr. (1996). Aconitases: a class of metalloproteins highly sensitive to nitric oxide synthesis. *Methods Enzymol*, *269*, 26-36.

Dutt, S., Hamza, I., & Bartnikas, T. B. (2022). Molecular Mechanisms of Iron and Heme Metabolism. *Annu Rev Nutr*, *42*, 311-335.

Ellinghaus, T. L., Marcellino, T., Srinivasan, V., Lill, R., & Kühlbrandt, W. (2021). Conformational changes in the yeast mitochondrial ABC transporter Atm1 during the transport cycle. *Sci Adv*, *7*(52), eabk2392.

Fan, C., & Rees, D. C. (2022). Glutathione binding to the plant AtAtm3 transporter and implications for the conformational coupling of ABC transporters. *Elife*, *11*.

Fenton, H. J. H. (1876). On a new reaction of tartaric acid. *Chem News*, *33*(190), 190.

Ferguson-Miller, S., & Babcock, G. T. (1996). Heme/Copper Terminal Oxidases. *Chem Rev*, *96*(7), 2889-2908.

Fleming, M. D., & Hamza, I. (2012). Mitochondrial heme: an exit strategy at last. *J Clin Invest*, *122*(12), 4328-4330.

Frey, A. G., Palenchar, D. J., Wildemann, J. D., & Philpott, C. C. (2016). A Glutaredoxin.BolA Complex Serves as an Iron-Sulfur Cluster Chaperone for the Cytosolic Cluster Assembly Machinery. *J Biol Chem*, *291*(43), 22344-22356.

Furuyama K, Kaneko K (2018). Iron metabolism in erythroid cells and patients with congenital sideroblastic anemia. *Int J Hematol,* 107(1):44-54.

Gari, K., Leon Ortiz, A. M., Borel, V., Flynn, H., Skehel, J. M., & Boulton, S. J. (2012). MMS19 Links Cytoplasmic Iron-Sulfur Cluster Assembly to DNA Metabolism. *Science*, *337*(6091), 243-245.

Gell, D. A. (2018). Structure and function of haemoglobins. *Blood Cells Mol Dis*, *70*, 13-42.

Gnandt, E., Dörner, K., Strampraad, M. F. J., de Vries, S., & Friedrich, T. (2016). The multitude of iron-sulfur clusters in respiratory complex I. *Biochim Biophys Acta*, *1857*(8), 1068-1072.

Gomes, C. M., & Santos, R. (2013). Neurodegeneration in Friedreich's ataxia: from defective frataxin to oxidative stress. *Oxid Med Cell Longev*, *2013*, 487534.

González-Cabo, P., Bolinches-Amorós, A., Cabello, J., Ros, S., Moreno, S., Baylis, H. A., . . . Vázquez-Manrique, R. P. (2011). Disruption of the ATP-binding cassette B7 (ABTM-1/ABCB7) induces oxidative stress and premature cell death in Caenorhabditis elegans. *J Biol Chem*, *286*(24), 21304-21314.

Goyal, M. M., & Basak, A. (2010). Human catalase: looking for complete identity. *Protein Cell*, *1*(10), 888-897.

Guengerich, F. P., Waterman, M. R., & Egli, M. (2016). Recent Structural Insights into Cytochrome P450 Function. *Trends Pharmacol Sci*, *37*(8), 625-640.

Gunshin, H., Mackenzie, B., Berger, U. V., Gunshin, Y., Romero, M. F., Boron, W. F., . . . Hediger, M. A. (1997). Cloning and characterization of a mammalian proton-coupled metal-ion transporter. *Nature*, *388*(6641), 482-488.

Góth, L., & Nagy, T. (2013). Inherited catalase deficiency: is it benign or a factor in various age related disorders? *Mutat Res*, *753*(2), 147-154.

Hamza, I., & Dailey, H. A. (2012). One ring to rule them all: trafficking of heme and heme synthesis intermediates in the metazoans. *Biochim Biophys Acta*, *1823*(9), 1617-1632.

Harrison, P. M., & Arosio, P. (1996). The ferritins: molecular properties, iron storage function and cellular regulation. *Biochim Biophys Acta*, *1275*(3), 161-203.

Hatefi, Y., & Stiggall, D. L. (1978). Preparation and properties of succinate: ubiquinone oxidoreductase (complex II). *Methods Enzymol*, *53*, 21-27.

Haunhorst, P., Hanschmann, E. M., Brautigam, L., Stehling, O., Hoffmann, B., Muhlenhoff, U., . . . Lillig, C. H. (2013). Crucial function of vertebrate glutaredoxin 3 (PICOT) in iron homeostasis and hemoglobin maturation [Research Support, Non-U.S. Gov't]. *Molecular biology of the cell*, *24*(12), 1895-1903.

Hausladen, A., & Fridovich, I. (1996). Measuring nitric oxide and superoxide: rate constants for aconitase reactivity. *Methods Enzymol*, *269*, 37-41.

Hederstedt, L. (2012). Heme A biosynthesis. *Biochim Biophys Acta*, *1817*(6), 920-927.

Horáková, E., Changmai, P., Paris, Z., Salmon, D., & Lukeš, J. (2015). Simultaneous depletion of Atm and Mdl rebalances cytosolic Fe-S cluster assembly but not heme import into the mitochondrion of Trypanosoma brucei. *Febs j*, *282*(21), 4157-4175.

Huang, M. L., Becker, E. M., Whitnall, M., Rahmanto, Y. S., Ponka, P., & Richardson, D. R. (2009). Elucidation of the mechanism of mitochondrial iron loading in Friedreich's ataxia by analysis of a mouse mutant. *Proc Natl Acad Sci U S A*, *106*(38), 16381-16386.

Iwahana, H., Oka, J., Mizusawa, N., Kudo, E., Ii, S., Yoshimoto, K., . . . Itakura, M. (1993). Molecular cloning of human amidophosphoribosyltransferase. *Biochem Biophys Res Commun*, *190*(1), 192-200.

Iwai, K. (2019). Regulation of cellular iron metabolism: Iron-dependent degradation of IRP by SCF(FBXL5) ubiquitin ligase. *Free Radic Biol Med*, *133*, 64-68.

Jiang, Z. Y., Woollard, A. C., & Wolff, S. P. (1990). Hydrogen peroxide production during experimental protein glycation. *FEBS Lett*, *268*(1), 69-71.

Kauppinen, R. (2005). Porphyrias. *Lancet*, *365*(9455), 241-252.

Kim, H. J., Khalimonchuk, O., Smith, P. M., & Winge, D. R. (2012). Structure, function, and assembly of heme centers in mitochondrial respiratory complexes. *Biochim Biophys Acta*, *1823*(9), 1604-1616.

Kim, Y. C., & Hummer, G. (2012). Proton-pumping mechanism of cytochrome c oxidase: a kinetic master-equation approach. *Biochim Biophys Acta*, *1817*(4), 526-536.

Kispal, G., Csere, P., Guiard, B., & Lill, R. (1997). The ABC transporter Atm1p is required for mitochondrial iron homeostasis. *FEBS Lett.*, *418*, 346-350.

Kispal, G., Csere, P., Prohl, C., & Lill, R. (1999). The mitochondrial proteins Atm1p and Nfs1p are essential for biogenesis of cytosolic Fe/S proteins. *EMBO J*, *18*(14), 3981-3989.

Knutson, M. D. (2007). Steap proteins: implications for iron and copper metabolism. *Nutr Rev*, *65*(7), 335-340.

Konstantinov, A. A., Siletsky, S., Mitchell, D., Kaulen, A., & Gennis, R. B. (1997). The roles of the two proton input channels in cytochrome c oxidase from Rhodobacter sphaeroides probed by the effects of site-directed mutations on time-resolved electrogenic intraprotein proton transfer. *Proc Natl Acad Sci U S A*, *94*(17), 9085-9090.

Kranz, R. G., Richard-Fogal, C., Taylor, J. S., & Frawley, E. R. (2009). Cytochrome c biogenesis: mechanisms for covalent modifications and trafficking of heme and for heme-iron redox control. *Microbiol Mol Biol Rev*, *73*(3), 510-528, Table of Contents.

Kruse, I., Maclean, A. E., Hill, L., & Balk, J. (2018). Genetic dissection of cyclic pyranopterin monophosphate biosynthesis in plant mitochondria. *Biochem J*, *475*(2), 495-509.

Kushnir, S., Babiychuck, E., Storozhenko, S., Davey, M. W., Papenbrock, J., De Rycke, R., . . . Van Montagu, M. (2001). A mutation of the mitochondrial ABC transporter Sta1 leads to dwarfism and chlorosis in the Arabidopsis mutant starik. *Plant Cell*, *13*, 89-100.

Kyhse-Andersen, J. (1984). Electroblotting of multiple gels: a simple apparatus without buffer tank for rapid transfer of proteins from polyacrylamide to nitrocellulose. *J Biochem Biophys Methods*, *10*(3-4), 203-209.

Laemmli, U. K. (1970). Cleavage of structural proteins during the assembly of the head of bacteriophage T4. *Nature*, *227*(5259), 680-685.

Li, J., & Cowan, J. A. (2015). Glutathione-coordinated [2Fe-2S] cluster: a viable physiological substrate for mitochondrial ABCB7 transport. *Chemical communications*, *51*(12), 2253-2255.

Li, K., Besse, E. K., Ha, D., Kovtunovych, G., & Rouault, T. A. (2008). Iron-dependent regulation of frataxin expression: implications for treatment of Friedreich ataxia. *Hum Mol Genet*, *17*(15), 2265-2273.

Li, P., Hendricks, A. L., Wang, Y., Villones, R. L. E., Lindkvist-Petersson, K., Meloni, G., . . . Gourdon, P. (2022). Structures of Atm1 provide insight into [2Fe-2S] cluster export from mitochondria. *Nat Commun*, *13*(1), 4339.

Lill, R. (2020). From the discovery to molecular understanding of cellular iron-sulfur protein biogenesis. *Biol Chem*, *401*(6-7), 855-876.

Lill, R., & Freibert, S. A. (2020). Mechanisms of Mitochondrial Iron-Sulfur Protein Biogenesis. *Annu Rev Biochem*, *89*, in press.

Lill, R., Srinivasan, V., & Muhlenhoff, U. (2014). The role of mitochondria in cytosolic-nuclear iron-sulfur protein biogenesis and in cellular iron regulation [Research Support, Non-U.S. Gov't]. *Current opinion in microbiology*, *22*, 111-119.

Liu, G., Anderson, Y., Camaschella, G., Chang, C., Nie, Y. (2016). Functional Analysis of GLRX5 Mutants Reveals Distinct Functionalities of GLRX5 Protein. *J Cell Biochem.*; 117(1):207-17.

Liu, G., Sil, D., Maio, N., Tong, W. H., Bollinger, J. M., Jr., Krebs, C., & Rouault, T. A. (2020). Heme biosynthesis depends on previously unrecognized acquisition of iron-sulfur cofactors in human amino-levulinic acid dehydratase. *Nat Commun*, *11*(1), 6310.

Maguire, A., Hellier, K., Hammans, S., & May, A. (2001). X-linked cerebellar ataxia and sideroblastic anaemia associated with a missense mutation in the ABC7 gene predicting V411L [Research Support, Non-U.S. Gov't]. *British journal of haematology*, *115*(4), 910-917.

Maio, N., Kim, K. S., Holmes-Hampton, G., Singh, A., & Rouault, T. A. (2019). Dimeric ferrochelatase bridges ABCB7 and ABCB10 homodimers in an architecturally defined molecular complex required for heme biosynthesis. *Haematologica*, *104*(9), 1756-1767.

Maio, N., Singh, A., Uhrigshardt, H., Saxena, N., Tong, W. H., & Rouault, T. A. (2014). Cochaperone binding to LYR motifs confers specificity of iron sulfur cluster delivery. *Cell Metab*, *19*(3), 445-457.

Malcovati, L., Della Porta, M. G., Pietra, D., Boveri, E., Pellagatti, A., Gallì, A., . . . Cazzola, M. (2009). Molecular and clinical features of refractory anemia with ringed sideroblasts associated with marked thrombocytosis. *Blood*, *114*(17), 3538-3545.

Manikandan, P., & Nagini, S. (2018). Cytochrome P450 Structure, Function and Clinical Significance: A Review. *Curr Drug Targets*, *19*(1), 38-54.

Martelli, A., Schmucker, S., Reutenauer, L., Mathieu, J. R. R., Peyssonnaux, C., Karim, Z., . . . Puccio, H. (2015). Iron regulatory protein 1 sustains mitochondrial iron loading and function in frataxin deficiency. *Cell Metab*, *21*(2), 311-323.

Martelli, A., Wattenhofer-Donzé, M., Schmucker, S., Bouvet, S., Reutenauer, L., & Puccio, H. (2007). Frataxin is essential for extramitochondrial Fe-S cluster proteins in mammalian tissues. *Hum Mol Genet*, *16*, 2651-2658.

Martinez, M., Fendley, G. A., Saxberg, A. D., & Zoghbi, M. E. (2020). Stimulation of the human mitochondrial transporter ABCB10 by zinc-mesoporphrin. *PLoS One*, *15*(11), e0238754.

Mayerhöfer, T. G., Pahlow, S., & Popp, J. (2020). The Bouguer-Beer-Lambert Law: Shining Light on the Obscure. *Chemphyschem*, *21*(18), 2029-2046.

Mayle, K. M., Le, A. M., & Kamei, D. T. (2012). The intracellular trafficking pathway of transferrin. *Biochim Biophys Acta*, *1820*(3), 264-281.

McCarthy, E. L., & Booker, S. J. (2017). Destruction and reformation of an iron-sulfur cluster during catalysis by lipoyl synthase. *Science*, *358*(6361), 373-377.

McKay, R., Druyan, R., Getz, G. S., & Rabinowitz, M. (1969). Intramitochondrial localization of delta-aminolaevulate synthetase and ferrochelatase in rat liver. *Biochem J*, *114*(3), 455-461.

Medlock, A., Swartz, L., Dailey, T. A., Dailey, H. A., & Lanzilotta, W. N. (2007). Substrate interactions with human ferrochelatase. *Proc Natl Acad Sci U S A*, *104*(6), 1789-1793.

Mendel, R. R. (2013). The molybdenum cofactor. *J Biol Chem*, *288*(19), 13165-13172.

Miao, R., Kim, H., Koppolu, U. M., Ellis, E. A., Scott, R. A., & Lindahl, P. A. (2009). Biophysical characterization of the iron in mitochondria from Atm1p-depleted Saccharomyces cerevisiae. *Biochemistry*, *48*(40), 9556-9568.

Miwa, S., Treumann, A., Bell, A., Vistoli, G., Nelson, G., Hay, S., & von Zglinicki, T. (2016). Carboxylesterase converts Amplex red to resorufin: Implications for mitochondrial H2O2 release assays. *Free Radic Biol Med*, *90*, 173-183.

Miyake, A., Higashijima, S., Kobayashi, D., Narita, T., Jindo, T., Setiamarga, D. H., . . . Takeda, H. (2008). Mutation in the abcb7 gene causes abnormal iron and fatty acid metabolism in developing medaka fish. *Dev Growth Differ*, *50*(9), 703-716.

Moe, E., Silveira, C. M., Zuccarello, L., Rollo, F., Stelter, M., De Bonis, S., . . . Todorovic, S. (2022). Human endonuclease III/NTH1: focusing on the [4Fe-4S] cluster and the N-terminal domain. *Chem Commun (Camb)*, *58*(90), 12568-12571.

Moraes, C. T., Diaz, F., & Barrientos, A. (2004). Defects in the biosynthesis of mitochondrial heme c and heme a in yeast and mammals. *Biochim Biophys Acta*, *1659*(2-3), 153-159.

Moroishi, T., Yamauchi, T., Nishiyama, M., & Nakayama, K. I. (2014). HERC2 targets the iron regulator FBXL5 for degradation and modulates iron metabolism. *J Biol Chem*, *289*(23), 16430-16441.

Muckenthaler, M. U., Rivella, S., Hentze, M. W., & Galy, B. (2017). A Red Carpet for Iron Metabolism. *Cell*, *168*(3), 344-361.

Munro, H. N., & Linder, M. C. (1978). Ferritin: structure, biosynthesis, and role in iron metabolism. *Physiol Rev*, *58*(2), 317-396.

Mühlenhoff, U., Hoffmann, B., Richter, N., Rietzschel, N., Spantgar, F., Stehling, O., . . . Lill, R. (2015). Compartmentalization of iron between mitochondria and the cytosol and its regulation. *European journal of cell biology*, *94*(7-9), 292-308.

Navarro-Sastre, A., Tort, F., Stehling, O., Uzarska, M. A., Arranz, J. A., Del Toro, M., . . . Lill, R. (2011). A fatal mitochondrial disease is associated with defective NFU1

function in the maturation of a subset of mitochondrial Fe-S proteins [Research Support, Non-U.S. Gov't]. *American journal of human genetics*, *89*(5), 656-667.

Netz, D. J., Pierik, A. J., Stümpfig, M., Mühlenhoff, U., & Lill, R. (2007). The Cfd1-Nbp35 complex acts as a scaffold for iron-sulfur protein assembly in the yeast cytosol. *Nat Chem Biol*, *3*(5), 278-286.

Netz, D. J., Stümpfig, M., Doré, C., Mühlenhoff, U., Pierik, A. J., & Lill, R. (2010). Tah18 transfers electrons to Dre2 in cytosolic iron-sulfur protein biogenesis. *Nat Chem Biol*, *6*(10), 758-765.

Neuspiel, M., Schauss, A. C., Braschi, E., Zunino, R., Rippstein, P., Rachubinski, R. A., . . . McBride, H. M. (2008). Cargo-selected transport from the mitochondria to peroxisomes is mediated by vesicular carriers. *Curr Biol*, *18*(2), 102-108.

Nikpour, M., Scharenberg, C., Liu, A., Conte, S., Karimi, M., Mortera-Blanco, T., . . . Hellstrom-Lindberg, E. (2013). The transporter ABCB7 is a mediator of the phenotype of acquired refractory anemia with ring sideroblasts [Research Support, Non-U.S. Gov't]. *Leukemia*, *27*(4), 889-896.

Ostermeier, C., & Michel, H. (1997). Crystallization of membrane proteins. *Curr Opin Struct Biol*, *7*(5), 697-701.

Ou, P., & Wolff, S. P. (1996). A discontinuous method for catalase determination at 'near physiological' concentrations of H2O2 and its application to the study of H2O2 fluxes within cells. *J Biochem Biophys Methods*, *31*(1-2), 59-67.

Pagon, R. A., Bird, T. D., Detter, J. C., & Pierce, I. (1985). Hereditary sideroblastic anemia: an X-linked recessive disorder. *J. Med. Gen.*, *22*, 267-273.

Pandey, A., Pain, J., Dziuba, N., Pandey, A. K., Dancis, A., Lindahl, P. A., & Pain, D. (2018). Mitochondria Export Sulfur Species Required for Cytosolic tRNA Thiolation. *Cell Chem Biol*, *25*(6), 738-748 e733.

Pandey, A. K., Pain, J., Dancis, A., & Pain, D. (2019). Mitochondria export iron-sulfur and sulfur intermediates to the cytoplasm for iron-sulfur cluster assembly and tRNA thiolation in yeast. *J Biol Chem*, *294*(24), 9489-9502.

Parkinson, M. H., Boesch, S., Nachbauer, W., Mariotti, C., & Giunti, P. (2013). Clinical features of Friedreich's ataxia: classical and atypical phenotypes. *J Neurochem*, *126 Suppl 1*, 103-117.

Patel, S. J., Frey, A. G., Palenchar, D. J., Achar, S., Bullough, K. Z., Vashisht, A., . . . Philpott, C. C. (2019). A PCBP1-BolA2 chaperone complex delivers iron for cytosolic [2Fe-2S] cluster assembly. *Nat Chem Biol*, *15*(9), 872-881.

Paul, V. D., & Lill, R. (2015). Biogenesis of cytosolic and nuclear iron-sulfur proteins and their role in genome stability [Review]. *Biochimica et biophysica acta*, *1853*(6), 1528-1539.

Pearson, S. A., Wachnowsky, C., & Cowan, J. A. (2020). Defining the mechanism of the mitochondrial Atm1p [2Fe-2S] cluster exporter. *Metallomics*, *12*(6), 902-915.

Peoc'h, K., Nicolas, G., Schmitt, C., Mirmiran, A., Daher, R., Lefebvre, T., . . . Puy, H. (2019). Regulation and tissue-specific expression of δ-aminolevulinic acid synthases in non-syndromic sideroblastic anemias and porphyrias. *Mol Genet Metab*, *128*(3), 190-197.

Phillips, J. D. (2019). Heme biosynthesis and the porphyrias. *Mol Genet Metab*, *128*(3), 164-177.

Pondarre, C., Antiochos, B. B., Campagna, D. R., Clarke, S. L., Greer, E. L., Deck, K. M., . . . Fleming, M. D. (2006). The mitochondrial ATP-binding cassette transporter Abcb7 is essential in mice and participates in cytosolic iron-sulphur cluster biogenesis. *Hum. Mol. Genet.*, *15*, 953-964.

Pondarre, C., Campagna, D. R., Antiochos, B., Sikorski, L., Mulhern, H., & Fleming, M. D. (2007). Abcb7, the gene responsible for X-linked sideroblastic anemia with ataxia, is essential for hematopoiesis. *Blood*, *109*(8), 3567-3569.

Popović, D. M. (2013). Current advances in research of cytochrome c oxidase. *Amino Acids*, *45*(5), 1073-1087.

Porter, D. J., & Spector, T. (1993). Dihydropyrimidine dehydrogenase. Kinetic mechanism for reduction of uracil by NADPH. *The Journal of biological chemistry*, *268*(26), 19321-19327.

Putnam, C. D., Arvai, A. S., Bourne, Y., & Tainer, J. A. (2000). Active and inhibited human catalase structures: ligand and NADPH binding and catalytic mechanism. *J Mol Biol*, *296*(1), 295-309.

Pérez-Mejías, G., Olloqui-Sariego, J. L., Guerra-Castellano, A., Díaz-Quintana, A., Calvente, J. J., Andreu, R., . . . Díaz-Moreno, I. (2020). Physical contact between cytochrome c(1) and cytochrome c increases the driving force for electron transfer. *Biochim Biophys Acta Bioenerg*, 148277.

Qi, W., Li, J., & Cowan, J. A. (2014). A structural model for glutathione-complexed iron-sulfur cluster as a substrate for ABCB7-type transporters [Research Support, N.I.H., Extramural]. *Chemical communications*, *50*(29), 3795-3798.

Reddi, A. R., & Hamza, I. (2016). Heme Mobilization in Animals: A Metallolipid's Journey. *Acc Chem Res*, *49*(6), 1104-1110.

Rhee, H. W., Zou, P., Udeshi, N. D., Martell, J. D., Mootha, V. K., Carr, S. A., & Ting, A. Y. (2013). Proteomic mapping of mitochondria in living cells via spatially restricted enzymatic tagging. *Science*, *339*(6125), 1328-1331.

Richardson, D. R., & Ponka, P. (1997). The molecular mechanisms of the metabolism and transport of iron in normal and neoplastic cells. *Biochim Biophys Acta*, *1331*(1), 1-40.

Robinson, K. M., von Kieckebusch-Guck, A., & Lemire, B. D. (1991). Isolation and characterization of a Saccharomyces cerevisiae mutant disrupted for the succinate dehydrogenase flavoprotein subunit. *J. Biol. Chem.*, *266*, 21347-21350.

Rutter, J., Winge, D. R., & Schiffman, J. D. (2010). Succinate dehydrogenase - Assembly, regulation and role in human disease. *Mitochondrion*, *10*(4), 393-401.

Salahudeen, A. A., & Bruick, R. K. (2009). Maintaining Mammalian iron and oxygen homeostasis: sensors, regulation, and cross-talk. *Ann N Y Acad Sci*, *1177*, 30-38.

San Francisco, B., Bretsnyder, E. C., & Kranz, R. G. (2013). Human mitochondrial holocytochrome c synthase's heme binding, maturation determinants, and complex formation with cytochrome c. *Proc Natl Acad Sci U S A*, *110*(9), E788-797.

Sanaker, P. S., Toompuu, M., Hogan, V. E., He, L., Tzoulis, C., Chrzanowska-Lightowlers, Z. M., . . . Bindoff, L. A. (2010). Differences in RNA processing underlie the tissue specific phenotype of ISCU myopathy [Case Reports Research Support, Non-U.S. Gov't]. *Biochimica et biophysica acta*, *1802*(6), 539-544.

Sanchez, M., Galy, B., Schwanhaeusser, B., Blake, J., Bähr-Ivacevic, T., Benes, V., . . . Hentze, M. W. (2011). Iron regulatory protein-1 and -2: transcriptome-wide definition of binding mRNAs and shaping of the cellular proteome by iron regulatory proteins. *Blood*, *118*(22), e168-179.

Schnackerz, K. D., Dobritzsch, D., Lindqvist, Y., & Cook, P. F. (2004). Dihydropyrimidine dehydrogenase: a flavoprotein with four iron-sulfur clusters [Research Support, Non-U.S. Gov't]. *Biochimica et biophysica acta*, *1701*(1-2), 61-74.

Schumann, U., & Subramani, S. (2008). Special delivery from mitochondria to peroxisomes. *Trends Cell Biol*, *18*(6), 253-256.

Schägger, H. (2006). Tricine-SDS-PAGE. *Nat Protoc*, *1*(1), 16-22.

Scientific, T. F. (2020). *Pierce BCA Protein Assay Kit: User Manual*. Retrieved 22.06.2023 from https://www.thermofisher.com/document-connect/document-connect.html?url=https://assets.thermofisher.com/TFS-

Assets%2FLSG%2Fmanuals%2FMAN0011430_Pierce_BCA_Protein_Asy_UG.pdf

Shaw, G. C., Cope, J. J., Li, L., Corson, K., Hersey, C., Ackermann, G. E., . . . Paw, B. H. (2006). Mitoferrin is essential for erythroid iron assimilation. *Nature*, *440*(7080), 96-100.

Shaw, G. C., Langer, N. B., Wang, Y., Li, L., Kaplan, J., Bloomer, J. R., & Paw, B. H. (2006). Abnormal Expression of Human Mitoferrin (SLC25A37) Is Associated with a Variant of Erythropoietic Protoporphyria [Meeting abstract]. *Blood*, *108*(11), 3.

Sheftel, A. D., & Lill, R. (2009). The power plant of the cell is also a smithy: the emerging role of mitochondria in cellular iron homeostasis. *Ann Med*, *41*(2), 82-99.

Sheftel, A. D., Richardson, D. R., Prchal, J., & Ponka, P. (2009). Mitochondrial iron metabolism and sideroblastic anemia. *Acta Haematol*, *122*(2-3), 120-133.

Sheftel, A. D., Stehling, O., Pierik, A. J., Elsasser, H. P., Muhlenhoff, U., Webert, H., . . . Lill, R. (2010). Humans possess two mitochondrial ferredoxins, Fdx1 and Fdx2, with distinct roles in steroidogenesis, heme, and Fe/S cluster biosynthesis [Research Support, Non-U.S. Gov't]. *Proceedings of the National Academy of Sciences of the United States of America*, *107*(26), 11775-11780.

Sheftel, A. D., Wilbrecht, C., Stehling, O., Niggemeyer, B., Elsasser, H. P., Mühlenhoff, U., & Lill, R. (2012). The human mitochondrial ISCA1, ISCA2, and IBA57 proteins are required for [4Fe-4S] protein maturation. *Mol Biol Cell*, *23*(7), 1157-1166.

Shimada, Y., Okuno, S., Kawai, A., Shinomiya, H., Saito, A., Suzuki, M., . . . Takahashi, E. (1998). Cloning and chromosomal mapping of a novel ABC transporter gene (hABC7), a candidate for X-linked sideroblastic anemia with spinocerebellar ataxia. *J Hum Genet*, *43*(2), 115-122.

Shirihai, O. S., Gregory, T., Yu, C., Orkin, S. H., & Weiss, M. J. (2000). ABC-me: a novel mitochondrial transporter induced by GATA-1 during erythroid differentiation. *EMBO J.*, *19*, 2492-2502.

Sikorska, K., Bernat, A., & Wroblewska, A. (2016). Molecular pathogenesis and clinical consequences of iron overload in liver cirrhosis. *Hepatobiliary Pancreat Dis Int*, *15*(5), 461-479.

Sinclair, J., & Hamza, I. (2015). Lessons from bloodless worms: heme homeostasis in C. elegans. *Biometals*, *28*(3), 481-489.

Sipos, K., Lange, H., Fekete, Z., Ullmann, P., Lill, R., & Kispal, G. (2002). Maturation of cytosolic iron-sulfur proteins requires glutathione. *J. Biol. Chem.*, *277*, 26944-26949.

Smith, P. M., Fox, J. L., & Winge, D. R. (2012). Biogenesis of the cytochrome bc(1) complex and role of assembly factors. *Biochim Biophys Acta*, *1817*(2), 276-286.

Srere, P. A. (1963). CITRYL-COA. AN SUBSTRATE FOR THE CITRATE-CLEAVAGE ENZYME. *Biochim Biophys Acta*, *73*, 523-525.

Srinivasan, V., Netz, D. J., Webert, H., Mascarenhas, J., Pierik, A. J., Michel, H., & Lill, R. (2007). Structure of the yeast WD40 domain protein Cia1, a component acting late in iron-sulfur protein biogenesis. *Structure*, *15*(10), 1246-1257.

Srinivasan, V., Pierik, A. J., & Lill, R. (2014). Crystal structures of nucleotide-free and glutathione-bound mitochondrial ABC transporter Atm1 [Research Support, Non-U.S. Gov't]. *Science*, *343*(6175), 1137-1140.

Srour, B., Gervason, S., Hoock, M. H., Monfort, B., Want, K., Larkem, D., . . . D'Autréaux, B. (2022). Iron Insertion at the Assembly Site of the ISCU Scaffold Protein Is a Conserved Process Initiating Fe-S Cluster Biosynthesis. *J Am Chem Soc*, *144*(38), 17496-17515.

Stehling, O., Jeoung, J. H., Freibert, S. A., Paul, V. D., Banfer, S., Niggemeyer, B., . . . Lill, R. (2018). Function and crystal structure of the dimeric P-loop ATPase CFD1 coordinating an exposed [4Fe-4S] cluster for transfer to apoproteins. *Proc Natl Acad Sci U S A*, *115*(39), E9085-E9094.

Stehling, O., & Lill, R. (2013). The role of mitochondria in cellular iron-sulfur protein biogenesis: mechanisms, connected processes, and diseases [Research Support, Non-U.S. Gov't]. *Cold Spring Harbor perspectives in biology*, *5*(8), a011312.

Stehling, O., Mascarenhas, J., Vashisht, A. A., Sheftel, A. D., Niggemeyer, B., Rösser, R., . . . Lill, R. (2013). Human CIA2A-FAM96A and CIA2B-FAM96B integrate iron homeostasis and maturation of different subsets of cytosolic-nuclear iron-sulfur proteins. *Cell Metab*, *18*(2), 187-198.

Stehling, O., Netz, D. J., Niggemeyer, B., Rosser, R., Eisenstein, R. S., Puccio, H., . . . Lill, R. (2008). Human Nbp35 is essential for both cytosolic iron-sulfur protein assembly and iron homeostasis [Research Support, N.I.H., Extramural Research Support, Non-U.S. Gov't Research Support, U.S. Gov't, Non-P.H.S.]. *Molecular and cellular biology*, *28*(17), 5517-5528.

Stehling, O., Paul, V. D., Bergmann, J., Basu, S., & Lill, R. (2018). Biochemical Analyses of Human Iron–Sulfur Protein Biogenesis and of Related Diseases. *Methods Enzymol.*, *599*, 227-263.

Stehling, O., Sheftel, A. D., & Lill, R. (2009). Chapter 12 Controlled expression of iron-sulfur cluster assembly components for respiratory chain complexes in mammalian cells. *Methods Enzymol*, *456*, 209-231.

Stehling, O., Vashisht, A. A., Mascarenhas, J., Jonsson, Z. O., Sharma, T., Netz, D. J., . . . Lill, R. (2012). MMS19 Assembles Iron-Sulfur Proteins Required for DNA Metabolism and Genomic Integrity. *Science*, *337*(6091), 195-199.

Stehling, O., Wilbrecht, C., & Lill, R. (2014). Mitochondrial iron–sulfur protein biogenesis and human disease. *Biochimie*, *100*, 61-77.

Steiner, H., Zollner, A., Haid, A., Neupert, W., & Lill, R. (1995). Biogenesis of mitochondrial heme lyases in yeast. Import and folding in the intermembrane space. *J. Biol. Chem.*, *270*, 22842-22849.

Stojanovski, B. M., Hunter, G. A., Na, I., Uversky, V. N., Jiang, R. H. Y., & Ferreira, G. C. (2019). 5-Aminolevulinate synthase catalysis: The catcher in heme biosynthesis. *Mol Genet Metab*, *128*(3), 178-189.

Swenson, S. A., Moore, C. M., Marcero, J. R., Medlock, A. E., Reddi, A. R., & Khalimonchuk, O. (2020). From Synthesis to Utilization: The Ins and Outs of Mitochondrial Heme. *Cells*, *9*(3).

Taketani, S., Adachi, Y., & Nakahashi, Y. (2000). Regulation of the expression of human ferrochelatase by intracellular iron levels. *Eur J Biochem*, *267*(15), 4685-4692.

Taketani, S., Kakimoto, K., Ueta, H., Masaki, R., & Furukawa, T. (2003). Involvement of ABC7 in the biosynthesis of heme in erythroid cells: interaction of ABC7 with ferrochelatase. *Blood*, *101*(8), 3274-3280.

Taylor, J. L., & Brown, B. L. (2022). Structural basis for dysregulation of aminolevulinic acid synthase in human disease. *J Biol Chem*, *298*(3), 101643.

Teschner, J., Lachmann, N., Schulze, J., Geisler, M., Selbach, K., Santamaria-Araujo, J., . . . Bittner, F. (2010). A novel role for Arabidopsis mitochondrial ABC transporter ATM3 in molybdenum cofactor biosynthesis. *Plant Cell*, *22*(2), 468-480.

Thomas, C., & Tampé, R. (2020). Structural and Mechanistic Principles of ABC Transporters. *Annu Rev Biochem*, *89*, 605-636.

Toompuu, M., Kärblane, K., Pata, P., Truve, E., & Sarmiento, C. (2016). ABCE1 is essential for S phase progression in human cells. *Cell Cycle*, *15*(9), 1234-1247.

Torraco, A., Stehling, O., Stümpfig, C., Rösser, R., De Rasmo, D., Fiermonte, G., . . . Carrozzo, R. (2018). ISCA1 mutation in a patient with infantile-onset leukodystrophy causes defects in mitochondrial [4Fe-4S] proteins. *Hum Mol Genet*, *27*(20), 3650.

Trounce, I. A., Kim, Y. L., Jun, A. S., & Wallace, D. C. (1996). Assessment of mitochondrial oxidative phosphorylation in patient muscle biopsies, lymphoblasts, and transmitochondrial cell lines. *Methods Enzymol*, *264*, 484-509.

Tsiftsoglou, A. S., Tsamadou, A. I., & Papadopoulou, L. C. (2006). Heme as key regulator of major mammalian cellular functions: molecular, cellular, and pharmacological aspects. *Pharmacol Ther*, *111*(2), 327-345.

Van Vranken, J. G., Na, U., Winge, D. R., & Rutter, J. (2015). Protein-mediated assembly of succinate dehydrogenase and its cofactors. *Crit Rev Biochem Mol Biol*, *50*(2), 168-180.

Vance, J. E. (2014). MAM (mitochondria-associated membranes) in mammalian cells: lipids and beyond. *Biochim Biophys Acta*, *1841*(4), 595-609.

Vashisht, A. A., Zumbrennen, K. B., Huang, X., Powers, D. N., Durazo, A., Sun, D., . . . Wohlschlegel, J. A. (2009). Control of iron homeostasis by an iron-regulated ubiquitin ligase [Research Support, N.I.H., Extramural Research Support, Non-U.S. Gov't]. *Science*, *326*(5953), 718-721.

Visconte, V., Rogers, H. J., Singh, J., Barnard, J., Bupathi, M., Traina, F., . . . Tiu, R. V. (2012). SF3B1 haploinsufficiency leads to formation of ring sideroblasts in myelodysplastic syndromes. *Blood*, *120*(16), 3173-3186.

Walden, W. E., Selezneva, A. I., Dupuy, J., Volbeda, A., Fontecilla-Camps, J. C., Theil, E. C., & Volz, K. (2006). Structure of dual function iron regulatory protein 1 complexed with ferritin IRE-RNA. *Science*, *314*(5807), 1903-1908.

Walton, P. A., Brees, C., Lismont, C., Apanasets, O., & Fransen, M. (2017). The peroxisomal import receptor PEX5 functions as a stress sensor, retaining catalase in the cytosol in times of oxidative stress. *Biochim Biophys Acta Mol Cell Res*, *1864*(10), 1833-1843.

Wang, H., Shi, H., Rajan, M., Canarie, E. R., Hong, S., Simoneschi, D., . . . Zheng, N. (2020). FBXL5 Regulates IRP2 Stability in Iron Homeostasis via an Oxygen-Responsive [2Fe2S] Cluster. *Mol Cell*, *78*(1), 31-41.e35.

Ward, D. M., & Cloonan, S. M. (2019). Mitochondrial Iron in Human Health and Disease. *Annu Rev Physiol*, *81*, 453-482.

Weiler, B. D., Brück, M. C., Kothe, I., Bill, E., Lill, R., & Mühlenhoff, U. (2020). Mitochondrial [4Fe-4S] protein assembly involves reductive [2Fe-2S] cluster fusion on ISCA1-ISCA2 by electron flow from ferredoxin FDX2. *Proc Natl Acad Sci U S A*, *117*(34), 20555-20565.

Wilkinson, N., & Pantopoulos, K. (2014). The IRP/IRE system in vivo: insights from mouse models. *Front Pharmacol*, *5*, 176.

Wu, M., Gu, J., Guo, R., Huang, Y., & Yang, M. (2016). Structure of Mammalian Respiratory Supercomplex I(1)III(2)IV(1). *Cell*, *167*(6), 1598-1609.e1510.

Xiong, S., Jia, Y., Li, S., Huang, P., Xiong, J., Mao, D., . . . Liu, L. (2021). The First Case Report of X-Linked Sideroblastic Anemia With Ataxia of Chinese Origin and Literature Review. *Front Pediatr*, *9*, 692459.

Yang, Q., Zhao, J., Zheng, Y., Chen, T., & Wang, Z. (2023). Microbial Synthesis of Heme b: Biosynthetic Pathways, Current Strategies, Detection, and Future Prospects. *Molecules*, *28*(8).

Ye, H., Jeong, S. Y., Ghosh, M. C., Kovtunovych, G., Silvestri, L., Ortillo, D., . . . Rouault, T. A. (2010). Glutaredoxin 5 deficiency causes sideroblastic anemia by specifically impairing heme biosynthesis and depleting cytosolic iron in human erythroblasts. *J Clin Invest*, *120*(5), 1749-1761.

Yien, Y. Y., Robledo, R. F., Schultz, I. J., Takahashi-Makise, N., Gwynn, B., Bauer, D. E., . . . Paw, B. H. (2014). TMEM14C is required for erythroid mitochondrial heme metabolism. *J Clin Invest*, *124*(10), 4294-4304.

Zang, J., Chen, H., Zhao, G., Wang, F., & Ren, F. (2017). Ferritin cage for encapsulation and delivery of bioactive nutrients: From structure, property to applications. *Crit Rev Food Sci Nutr*, *57*(17), 3673-3683.

Zeida, A., Trujillo, M., Ferrer-Sueta, G., Denicola, A., Estrin, D. A., & Radi, R. (2019). Catalysis of Peroxide Reduction by Fast Reacting Protein Thiols. *Chem Rev*, *119*(19), 10829-10855.

Zhang, Y., Lyver, E. R., Nakamaru-Ogiso, E., Yoon, H., Amutha, B., Lee, D.-W., . . . Dancis, A. (2008). Dre2, a conserved eukaryotic Fe/S cluster protein, functions in cytosolic Fe/S protein biogenesis. *Mol. Cell. Biol.*, *28*, 5569-5582.

Zheng, L., White, R. H., Cash, V. L., & Dean, D. R. (1994). Mechanism for the desulfurization of L-cysteine catalyzed by the nifS gene product. *Biochemistry*, *33*, 4714-4720.

Zhong, H., Janer, A., Khalimonchuk, O., Antonicka, H., Shoubridge, E. A., & Barrientos, A. (2023). BOLA3 and NFU1 link mitoribosome iron-sulfur cluster assembly to multiple mitochondrial dysfunctions syndrome. In.

Zhou, M., Diwu, Z., Panchuk-Voloshina, N., & Haugland, R. P. (1997). A stable nonfluorescent derivative of resorufin for the fluorometric determination of trace hydrogen peroxide: applications in detecting the activity of phagocyte NADPH oxidase and other oxidases. *Anal Biochem*, *253*(2), 162-168.

Zhou, S., Kachhap, S., & Singh, K. K. (2003). Mitochondrial impairment in p53-deficient human cancer cells. *Mutagenesis*, *18*(3), 287-292.

11. Appendix

11.1 Akademische Lehrer

Meine akademischen Lehrenden in Marburg waren (in alphabetischer Reihenfolge ohne akademischen Grad):

Adamkiewicz
Adeberg
Adhikary
Aigner
Albers
Arndt
Bartsch
Bauer S.
Bauer U.
Baum
Becker A.
Becker K.
Becker S.
Bender
Bertoune
Bette
Bliemel
Boekhoff
Bogdan
Bösner
Boss
Bonaterra
Braun
Braymer
Brehm
Buchholz
Burchert
Cetin
Czubayko
Decher
del Rey
Denkert
Denzer
Dietz
Dinges
Donner-Banzhoff
Elsässer
Eschbach
Feuser
Fülber
Freibert
Frink
Fritz
Fuchs-Winkelmann
Geisthoff
Geks
Geraedts
Ghazy
Görg
Greim
Gress
Grgic
Graumann
Hantschel
Hellinger
Hertl
Hildebrand
Hirsch
Hoch
Holzer
Homm
Horodko
Hoyer
Huber
Irqsusi
Jakob
Jerrentrup
Kalder
Kann
Kanngießer
Keber
Kemmling
Kerwat
Kinscherf
Kircher
Kirschbaum
Klaus
Knake
Knorrenschild
Köhler G.
Köhler S.
Kolb-Niemann
Koolmann
Kortus-Götze
Lill
Lohoff
Lüsebrink
Luster
Mahnken
Maier
Maisner
Mandic
Maurer
Meissel
Mendoza
Milani
Mirow
Moll
Moosdorf

Mühlenhoff	Rost	Streubel
Mutters	Ruchholtz	Stuck
Neff	Rust	Swaid
Neubauer	Sahmland	Thieme
Neumüller	Schäfer	Timmermann
Nimsky	Schieffer	Ulrich
Oberkircher	Schmidt	Vogelmeier
Oberwinkler	Scholz	Vogt
Oliver	Schu	Vorwerk
Opitz	Schumacher	Wagner
Pagenstecher	Schütz	Weber
Pankuweit	Schwarz	Weihe
Pedrosa	Seifart	Westermann
Pehl	Seitz	Wiese
Peterlein	Sekundo	Wilhelm
Plant	Sevinc	Witzleb
Preisig-Müller	Skevaki	Worzfeld
Quint	Sommer	Wrocklage
Rastan	Sonanini	Wulf
Rakwalska-Bange	Stehling	Zacharis
Reese	Steininger	Ziring
Renz	Stibane	Zwermann

Meine akademischen Lehrenden in München waren (in alphabetischer Reihenfolge ohne akademischen Grad):

Arnholdt	Juchem	Neuerburg
Böcker	Kauke	Peterß
Brenner	Klauser	Pichlmaier
Fertmann	Krötz	Schmoeckel
Hagl	Kur	Schneider
Holzapfel	Michel	Sienel
Joskowiak	Müller	

11.2 Danksagung

Nicht nur Recherche, zahlreiche Experimente und eine lange Schreibphase führten zur Fertigstellung dieser Arbeit. Dahinter stecken viele lange, später vergessene Tage der Arbeit, viele prüfende Augen und anleitende Hände. Einigen bemerkenswerten Unterstützern während der Arbeitsphase dieser Dissertation möchte ich daher besonders danken.

Die Forschung und die gesamte Arbeit an dieser Thesis wären nicht ohne die Hilfe meines Doktorvaters Herrn Prof. Dr. Roland Lill sowie meiner Betreuer Herrn Dr. Oliver Stehling und Frau Dr. Linda Boss möglich gewesen.

Herr Prof. Dr. Lill ermöglichte mir die intensive Forschungszeit und schenkte mir das Vertrauen, auf dem Gebiet seiner besonderen Expertise zu arbeiten und zahlreiche Erfahrungen zu sammeln. Meine Motivation, als Medizinerin den Einstieg in die Welt der naturwissenschaftlichen Grundlagenforschung zu finden, hat er ab dem ersten Tag unterstützt und dafür bin ich sehr dankbar.

Ein besonderer Dank gilt Herrn Dr. Stehling. Monatelang opferte er seine Zeit, um mich zuerst in den Laboralltag einzuarbeiten, zuletzt mit mir diese Arbeit durchzusprechen, gab mir so viele hilfreiche Tipps. Seine Anmerkungen waren so detailliert wie weitsichtig, was, da bin ich überzeugt, zur Gänze dieser Thesis beitrug. Er hatte immer ein offenes Ohr und eine passende Antwort auf meine zahlreichen Fragen. Auch Frau Dr. Boss gilt ein großer Dank für die sowohl fachliche, aber auch mentale Unterstützung.

So gilt Herrn Prof. Dr. Lill, Herrn Dr. Stehling und Frau Dr. Boss sowie dem gesamten Team des zellbiologischen Instituts mein Dank für die Geduld und Unterstützung, die Hilfestellungen und Anmerkungen. Ich hatte großes Glück, mit einem so tollen Team zusammenzuarbeiten.

Auch meiner Familie und meinen Freunden gilt großer Dank. Sie motivierten mich und hielten mir den Rücken frei, damit ich mich auf meine Arbeit konzentrieren konnte. Ob die ersten Jahre während der Laborarbeit oder während der Schreibphase, auf ihren Rat konnte ich immer bauen.

Danke für eure Unterstützung.